LBL-38228
UC-401

Lawrence Berkeley Laboratory
UNIVERSITY OF CALIFORNIA

CHEMICAL SCIENCES DIVISION

The Reaction Dynamics of Alkali Dimer Molecules and Electronically Excited Alkali Atoms with Simple Molecules

H. Hou
(Ph.D. Thesis)

December 1995

Prepared for the U.S. Department of Energy under Contract Number DE-AC03-76SF00098

LBL-38228
UC-401

The Reaction Dynamics of Alkali Dimer Molecules and Electronically Excited Alkali Atoms with Simple Molecules

Hongtao Hou

Department of Chemistry
University of California, Berkeley

and

Chemical Sciences Division
Lawrence Berkeley National Laboratory
University of California
Berkeley, California 94720

December 1995

This work was supported by the Director, Office of Energy Research, Office of Basic Energy Sciences, Chemical Sciences Division, of the U.S. Department of Energy under Contract No. DE-AC03-76SF00098.

The Reaction Dynamics of Alkali Dimer Molecules and Electronically Excited Alkali Atoms with Simple Molecules

by

Hongtao Hou

B. S. (University of Science and Technology of China) 1989

A dissertation submitted in partial satisfaction of the

requirements for the degree of

Doctor of Philosophy

in

Chemistry

in the

GRADUATE DIVISION

of the

UNIVERSITY of CALIFORNIA, BERKELEY

Committee in charge:

Professor Yuan T. Lee, Chair

Professor Alexander Pines

Professor Alan M. Portis

1995

Abstract

The Reaction Dynamics of Alkali Dimer Molecules and Electronically Excited Alkali Atoms with Simple Molecules

by

Hongtao Hou

Doctor of Philosophy in Chemistry

University of California at Berkeley

Professor Yuan T. Lee, Chair

This dissertation presents the results from the crossed molecular beam studies on the dynamics of bimolecular collisions in the gas phase. The primary subjects include the interactions of alkali dimer molecules with simple molecules, and the inelastic scattering of electronically excited alkali atoms with O_2.

The reaction of the sodium dimers with oxygen molecules is described in Chapter 2. Two reaction pathways were observed for this four-center molecule-molecule reaction, i.e. the formations of NaO_2 + Na and NaO + NaO. NaO_2 products exhibit a very anisotropic angular distribution, indicating a direct spectator stripping mechanism for this reaction channel. The NaO formation follows the bond breaking of O_2, which is likely a result of a charge transfer from Na_2 to the excited state orbital of O_2^-. The cross sections for these two reaction channels were measured to be 0.8 $Å^2$ and 2 $Å^2$, respectively.

The scattering of sodium dimers from ammonium and methanol produced novel molecules, $NaNH_3$ and $Na(CH_3OH)$, respectively. These experimental observations, as well as the discussions on the reaction dynamics and the chemical bonding within these molecules, will be presented in Chapter 3. The lower limits for the bond dissociation energies of these molecules are also obtained.

Finally, Chapter 4 describes the energy transfer between oxygen molecules and electronically excited sodium atoms. Long-lives Rydberg states Na were produced in the scattering of Na(4D) from O_2 molecules, with most of the translational energy converted into the electronic excitation of Na. In the parallel experiments replacing O_2 by N_2, NO and CO, no Rydberg signal were recorded, suggesting the participation of the ionic state $Na^+...O_2^-$. A simple model is used to demonstrate the importance of the translational energy in determining outcomes of the collisions.

To my family.

Table of Contents

Chapter 4

List of Tables

Acknowledgments

First I would like to express my gratitude to Professor Yuan T. Lee for providing me with this great opportunity to continue my education in his research group at Berkeley. In the past six years I have benefitted the most not only from Yuan's deep scientific insight which guides me in my quest for the laws of the nature, but also from his everlasting optimism and constant encouragement which has been, and will always be, the endless inspiration in my expedition of life.

Thanks also to Professor Xing-Xiao Ma and Professor Shu-Qin Yu who taught me in the college and have since become a great support in my scientific career. Their devotion to education and scientific research sets an excellent example to me.

On my first day becoming a Lee Group member, Yuan led me to the A machine, where I teamed up with H. Floyd Davis and Arthur G. Suits, both among the most devoted scientists that I have ever met. They taught me patiently the basics of running the then-formidable crossed beam apparatus, correcting numerous mistakes in my learning processes. Last year, I visited Floyd and his brand new, nearly empty lab at Cornell University. Two months ago, when I met Floyd again, I was excited to see that in less than one year, he has made his lab running and very productive. Arthur returned to Berkeley last year, tirelessly taking the tremendous responsibilities of superintending the lab, managing a beam line at the Advanced Light Source of Lawrence Berkeley National Laboratory, and many other duties. With him I have had the most frequent discussions which have been so constructive and helpful for me to reach the results presented in this dissertation. At my entry, Mike Covinsky had already completed his tenure on the A Machine, but my few

conversations with him were educational and memorable.

The experiments reported in this thesis were carried out in almost five years. Shortly after I started these projects, Vladislav Sadchenko came to the Lee Group and offered his help on the A Machine. He is a wonderful young man with strong enthusiasm and good training in science. Vlad is now working on his Ph. D. degree at the University of Minnesota and I wish him the best in his future. During my last year in the Lee Lab, I enjoyed the pleasure of working with Kueih-Tzu Lu, who has such a delightful personality and positive attitude toward various challenges. She went back to Taiwan to start her scientific career and I am sure that I will hear good news from her before long.

There are many individuals who helped me through my years at Berkeley. My running two ring dye lasers would never have come to realization without Dr. Marcus J. J. Vrakking, Allan Bracker and Dr. James Chesko teaching me how at the very beginning. Dr. Jingsong Zhang and Dr. Tzong Tsong Miau were particularly helpful when I was stuck by scientific and technical problems. Dr. Jim Meyers and Dr. John Price impressed me by their willingness to take responsibility whenever there was a need in the group. I also enjoyed very fruitful discussions on the photodissociation experiments and scientific problems in general with Dr. Simon North and Dr. Domenico Stranges.

I have benefitted from Dr. Jinchun Xie, Dr. Zhifeng Liu, Dr. Xueming Yang and Dr. Gang-Yu Liu more than the scientific discussions. They have also shared so much of their knowledge of Chinese history, politics and culture with me. "Too bad" they all took jobs in scientific research. I would also like to thank Dr. Deon Anex, Dr. Pam Chu, Dr. Toshinori Suzuki, Dr. Laura Smoliar, Cheryl Longfellow, Cindy Berrie, David Blank, Dr. Kim Prather and Dr. Ralf Ingo-Kaiser for their generous support.

Our chemistry department was recently rated number one in research in the nation. This honor is inseparable from the endeavor of the staff in the department. Among them, Beth Murphy has been looking after me since day one that I am here. Ann Lawhead, Daina Tekorius, and Marian Grebanier have helped me to survive without having to struggle in an ocean of paper work. The machine shop and the electronic shop were the rescuers whenever something failed on my apparatus. Special thanks to Bob Conroy, who works in the welding shop of Lawrence Berkeley National Laboratory. He helped so much with the designing and machining of the high temperature oven, making the experiments possible.

I am deeply indebted to every member of my family. I owe my education to my parents, who were both excellent chemistry students in college but did not have the opportunity to continue after their graduation due to the infamous Cultural Revolution in China. I hope their dreams will become true in me. Mr. and Mrs. Harding warmly welcomed me into their house on my first day in the United States and since then led me gradually into this great society. Yuezhong Du, Kun Liu and Qing Wang are like big brothers, looking after me during my tenure in Berkeley.

Finally I owe special thanks to my wife, Sophie, for her everlasting support without which all my effort would be fruitless. Together we struggle, we endure the hardships, we enjoy the good times, and we succeed.

Chapter 1

Introduction to the Thesis

The Crossed Molecular Beam Apparatus

The experimental results reported in this thesis were carried out on a crossed molecular beam machine which has been detailed previously. [1] [2] [3] Some general methods for operating this machine will be outlined briefly in each chapter whenever it is necessary. The scope of this chapter is to describe the parts of the apparatus that are directly relevant to the specific experiments and to summarize the operation conditions for the measurements.

The experiments were performed using continuous supersonic atomic/molecular beams. A beam containing either sodium atoms or sodium dimer molecules, designated as the primary beam, crosses a molecular beam, the secondary beam, at 90^{o} in a vacuum chamber under single collision conditions. The geometric plane defined by these two beams will be named the scattering plane hereafter. In the studies of the energy transfer between oxygen molecules and electronically excited sodium atoms, two CW ring dye lasers pumped by Ar^{+} lasers were used. The laser beams were sent through the interaction region of the primary and secondary beams, perpendicular to the scattering plane. A triply differentially pumped UHV detector equipped with an electron bombardment ionizer, [4] a quadrupole mass spectrometer and a Daly ion counter [5] rotates about the interaction region in the scattering plane so that the laboratory angular distributions of the scattering products can be measured. By using a mechanical chopper wheel (either single shot or pseudo-random sequence [6]) at the entrance of the detector, the velocity distributions of

the scattered products can be measured.

The High Temperature Oven Assembly

The primary beam is generated by a high temperature oven assembly originally designed for studies involving barium atoms. [7] A schematic of this oven assembly is shown in Figure 1.1. The heart of this assembly is an oven made of refractory metal. The oven body has a concentric double wall structure. During operation, an AC current (typically 400 A at 1.4 V) passes across the outer layer to provide the heating, and the outer layer in turn radiatively heats up the inner layer which contains alkali metal. This configuration can effectively reduce the temperature instability caused by the varying resistance of the loaded oven due to the evaporation of the alkali metal. The oven is spring loaded against the front electrode so that more heating power is dissipated at the front nozzle due to the higher contact resistance. In this way the nozzle can be maintained ~ 200 K hotter than the oven body so as to prevent clogging of the nozzle. A second heater made of high density graphite is placed around the oven body to provide further control of the vaporization temperature. Tantalum sheets are extensively used as radiation shield in this oven assembly to minimize heat loss. After supersonic expansion, the alkali beam is skimmed at ~ 0.75 cm down stream by a stainless steel skimmer which is also heated to prevent clogging. For the sodium beam, the oven is made of molybdenum, whereas for lithium experiments which are not described in this thesis, a tantalum oven was used because lithium is extremely corrosive to molybdenum. This oven assembly can be operated within a wide temperature range up to ~1500 K so that an intense alkali metal atom beam can be generated without difficulty.

The Primary Beam

Sodium dimers are stable molecules with a bond dissociation energy of 17.5 kcal/mol. [8] This bond strength is very large compared with the Van der Waals interaction so the dimer molecules are always present in the sodium vapor in appreciable amount. In theory, the dimer intensity can be raised to any desired level for the experiment simply by increasing the body temperature of the oven. However, in practice, the sodium vapor pressure has to be kept low enough to allow at least a few hours of stable run-time for signal average. For the dimer experiments the optimal operation conditions can be estimates as follow. First let us review the equilibrium properties of a gaseous mixture containing sodium vapor at certain temperature and pressure. If we assume that the vapor pressure of sodium is low enough so that the influence of trimer and larger clusters on the equilibrium are negligible, then we need only to consider the equilibrium process:

$$Na(g) + Na(g) + M \Leftrightarrow Na_2(g) + M, \qquad \text{(i)}$$

where M is an arbitrary third body. The equilibrium constant K(T) for Reaction (i) can be calculated from the thermodynamic data obtained from standard handbooks [9] and the results are listed in Table 1 on page 13. The vapor pressure of sodium is also listed in the same table for corresponding temperatures. From these results we can calculate the molar fraction of the sodium dimer in the sodium vapor at different temperatures. Similar calculation is also done for the cases when there is a buffer gas of certain pressure in the mixture. Table 2 on page 13 and Figure 1.2 present the molar fraction of sodium dimer in the sodium vapor as a function of temperature under different pressure of the buffer gas. Interestingly, each curve (except the one for neat sodium) shows a maximum corresponding to an optimal temperature for making the dimer molecules the most efficiently. This

optimal peak tends to shift to lower temperature when the buffer gas pressure decreases. It is also evident that at the same temperature, the less buffer gas, the higher the dimer fraction in the sodium vapor.

On the other hand, in a crossed beam experiment, the intensity of the beam is scaled by the pressure of the molecules behind the nozzle. In Table 3 on page 14 and Figure 1.3 the partial pressure of sodium dimers under the same conditions as those in the above mentioned calculations is given for various temperatures. Unlike the molar fraction curves in Figure 1.2, the partial pressure of the sodium dimers increases monotonically with the temperature, primarily due to the exponential increase of the vapor pressure of the sodium.

These thermodynamic calculations provide us with very important guidances in the search for the optimal experimental conditions. Take the neat sodium vapor for example: at temperatures below 850 K, the dimer formation is rather efficient but the overall vapor pressure of the sodium is too low for the scattering experiment. At a temperature higher than 1100 K, sodium dimers are formed in large quantity but less efficiently so that most of the sodium in the gas is in monomer form and wasted. Consequently the optimal operation temperature is somewhere between 900 K and 1000 K. Meanwhile, in the sense to study the reaction dynamics, we wish to be able to change the collisional energy of the particle system. For this purpose, as well as for obtaining a better supersonic expansion, a mixture of sodium vapor with helium or neon is frequently used to generate a seeded beam.

After the optimal operation conditions are set, the stable run-time for each load of alkali metal can be estimated. Assuming the expansion is carried out through a 0.2 mm

dia. nozzle at 1250°K with a stagnation pressure (p_s) of 660 torr (~15% molar fraction of Na in He, experimental value). The amount of gas that flows into the vacuum chamber can be estimated to be 0.02 l/s using the equation: [10]

$$S = 3.64(T/M)^{1/2}A \text{ liters/second,} \qquad (1.1)$$

where T is the nozzle temperature (K), M is the average molecular weight (g/mol), and A is the area of the nozzle cross section (cm^2). This is equivalent to a net sodium flow of 1.6 g/hr. The inner can of the oven body can hold ~ 20 g of sodium (300 × 0.5 cm dia. spheres). Under these conditions, the maximum run-time is only 12.5 hours. Usually during an operation cycle, the beam intensity is not stable in the first and the last two hours. As a result, the effective run-time is only ~ 8 hours for a full load of sodium. For a neat sodium beam, the nozzle conductance is much lower (~ 0.8 g/hr) so the run-time is much longer (~ 20 hours), with sacrifices of the beam intensity and beam quality.

In practice, dimer formation processes could be much more complicated than the situations under the equilibrium conditions. [11] Kinetics models for dimerization usually require tedious fluid mechanics analysis and they are often inaccurate because the mechanisms for dimerization used in these models are much simplified compared to the real cases. Experimentally, the fragmentation of the dimers in the mass spectrometer and the mass dependent sensitivity of the detector pose severe difficulties in determining the fraction of dimers. Only in limited cases where the kinematics are favorable, scattering experiments do provide some important information on the dimer composition in the beam.

The Newton diagram for Na/Na_2 (neat) + Ne(neat, room temperature) is shown in Figure 1.4. The measurement of the relative dimer concentration was carried in three steps. First, time of flight spectra are measured at certain angles for Na^+ (m/e = 23), which

could be from either the scattered Na or the fragmentation of the scattered Na_2. Because the elastically scattered sodium monomers and dimers fly at different velocities (e.g. at 40°, the laboratory velocity for the fast monomers is 1423 m/s, while that for the dimers is 1061 m/s), we expect to see two peaks in each time of flight spectrum. For the present configuration of the detector, the neutral flight distance is 16.74 cm, so the fast and slow Na^+ arrive at 118 μs and 158 μs, respectively. In theory, if these two peaks are separated well enough in the spectrum, the areas under these peaks can be computed with good accuracy, which will be designated as S_{Na} and S_{Na2}, respectively. Second, time of flight spectra of the Na_2^+ signal are also measured at the same angles. The area under the elastically scattered Na_2^+ peak can be calculated as S_{Na2}'. If the resolution of the mass spectrometer is set low enough such that Na^+ and Na_2^+ have roughly the same transmission, the ratio

$$\eta_{Na2} = S_{Na2}/(S_{Na2} + S_{Na2}') \qquad (1.2)$$

gives the fraction of the sodium dimers that dissociate to Na^+ in the detector. The third step is to measure the Na^+ and Na_2^+ signal on the beam axis with the same detector sensitivity and secondary beam off to get the respective intensities S_{Na}^0 and S_{Na2}^0. The fraction of the dimer in the sodium vapor is then:

$$f_{Na2} = (S_{Na2}^0/(1 - \eta_{Na2}))/(S_{Na2}^0 + S_{Na}^0). \qquad (1.3)$$

In practice, however, this method suffers severe restraints besides the requirement that the detector have the same sensitivity to Na and Na_2. First, this scheme can be applied only in the situations when the primary beam is very slow so that the scattered Na and Na_2 are well separated in their velocities. For the seeded beams, because the center-of-mass of the monomer-secondary and dimer-secondary systems move closer to the pri-

mary beam, the velocities of the scattered monomers and dimers are less different, and the corresponding time of flight peaks are less separated. Second, the monomer and dimer peaks are well separated only at large lab angles where the intensity of the scattered dimers is extremely low. And third, the most serious drawback of this method, is the intrinsic spread of the beam. Under a "soft" expansion (i.e. for neat sodium vapor of 50 — 100 torr), the typical speed ratio of the beam, $v/\Delta v$, is ~ 5, corresponding to FWHM of ~ 30 μs. The spread for the recorded time of flight peaks is even wider due to the velocity distribution of the secondary beam and the instrumental broadening. As a result, the dimer peak could well be buried under the monomer peak. In Figure 1.5, the time of flight spectra for the elastically scattered Na^+ and Na_2^+ off a neat neon beam at a lab angle of 40 degrees are shown. These two spectra are normalized to the same arbitrary averaging time. It is immediately evident that the Na_2^+ signal is very weak at this angle. After almost 4 hours of signal averaging, the peak is barely seen. Fortunately in the Na^+ spectrum, we can see a fast peak which is the elastic scattering of Na, and a slow peak which is from the fragmentation of elastically scattered Na_2^+. In the figure, the lines are the fit to the data using simple Gaussian curves. In the Na^+ spectrum, the areas under the data and the Gaussian curve are 4430 and 2283 (arbitrary unit), respectively. The difference between these two values is taken to be the total signal for the fragmented Na_2^+. The area under the Na_2^+ curve is 239. According to Equation (1.2), the fragmentation ratio of Na_2 can be calculated to be 87%.

Figure 1.6 shows the time of flight spectra for Na^+ and Na_2^+ measured on the primary beam axis with the secondary beam turned off. The slow peak in the Na_2^+ spectrum (indicated by arrow) should be neglected since it is from the field ionization of the Ryd-

berg sodium atoms generated by electron bombardment. The areas under these curves are 8861 and 85 (arbitrary unit) for Na^+ and Na_2^+, respectively. From Equation (1.3), the fraction of Na_2 in the sodium vapor is ~ 7%. This value is consistent with the results shown in Figure 1.2 for the neat sodium vapor at a nozzle temperature of ~ 1250 K. The fraction of Na_2 in a seeded beam is difficult to measure, however, based on the measurement for the neat Na vapor, its true value should be reasonably close to the calculated value shown in Figure 1.2.

Detector Calibration

In the experiments we need to measure both the angular and the velocity distributions of the product molecules to get a full picture of the scattering processes. This can be achieved with the rotatable universal detector, which is schematically drawn in Figure 1.7 to illustrate the detection techniques. The molecules to be detected will first pass through a series of defining slits before they arrive at the electron bombardment ionizer, which is housed in an ultrahigh vacuum (10^{-10} torr) chamber. Roughly one out of 10^4 molecules arriving at the ionization region will be ionized upon electron impact. The ions so produced then undergo mass selection by the quadrupole mass spectrometer and finally are counted at the Daly ion detector. The criteria for the design of this universal detector have been described recently. [12]

In a typical experiment to measure the time of flight spectra, a mechanical chopper wheel is mounted at the entrance of the detector, serving the purposes of modulating the signal and providing a time reference. The intensity of the scattering signal is then recorded as a function of flight time to the Daly detector starting from the position of the chopper wheel. The total flight time can be divided into two parts: the neutral flight time,

$t_{neutral}$, and the ion flight time, t_{ion}. $t_{neutral}$ is the duration for the neutral molecules to travel from the chopping wheel to the ionizer so it contains information on the velocity of the molecules. t_{ion} is the time the ions spend for the rest of the flight path and depends on the geometry and voltage settings of the detector only. It can be shown that t_{ion} is proportional to the mass-to-charge ratio of the ions in consideration. i. e.,

$$t_{ion} = \alpha(m/e)^{1/2}, \qquad (1.4)$$

where α is a function of the electric field potential and is designated as the ion flight constant.

To measure α, a supersonic beam of a polyatomic molecule, e. g. CF_2Cl_2, is prepared and the time of flight spectra are recorded for various daughter ions produced by electron impact. Obviously $t_{neutral}$ is the same for all the ions having a common parent molecule. So the differences in their flight time are solely due to the disparity in their mass-to-charge ratios, assuming that the momenta from the fragmentation are small compared with the interaction between the ions and the electric field. A plot of the flight time at the maximum intensity vs. the square root of the mass-to-charge ratio is shown in Figure 1.8 for measurements with the chopping wheel spinning clockwise (CW) and counterclockwise (CCW). A linear least square fit to each measurement gives the ion flight constant as the slope of the line. The difference between CW and CCW results is due to the mechanical offset of the wheel, which has to be account for in the flight time measurement.

Now that the neutral flight time can be measured accurately, we need to measure the nominal neutral flight distance, L, from the chopping wheel to the ionizer to be able to obtain the velocity of the molecules. To determine L, the time of flight spectra of the

supersonic beams of various inert gases are recorded. For a good expansion, the terminal group velocity for an inert gas is:

$$v_{terminal} = (5RT/M)^{1/2}, \qquad (1.5)$$

where R is the gas constant, T is the nozzle temperature and M is the mass of the atom. It is therefore possible to assume a neutral flight distance and calculate the group velocity based on the measured time of flight spectra for the inert gases. By comparing the results with the values obtained by Equation (1.5) and iterating the above procedure, L can be precisely determined.

Under these conditions the neutral flight time is:

$$t_{neutral} = L/v_{terminal} = \beta M^{1/2}, \qquad (1.6)$$

where $\beta = L/(5RT)^{1/2}$. If we consider the singly charged ions whose mass to charge ratio is equal to M, we will have for the flight time t:

$$t = t_{neutral} + t_{ion} = (\beta + \alpha)M^{1/2}. \qquad (1.7)$$

Figure 1.9 shows the recorded flight time for He, Ne and Ar vs. the square root of their masses. A linear least square fit gives the value $(\alpha + \beta)$ as the slope. Using the measured values for α and T, L can be determined.

The Reactions of Alkali Atoms and Dimers

The pioneering studies of the alkali atom reactions with halogen molecules ($M + X_2$) were performed in the late 1920s and 1930s by M. Polanyi and coworkers. [13] Their experiments brought attention to the surprisingly large size of the cross sections for the $M + X_2$ reactions. The simplest-model to explain these large cross sections is the "Harpooning" model first proposed by Polanyi and further developed by Magee. [14] In this model

the reaction occurs as a result of the transfer of the valence electron of the alkali atom to the halogen molecule. The reaction is then completed by the action of the resulting Coulomb force. The rapid electron transfer from the alkali atom to the halogen molecule occurs in the region between the covalent M-X_2 and the ionic M^+-X_2^- potential energy curves. If one neglects the nonadiabatic interactions between the ionic and covalent states, and the van der Waals interactions at long range, the crossing distance can be obtained from:

$$R_c = \frac{14.4}{IP(M) - EA(X_2)} \text{ (Å)}. \qquad (1.8)$$

Here IP(M) is the ionization potential for the alkali atom and $EA(X_2)$ is the vertical electron affinity of the halogen molecule, both in electron volts. Following this simple idea of electron jump, the cross sections for the dynamical processes of alkali atoms are usually described to be:

$$\sigma = p(\pi R_c^2), \qquad (1.9)$$

where p is usually a function of the collisional energies and the topologies of the potential energy surfaces. p is different for each individual theoretical model, the simplest being equal to 1 which can provide a very satisfactory description for the $M + X_2 \rightarrow MX + X$ reactions.

With the application of molecular beam techniques and the advances in vacuum and mass spectrometry technologies, a vast number of reactive scattering processes as well as inelastic scattering processes have been investigated since the 1960s. [15] These results reveal that the alkali reactions exhibit a broad spectrum of dynamical behaviors which are often amenable to simple model interpretations, e. g., "stripping" [16] (M/M_2 +

X_2) and "rebound" [17] ($M + CH_3X$) mechanisms, direct interaction ($M + X_2$ and CH_3X) and long-lived or osculating complexes [18] ($M + M'X$), impulsive energy transfer and statistical energy partition, etc. Currently lasers are being used widely to prepare electronically excited alkali atoms for studies of the reactions and the energy transfer processes. During the entire period of chemical dynamics studies, alkali family members have played active and important roles because of their unique physical properties such as low ionization potentials, the generally large reaction cross sections, the readiness for laser excitation, and the readiness to form dimers, to name just a few. In the following chapters, it will be demonstrated from the results of the alkali dimer reactions and the energy transfer of the electronically excited alkali atoms that alkali metal systems still generate unceasing excitement in the field of chemical dynamics.

Tables

Table 1: Thermodynamic properties of sodium vapor

T(K)	$G_f(Na)$ (kj/mol)	$G_f(Na_2)$ (kj/mol)	K ($2Na \Leftrightarrow Na_2$)	Sodium Vapor (torr)
300	76.636	103.87	3.9953e+08	3.7023e-11
400	66.753	91.873	2.7330e+05	1.1604e-06
500	57.626	81.481	3372.8	0.00057847
600	48.676	71.547	176.40	0.036369
700	39.919	61.966	21.558	0.70040
800	31.263	52.667	4.4027	6.4387
900	22.710	43.601	1.2752	36.154
1000	14.246	34.740	0.47167	143.76
1100	5.8650	26.064	0.20861	444.76

Table 2: The fraction of Na_2 in sodium vapor at various buffer pressures

T (K)	600torr buffer	500torr buffer	400torr buffer	300torr buffer	200torr buffer	100torr buffer	0 torr buffer
300	0.0000	0.0000	0.0000	0.0000	0.0001	0.0001	0.9999
400	0.0005	0.0006	0.0008	0.0011	0.0016	0.0032	0.9981
500	0.0032	0.0039	0.0048	0.0064	0.0096	0.0188	0.9829
600	0.0105	0.0125	0.0155	0.0205	0.0302	0.0570	0.9275
700	0.0239	0.0285	0.0351	0.0457	0.0657	0.1169	0.8066
800	0.0428	0.0505	0.0614	0.0785	0.1090	0.1794	0.6236
900	0.0636	0.0738	0.0879	0.1089	0.1433	0.2109	0.4236
1000	0.0776	0.0877	0.1008	0.1187	0.1444	0.1848	0.2590
1100	0.0758	0.0826	0.0908	0.1007	0.1132	0.1292	0.1505

Table 3: Partial pressure of Na_2 (torr) in buffer gas

T(K)	600torr buffer	500torr buffer	400torr buffer	300torr buffer	200torr buffer	100torr buffer	0 torr buffer
300	0.0000	0.0000	0.0000	0.0000	0.0000	0.0000	0.0000
400	0.0000	0.0000	0.0000	0.0000	0.0000	0.0000	0.0000
500	0.0000	0.0000	0.0000	0.0000	0.0000	0.0000	0.0006
600	0.0004	0.0005	0.0006	0.0007	0.0011	0.0021	0.0337
700	0.0168	0.0199	0.0246	0.0320	0.0460	0.0819	0.5649
800	0.2758	0.3249	0.3956	0.5057	0.7019	1.1549	4.0154
900	2.2977	2.6671	3.1791	3.9373	5.1804	7.6236	15.316
1000	11.152	12.604	14.495	17.062	20.759	26.573	37.233
1100	33.734	36.758	40.382	44.807	50.336	57.447	66.952

References

[1] Y. T. Lee, J. D. McDonald, P. R. LeBreton, and D. R. Herschbach, Rev. Sci. Instrum. **40**, 1402 (1969).

[2] P. E. Siska, J. M. Parson, T. P. Schaefer, and Y. T. Lee, J. Chem. Phys. **55**, 5762 (1971).

[3] Y. T. Lee in: *Atomic and Molecular Beam Methods, Vol. 1*, edited by G. Scoles, Oxford University Press, New York (1988).

[4] G. O. Brink, Rev. Sci. Instrum. **37**, 857 (1966).

[5] N. R. Daly, Rev. Sci. Instrum. **31**, 264 (1960).

[6] (a) G. Comsa, R. David, and B. J. Schumacher, Rev. Sci. Instrum. **52**, 789 (1981).
(b) R. David, K. Kern, P. Zeppenfeld, and G. Comsa, Rev. Sci. Instrum. **57**, 2771 (1986).

[7] H. F. Davis, Ph. D. Thesis, University of California at Berkeley (1992).

[8] D. R. Lide, Editor-in-Chief, *CRC Handbook of Chemistry and Physics*, 74th edition (1993-1994).

[9] JANAF Thermochemical Tables, 3rd ed., J. Physical and Chemical Ref. Data, 14 (1985), Supp. No.1.

[10] A. Berman, *Vacuum Engineering Calculations, Formulas, and Solved Exercises*, Academic Press, Inc. (1992).

[11] D. R. Miller in: *Atomic and Molecular Beam Methods, Vol. 1*, edited by G. Scoles, Oxford University Press, New York (1988).

[12] A. G. Suits and Y. T. Lee in Atomic, Molecular and Optical Physics Reference Book, G. Drake, Ed., American Institute of Physics, New York (1994).

[13] M. Polanyi, *Atomic Reactions*, Williams & Norgate, London (1932).

[14] J. L. Magee, J. Chem. Phys. **8**, 687 (1940).

[15] (a) R. D. Levine and R. B. Bernstein, *Molecular Reaction Dynamics and Chemical Reactivity*, Oxford University Press, New York (1987). (b) R. R. Herm in: *Alkali Halide Vapors*, P. Davidovits and D. L. McFadden ed., Academic Press, New York (1979).

[16] (a) S. Datz, and R. E. Minturn, J. Chem. Phys. **41**, 1153 (1964). (b) R. E. Minturn, S. Datz, and R. L. Becker, J. Chem. Phys. **44**, 1149 (1966). (c) K. R. Wilson, G. H. Kwei, J. A. Norris, R. R. Herm, J. H. Birely, and D. R. Herschbach, J. Chem. Phys. **41**, 1154 (1964). (d) J. H. Birely, R. R. Herm, K. R. Wilson, and D. R. Herschbach, J. Chem. Phys. **47**, 993 (1967).

[17] (a) D. R. Herschbach, G. H. Kwei, and J. A. Norris, J. Chem. Phys. **34**, 1842

(1961). (b) D. R. Herschbach, Disc. Faraday Soc., 33, 149 (1962).

[18] W. B. Miller, S. A. Safron, and D. R. Herschbach, J. Chem. Phys. **56**, 3581 (1972).

[19] H. F. Davis, A. G. Suits, Y. T. Lee, C. Alcaraz, and J. -M. Mestdagh, J. Chem. Phys. **98**, 9595 (1993), and the references therein.

[20] (a) I. V. Hertel, H. Hofmann, and K. A. Rost, J. Chem. Phys. **71**, 674 (1979). (b) G. Jamieson, W. Reiland, C. P. Schulz, H. U. Tittes, and I. V. Hertel, J. Chem. Phys. **81**, 5805 (1984).

Figure Captions

Figure 1.1 Schematic drawing of the oven assembly for generating the Na/Na_2 beam.

Figure 1.2 The molar fraction of sodium dimer in the sodium vapor as a function of temperature under different pressure of the buffer gas.

Figure 1.3 The partial pressure of sodium dimers as a function of temperature under different pressure of the buffer gas.

Figure 1.4 Newton Diagram for Na(neat) and Ne(neat). Ther numbers mark the velocities for each scattered signal.

Figure 1.5 Time of flight spectra of the elastically scattered Na and Na_2^+ at 40^o off a neat neon beam.

Figure 1.6 Time of flight spectra of the Na^+ and Na_2^+ on the primary beam axis. The slow peak in the Na_2^+ spectrum (indicated by arrow) should be neglected since it is from the field ionization of the Rydberg sodium atoms generated by electron bombardment.

Figure 1.7 Schematic drawing of the rotatable detector. c.c. is the interaction region of the molecular beams. The products pass through a series of defining slits

before they reach the electron bombardment ionization region (1). The ions are then mass selected by the quadrupole mass filter (2) and focused by ion lenses (3) into the Daly ion counter, which houses a high voltage electrode (4) and a scintillator-PMT assembly (5).

Figure 1.8 Flight time of the fragments of CF_2Cl_2 vs. $M^{1/2}$. The slope is the ion flight constant.

Figure 1.9 Flight time of helium, neon, and argon beams vs. the square roots of their masses, plotted for both CW and CCW spinning of the wheel.

Figures

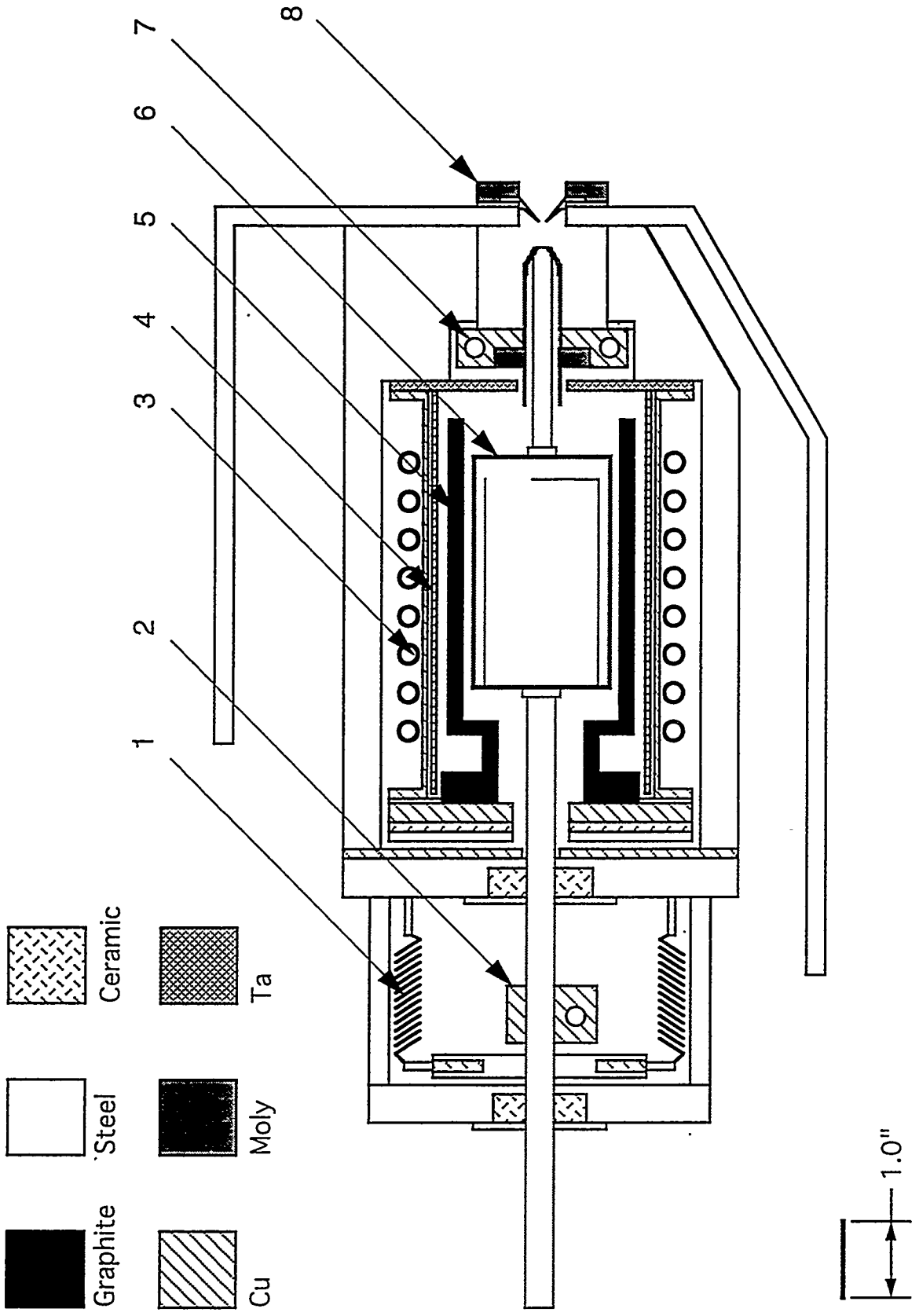

Figure 1.1

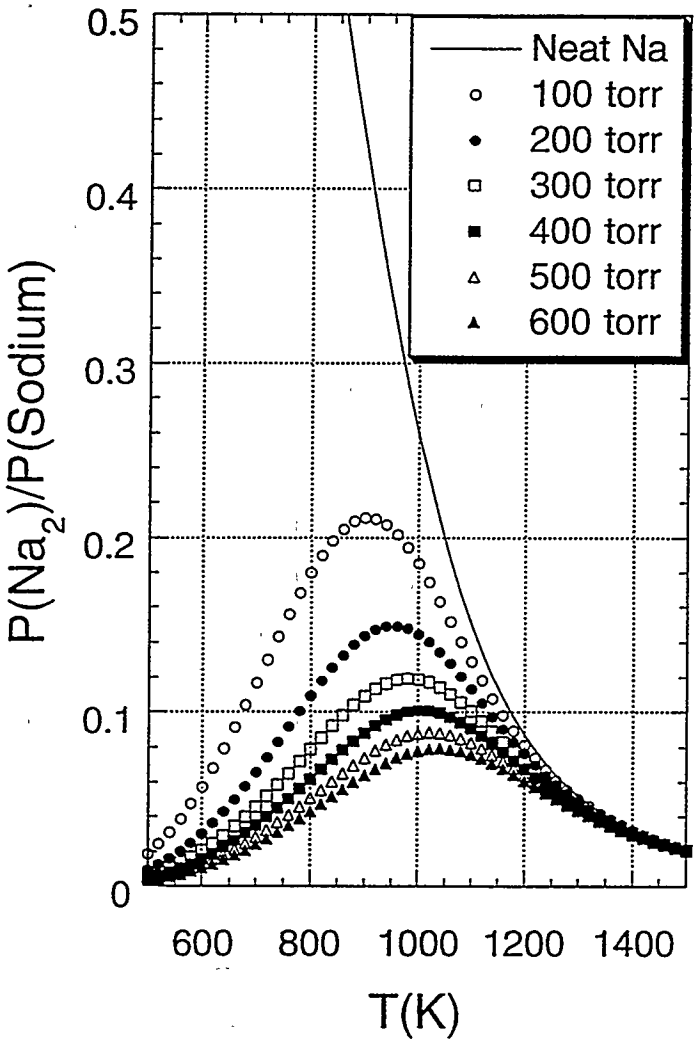
0.5
0.4
0.3
0.2
0.1
0
P(Na2)/P(Sodium)
600
800
1000
1200
1400
T(K)
Neat Na
100 torr
200 torr
300 torr
400 torr
500 torr
600 torr

Figure 1.2

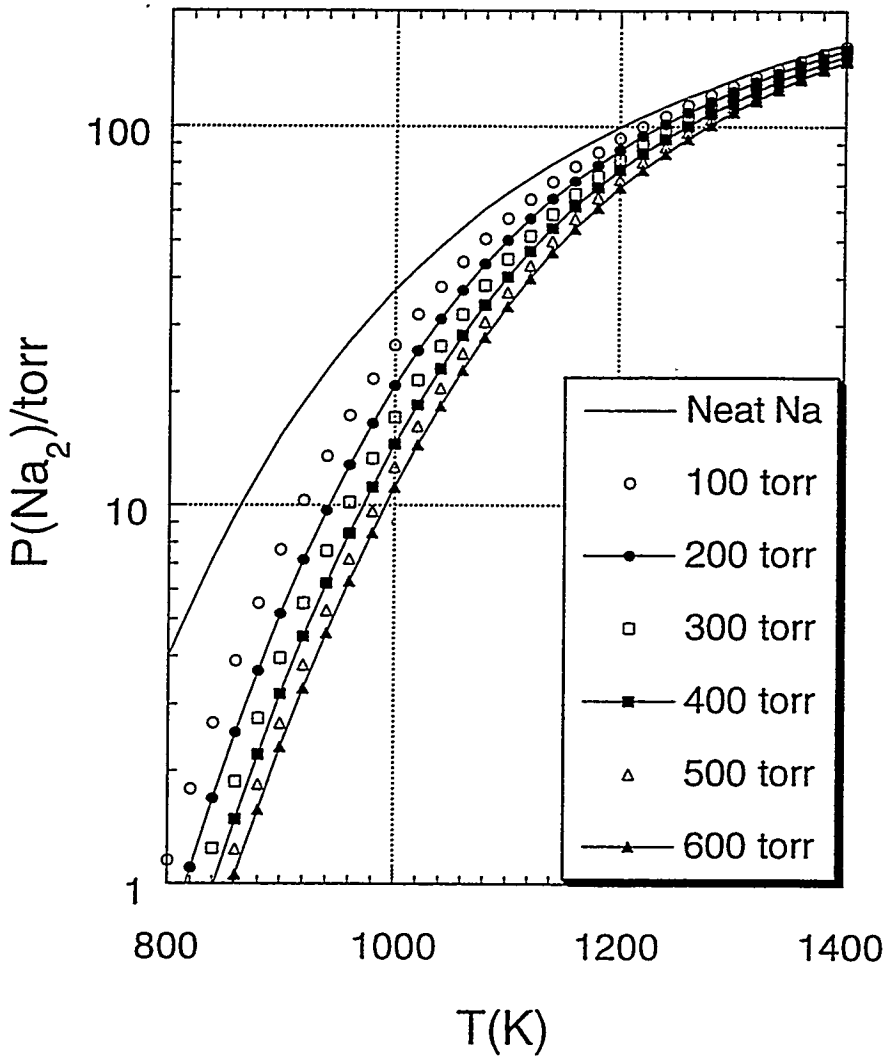
100
10
1
P(Na2)/torr
800
1000
1200
1400
T(K)
Neat Na
100 torr
200 torr
300 torr
400 torr
500 torr
600 torr

Figure 1.3

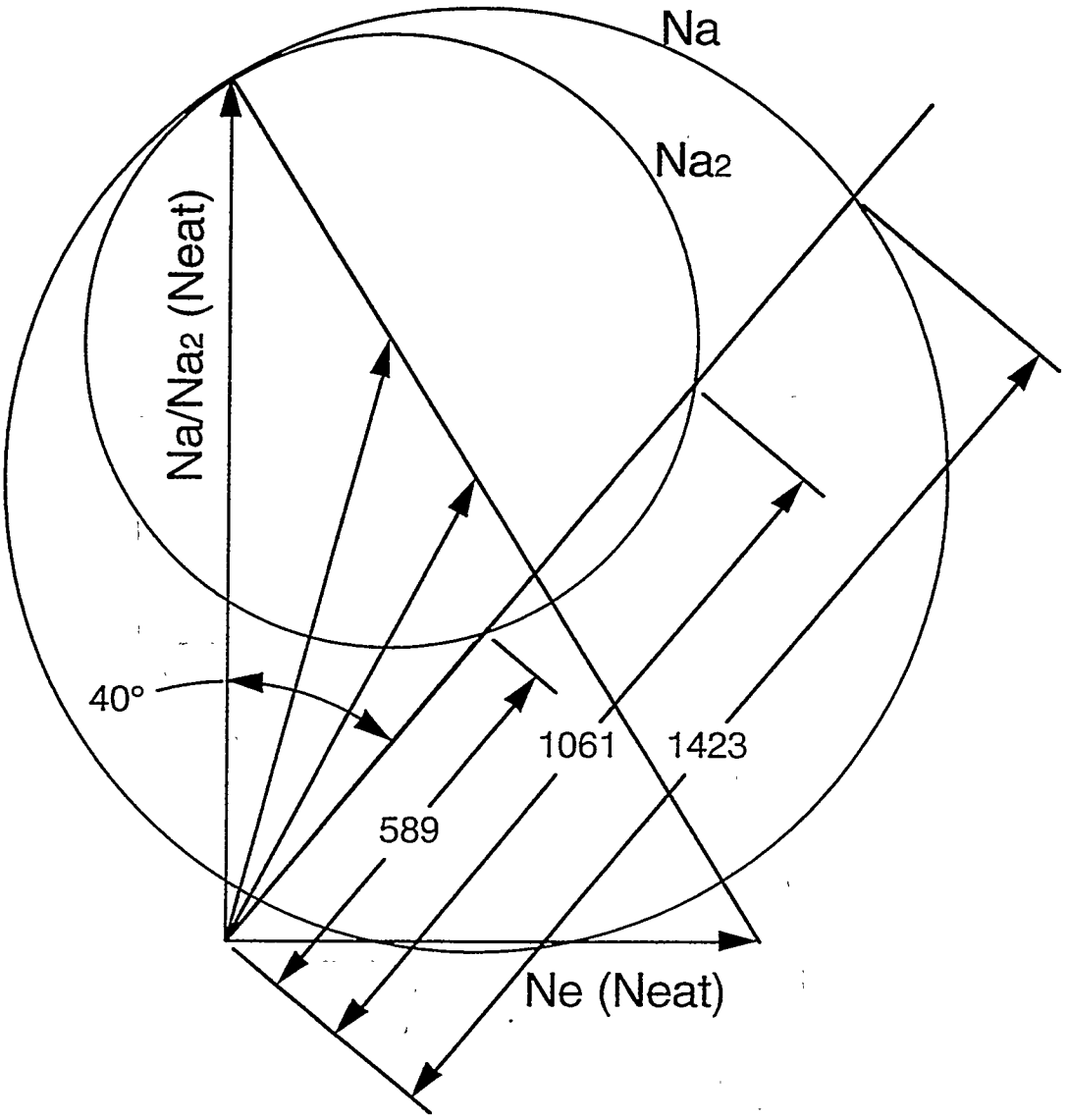

Figure 1.4

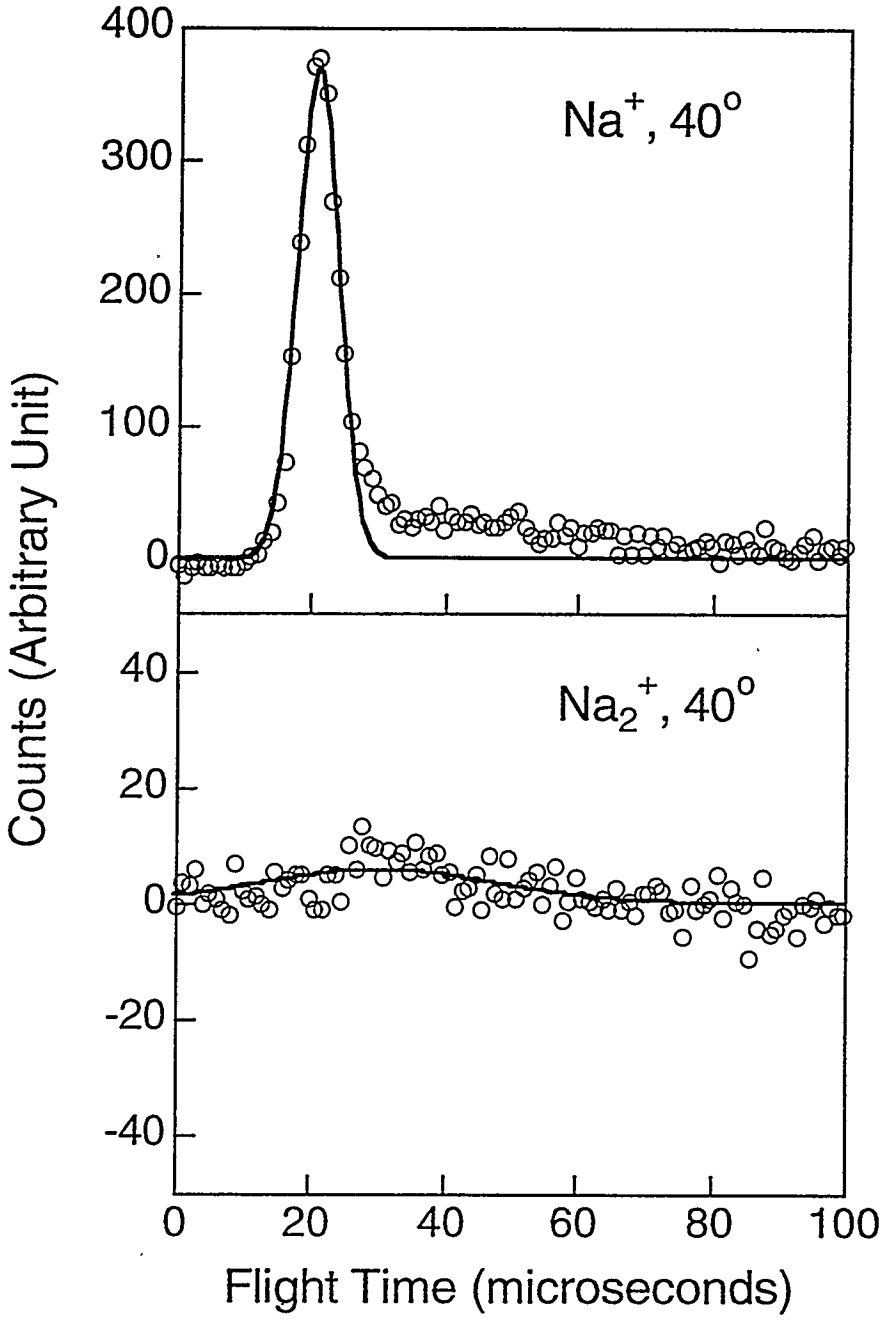
400
300
200
100
0
Na+, 40°
40
20
0
-20
-40
Na2+, 40°
Counts (Arbitrary Unit)
0
20
40
60
80
100
Flight Time (microseconds)

Figure 1.5

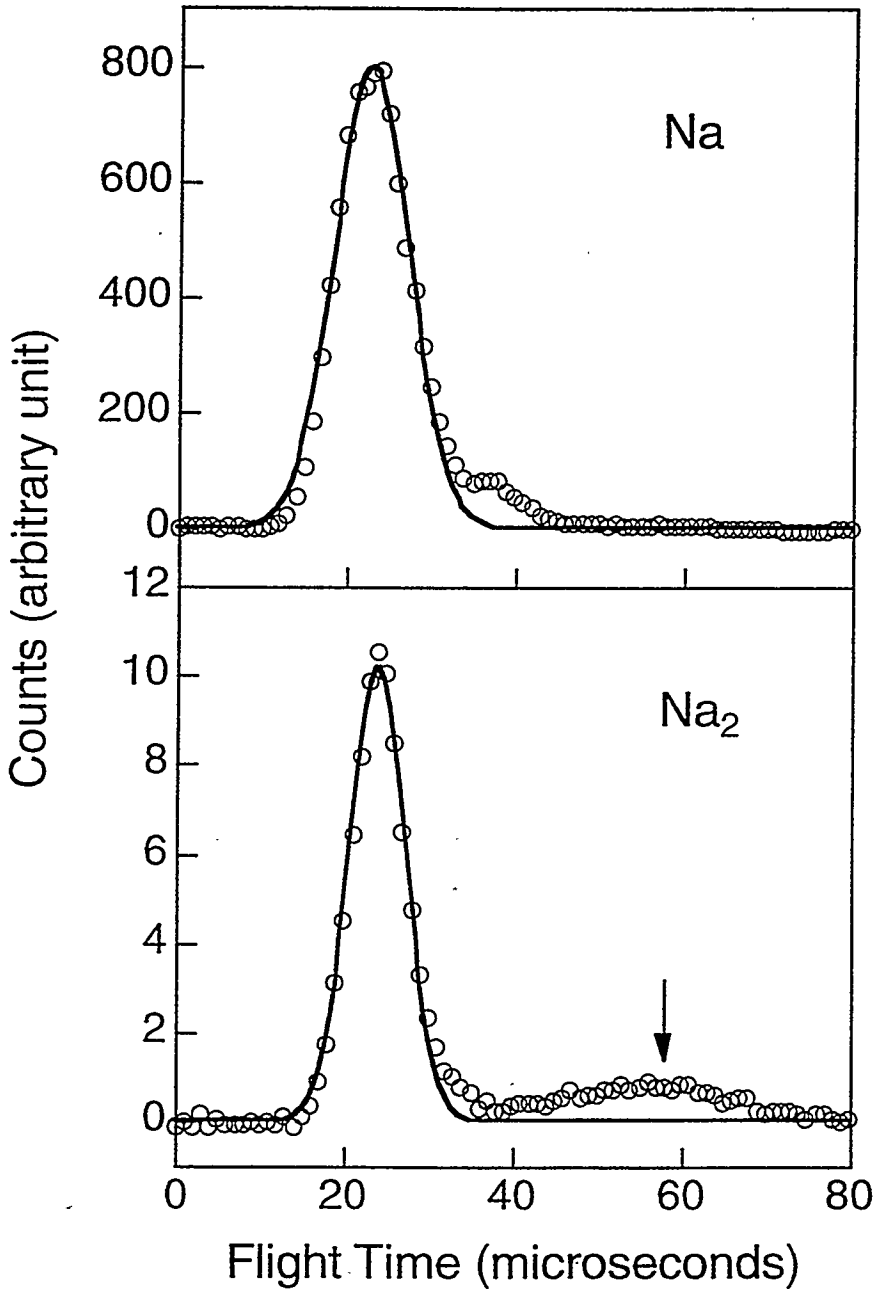
800
600
400
200
0
Na
12
10
8
6
4
2
0
Na_2
0
20
40
60
80
Counts (arbitrary unit)
Flight Time (microseconds)

Figure 1.6

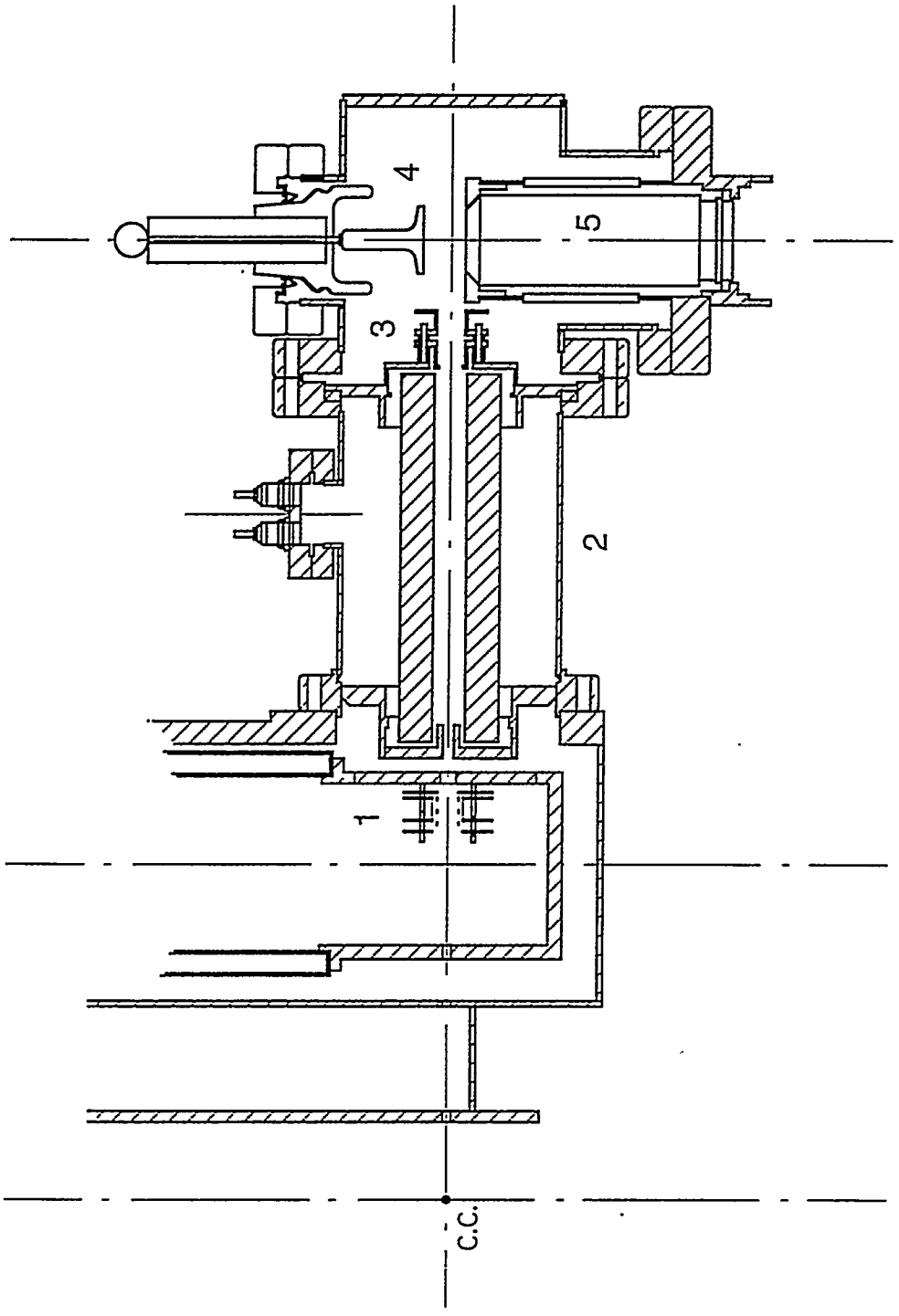

Figure 1.7

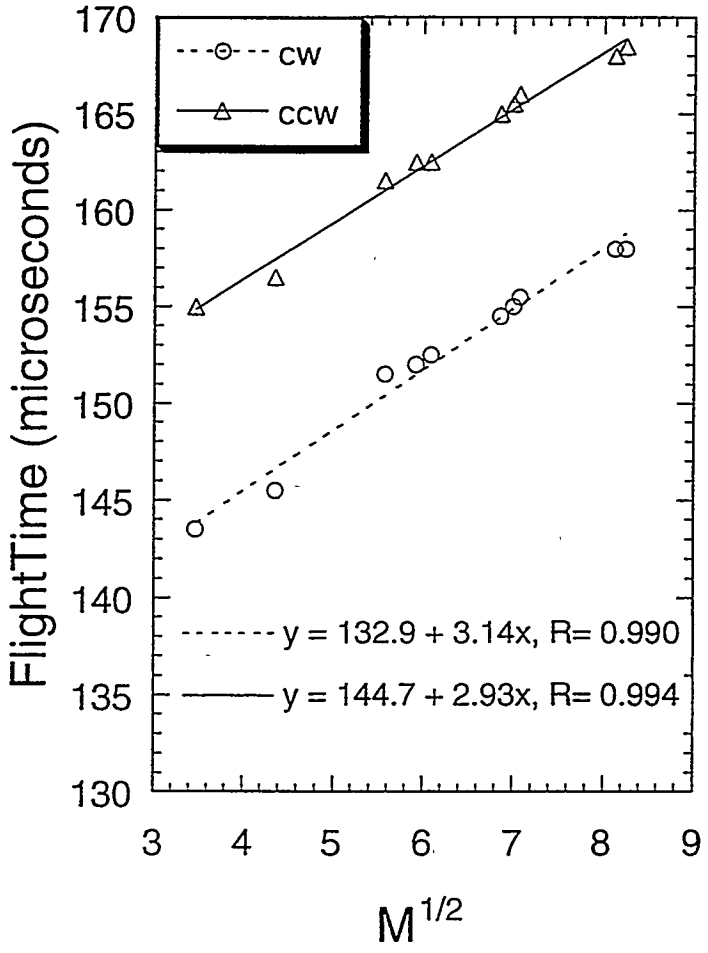
170
165
160
155
150
145
140
135
130
FlightTime (microseconds)
cw
ccw
y = 132.9 + 3.14x, R= 0.990
y = 144.7 + 2.93x, R= 0.994
3
4
5
6
7
8
9
M1/2

Figure 1.8

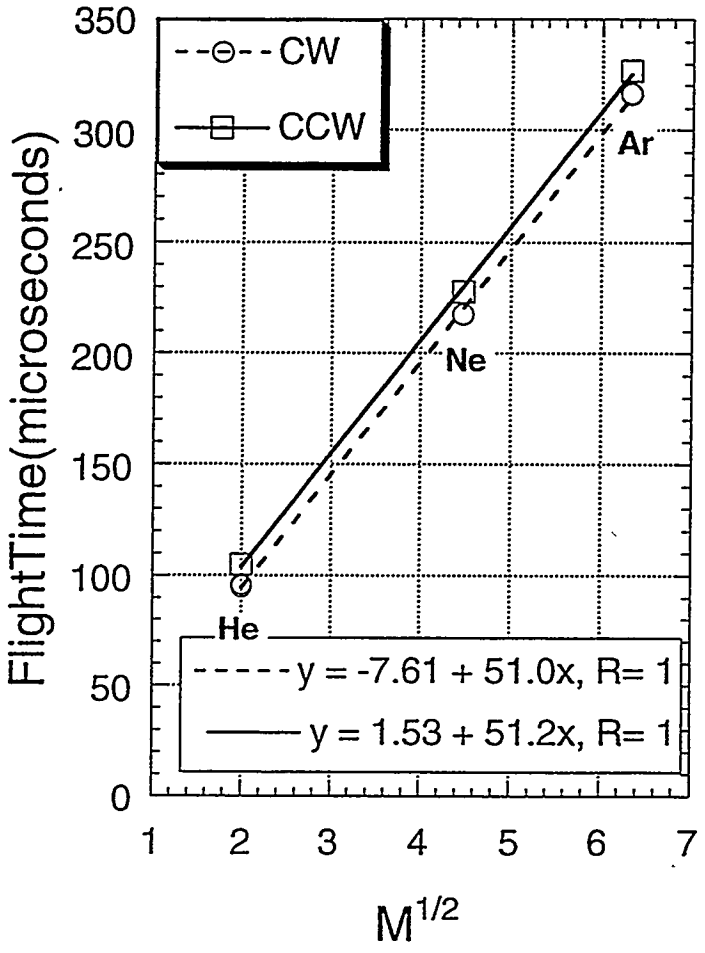
350
300
250
200
150
100
50
0
FlightTime(microseconds)
CW
CCW
Ar
Ne
He
y = -7.61 + 51.0x, R= 1
y = 1.53 + 51.2x, R= 1
1
2
3
4
5
6
7
M1/2

Figure 1.9

Chapter 2

The Reactions of Na_2 with Oxygen Molecules*

Abstract

The reactions of Na_2 with O_2 were studied in a crossed-beam experiment at collision energies (E_c) of 8 and 23 kcal/mol. The formation of NaO_2 + Na was observed at both collision energies, with the angular distributions of NaO_2 in the center of mass coordinates peaking strongly forward with respect to the direction of the O_2 beam, suggesting that the reaction is completed in a time scale that is shorter than one rotational period of the molecular system. From the velocity distribution of the products, we found that the newly formed NaO_2 molecules are internally excited, with less than 20% of the available energy appearing in the translational motion of the separating products. These results indicate a "spectator stripping" mechanism for the reaction, with the O_2 stripping one Na off the Na_2 molecules. At E_c = 23 kcal/mol, the cross section for this reaction channel, σ_{NaO2}, is estimated to be 0.8 $Å^2$. Another reaction channel which produces NaO + NaO was seen at E_c = 23 kcal/mol. The angular distribution for NaO is broad and forward-backward symmetric in the center of mass frame. A substantial fraction of the available energy is released into the relative motion of the products. This reaction is likely to proceed on an excited potential energy surface since a charge transfer to the excited O_2^- orbitals seems necessary for breaking the O-O bond. The measurement yields a bond energy of

---

* This chapter is based on H. Hou, K. T. Lu, V. Sadchenko, A. G. Suits, and Y. T. Lee, in "Gas Phase Chemical Reaction Systems: Experiments and Models: 100 years after Max Bodenstein", edited by G. C. Schatz and H. Volpp, (1996), in press. The experimental work is that of H. Hou, who is the responsible author.

60 kcal/mol for the Na-O molecule, and a total cross section of 2 $Å^2$ for this reaction channel at E_c = 23 kcal/mol.

Introduction

The reactions of alkali metals (M) with oxygen molecules have been studied for decades. In combustion processes, alkali atoms can rapidly form superoxides, MO_2, in an oxygen rich flame through recombination reactions such as $M + O_2 + N \rightarrow MO_2 + N$ (where N is a third body). [1] [2] [3] The knowledge of the rate constants for these reactions and that for the unimolecular decomposition of MO_2 is essential for modelling the kinetics of the combustion processes and calculating the composition of the free radicals in the flame. However, the alkali dimer reactions, which also produce MO_2, were often neglected in kinetics modelling because there was less information for these reactions. Although the concentration of the dimers in a flame is much lower than that of the monomers, it is still appreciable owing to the covalent bonding in the alkali dimer molecules, which is nearly 1 eV in strength. Furthermore, reactions of the dimers could be significant also because they produce MO_2 via direct bimolecular reactions, which is expected to be faster than the three body recombinations between M and O_2. Therefore taking the dimer reactions into consideration could make substantial improvements over the existing kinetics models.

The various collisional processes of alkali atoms with oxygen molecules have been investigated extensively during the past fifteen years, especially the electronic excitations of the alkali atoms $M + O_2 \rightarrow M^* + O_2$ at collision energies of 2 ~ 10 eV. [4] In the Na + O_2 collision, Na D-line fluorescence was observed as the collision energy was increased above the $3P \leftarrow 3S$ excitation energy of 2.1 eV, with its intensity becoming stronger as the

collision energy was increased. The cross section for this process was found to be 26 $Å^2$ at a collision energy of 5 eV. When the collision energy was above 8 eV, fluorescence from higher electronic states appeared. The inelastic scattering experiment of Na(4D) + O_2 carried out in our lab [5] showed that the translational energy of the reactants could effectively promote Na to long-lived Rydberg states ($\tau \geq 320$ μs). Kleyn and coworkers carried out landmark investigations of the charge transfer processes $M + O_2 \rightarrow M^+ + O_2^-$ at collision energies ranging from 4 to 2000 eV. [6] [7] In their experiment, the relative velocity of the reactants was so fast that the "collision time" was comparable with the vibrational period of the O_2^- ($\omega_e = 1089\ cm^{-1}$) [8]. Because the electron transfer probability and the critical distance vary strongly as a function of the internuclear distance of O_2^-, these authors observed oscillations in the differential cross sections. These results clearly demonstrate that the measurements of angular distributions of the scattered molecules reveal not only the average lifetime of the collision complexes using the picosecond rotational period as an inherent clock, but also, in the cases of charge transfer, the vibrational motions of the reaction intermediates on the time scale of ~100 femtoseconds. In all these processes mentioned above, charge transfer from alkali metal to O_2 molecules was undoubtedly the essential first step to account for the change of the electronic states of the alkali atoms in these experiments; and the behavior of the ionic intermediate $M^+O_2^-$ determines the outcome of the scattering. The chemical reaction $M + O_2 \rightarrow MO + O$ however, was not seen in the previous studies.

Alkali dimers have many interesting properties [8] [9] [10] that make their chemistry unique. The ionization potentials of the dimer molecules are lower than those of the corresponding monomers such that when dimers interact with electron accepting molecules, the

ionic and covalent potential energy surfaces cross at larger intermolecular distances, which could strongly affect the charge transfer probabilities and the overall reaction cross sections. The bond lengths of M_2 and M_2^+ are extraordinarily long (e. g. 3.0 Å for Na_2, 3.5 Å for Na_2^+) and although the bond length of M_2^+ is longer, the bond dissociation energy of M_2^+ ion is ~50% higher than those of M_2 neutrals. The covalent bonds of the alkali dimers are abnormally weak, with the bond dissociation energies lower than 1 eV, making many chemical reactions involving the cleavage of the alkali dimer bonds exoergic.

Figger and coworkers [11] observed chemiluminescence in their crossed-beam experiment of alkali metal dimers with oxygen molecules. In the reactions of Cs_2, Rb_2, K_2 and Li_2, D-line emission as well as continuous chemiluminescence from the collision zone were recorded. They attributed this emission to the formation of electronically excited products from the reactions $M_2 + O_2 \rightarrow MO_2 + M^*$ and $M_2 + O_2 \rightarrow MO_2^* + M$. No emission was observed for the Na_2 reactions due to their lower exothermicities.

Very recently, Goerke and coworkers [12] reported the results of their studies on the reactions of sodium clusters with oxygen molecules using photoionization and ion time-of-flight as detection methods. $Na_nO(2 \le n \le 4)$ and $Na_mO_2(2 \le m \le 6)$ products were detected for the reactions of $Na_x(3 \le x \le 8)$ with O_2. Angular distributions of $Na_nO(2 \le n \le 4)$ and $Na_mO_2(2, 3, 5)$ showed strong forward scattering with respect to the sodium cluster beam in the center of mass frame. Although the energy distributions of the products were not measured, their experimental data suggested that most of the exothermicity remained in the internal degrees of freedom of the products. The cross sections for the reactions were determined to be 50 ~ 80 $Å^2$, which led to their conclusion that electron harpoon-

ing [13] [14] [15] [16] was the first step in the course of the reactions. However, these authors did not include Na_2 reactions in their considerations. Due to the high ionization potential of NaO and NaO_2 they were not able to detect these molecules with the photon energy used in their experiments, although the presence of these molecules was almost certain.

This chapter presents our results from crossed-beam studies of the reactions of sodium dimers with oxygen molecules. For this seemingly simple chemical system, there are at least four distinct reaction pathways that were energetically accessible under our experimental conditions:

$$Na_2 + O_2 \rightarrow NaO_2 + Na, \quad \text{(i)}$$

$$Na_2 + O_2 \rightarrow Na_2O + O, \quad \text{(ii)}$$

$$Na_2 + O_2 \rightarrow NaO + NaO, \quad \text{(iii)}$$

$$Na_2 + O_2 \rightarrow Na + Na + O_2. \quad \text{(iv)}$$

The energetics for these reactions [8] [9] [10] are plotted in Figure 2.1. Reaction (i) is the only exothermic reaction and it becomes Reaction (iv) in the case when the internal excitation of NaO_2 along the $Na–O_2$ bond exceeds its dissociation limit. In our experiment, we measured the angular and velocity distribution of the products at two collision energies, which enabled us to identify the important reaction channels and learn the dynamics underlying these molecule-molecule collision processes.

Experimental

The details of the crossed-beam apparatus used in our experiment can be found in many earlier publications. [17] [18] Briefly, the primary source generates a supersonic beam of sodium vapor/inert gas mixture. Either helium or neon were used as the carrier gas. The Na_2 concentration was about 5% molar fraction of the total sodium in the beam

when He was used as carrier gas. No substantial amount of trimers or larger clusters was detected under our experimental conditions. The Na_2 beam was crossed at 90° by a neat oxygen supersonic beam in the main collision chamber under single collision conditions. The O_2 source nozzle was heated to 473°K to prevent cluster formation. At this temperature, the fraction of O_2 in the v = 1 (ω_e = 1580 cm^{-1}) state is less than 1% assuming insufficient cooling during the expansion. Both sources were doubly differentially pumped. The beams were skimmed and collimated to 2° FWHM in the collision chamber. Under these conditions, the collision energies for the reaction could be varied from 8 kcal/mol to 23 kcal/mol. The rotatable detector used in this experiment was described in the previous chapter. Under our experimental conditions, we were unable to measure the signal close to the Na_2 beam. At these angles, the number density of elastically scattered Na was very high such that a certain fraction of scattered Na could be excited to long-lived Rydberg states by electron bombardment and subsequently field-ionized in the ion counting region. The mass spectrometer was "transparent" to these Rydberg atoms so they produced strong interference at all the masses of interest. We also recorded the spectra for O and O_2 but the effort to extract any information related to these reactions was not successful because of the high background of oxygen in the mass spectrometer and the intense nonreactive scattering of the O_2.

Results and Kinematic Analysis

In our experiment, we observed an NaO^+ (m/e = 39) signal which was unambiguously from the reactive scattering since it contains both Na and O. The monomer reaction $Na + O_2 \rightarrow NaO + O$ has very large endothermicity (ΔD_0 = + 58 kcal/mol [9]). Under our experimental conditions, even the highest collision energy for $Na + O_2$ was not sufficient

for this reaction. Thus the observed NaO^+ signal must be from the reactions of sodium dimers with oxygen molecules. This result is in contradiction with that reported by Goerke et al. [12] who explicitly ruled out the possibility of the dimer reactions in their similar experiment. Neither NaO_2^+ nor Na_2O^+ signal was seen under our experimental conditions. However this does not necessarily mean that only Reaction (iii) took place. In the ionization region, electron impact fragmentation is severe, especially for the internally excited molecules. Both NaO_2 from Reaction (i) and Na_2O from Reaction (ii) could fragment completely and both molecules could form NaO^+. Additional analysis on the kinematics and dynamics of the reactions have to be made in order to identify the actual reaction pathway(s).

Collision Energy at 8 kcal/mol

The Newton diagram [19] [20] [21] for $Na_2 + O_2$ at a nominal collision energy of 8 kcal/mol is shown in Figure 2.2. Θ_{CM} denotes the laboratory angle of the center of mass velocity vector for $Na_2 + O_2$. For future discussion, we also plot the center of mass velocity (dotted line) for $Na + O_2$, which extends an angle of Θ_m from the Na_2 beam. The direction of the Na_2 velocity in the center of mass frame is defined as 0^o hereafter. At this collision energy, only Reaction (i) could take place, so the observed NaO^+ signal was entirely due to the fragmentation of NaO_2 products. The solid circle in Figure 2.2 encloses the zone within which NaO_2 might appear. Figure 2.3 shows the NaO^+ time-of-flight spectra recorded at several laboratory angles. Beyond the range of these angles, the signal became too weak to observe the time-of-flight peaks. It was observed that most NaO_2 products appeared around Θ_m. Signal intensities obtained by integrating the time-of-flight spectra are plotted in Figure 2.4 to give the laboratory angular distribution for

NaO_2. Compared with the range of the NaO_2 circle in the Newton diagram, the NaO_2 angular distribution was very narrow.

In Figure 2.3 and Figure 2.4, the solid lines are the computer simulation of the data obtained by assuming the center of mass translational energy distribution (P(E)) and angular distribution ($T(\theta)$) shown in Figure 2.5. Peaking in the direction of the O_2 beam (180^o), the angular distribution shows remarkable anisotropy, with all the NaO_2 products scattered into the hemisphere toward the O_2 beam. This anisotropy indicates that the reaction takes place during a time that is shorter than the rotational period of the molecular system so that the products are separated before they lose the information of the well defined approaching direction of the reactants. [21] At this collision energy, the total available energy for the reaction ($E_c + \Delta D_0$) is 34 kcal/mol, of which only an average of 2.6 kcal/mol appears in the translational motion of the products (cf. P(E) in Figure 2.5). The rest of the energy has to become the internal excitation of the NaO_2 molecules. When NaO_2 is ionized to form NaO_2^+, the binding energy between Na^+ and O_2 becomes weaker and the internal excitation initially stored in NaO_2 is likely to remain in NaO_2^+ and causes the complete dissociation of NaO_2^+ into Na^+ and O_2. This is probably the reason why the NaO_2^+ parent ion was not detected. However when NaO_2 is excited to higher electronic states during electron impact ionization, the dissociative ionization can produce a stable NaO^+ ion.

Collision Energy at 23 kcal/mol

All the dimer reactions (i) – (iv) became energetically accessible at a collision energy of 23 kcal/mol. The Newton diagram for this collision energy is shown in Figure 2.6. For Reaction (ii), the available energy was only 5 kcal/mol. The heavier products

Na_2O (compared with O) have to be limited in the small circle. On the other hand, NaO molecules produced by Reaction (iii) are much less confined because there is slightly more available energy (9 kcal/mol) and no disparity in the masses of the products. The time-of-flight spectra of NaO^+ recorded at different laboratory angles are plotted in Figure 2.7, and the laboratory angular distribution of the NaO^+ intensity is shown in Figure 2.8. There are clearly two features in the time-of-flight spectra. Both features exist well out of the Na_2O limit which indicates clearly that the observed signal was not from Reaction (ii). The slow peaks which appear at ~120 μs have a very narrow angular distribution, with the intensity peaking sharply around Θ_m. The angular and velocity distributions of this slow signal bear such strong resemblance to those of the NaO_2 products we saw at low collision energy that we can with little doubt assign this signal to the same reaction channel. The fast peaks, arriving at ~70 μs, have very different characteristics than those of the NaO_2 products. Appearing weak at all angles and becoming only slightly stronger at small angles, these fast peaks have much less variation in intensity, an indication of products with larger recoil velocities and broader laboratory angular distributions. Therefore this fast signal is, without any doubt, the NaO products from Reaction (iii).

The simulation of the time-of-flight and angular distribution data was done by assuming an independent set of P(E) and $T(\theta)$ for each reaction channel. An additional parameter γ was assigned to each reaction channel to weight its contribution to the observed signal. The total fits are plotted as solid lines in Figure 2.7 and Figure 2.8. The dotted lines and the dashed lines show the contributions from Reaction (i) and Reaction (iii), respectively. Figure 2.9 shows the P(E) and $T(\theta)$ for Reaction (i). As mentioned above, these distributions are similar to those at low collision energy. $T(\theta)$ again peaks

sharply at the direction of O_2 beam with all the NaO_2 scattered into the O_2 hemisphere, showing strong anisotropy. Among the 49 kcal/mol available energy, only an average of ~8 kcal/mol was released into the translational energy of the separating products. The P(E) had a sharp rising edge at ~7 kcal/mol, which indicates that the internal energy of NaO_2 could not exceed 42 kcal/mol or else the NaO_2 molecule could not be held together. The subsequent result is the collisional dissociation making Na + Na + O_2. Therefore this sharp rising edge in P(E) marks the onset of Reaction (iv), which requires at least the energy to break the Na-Na bond. The collision energy of 23 kcal/mol less the cut off energy of 7 kcal/mol in the P(E) is then our experimental measurement of the Na-Na bond dissociation energy. This result of 16 kcal/mol is in agreement with the well known value in the literature. [9]

Figure 2.10 shows the P(E) and T(θ) used in the simulation of Reaction (iii). The angular distribution is quite broad. The forward-backward symmetry in the product angular distribution is a prerequisite rather than an experimental result because in this reaction two identical molecules are always produced with exactly opposite center of mass velocities. Under such conditions the angular distribution does not tell us the time duration of the reaction, which is the important information for dynamics studies. The P(E) distribution shows that an average of 3 kcal/mol is released in the translational motion of the products. The high energy cut off at 5.5 kcal/mol in P(E) allows us to estimate Na-O bond strength. From conservation of energy, there is the following relation between the energies of the reactants and the products:

$$E'_{trans} + E'_{int} = E_{trans} + E_{int} + \Delta D_0, \qquad (2.1)$$

where E_{trans} and E'_{trans} are the center of mass translational energies of the reactants and

products, respectively. Similarly, E_{int} and E'_{int} are the internal energies, i.e. the total electronic, vibrational and rotational energies, in the reactants and the products, respectively. ΔD_0 is the change of the bond dissociation energy for the reaction. E_{int} is assumed to be negligible for the supersonic beams. E'_{trans} reaches its maximum value when E'_{int} is a minimum, which will be assumed to be zero. Namely at the highest translational energy release, both NaO products are assumed to be in the ground state. From Equation (2.1) and the maximum translational energy release in P(E), we calculated the change of bond dissociation energy ΔD_0 for Reaction (iii) to be -17 kcal/mol. Using the accurately known values of D_0(O-O), 119 kcal/mol, and D_0(Na-Na), 18 kcal/mol, [9] we obtained D_0(Na-O) = 60 kcal/mol, which can be compared with the literature value of 61.2 ± 4.0 kcal/mol. [9]

From the best fit, the relative contributions of these two reactions to the observed signal at m/e = 39 are:

$$\gamma_i : \gamma_{iii} = 1 : 1.8. \qquad (2.2)$$

In Equation (2.2), we use the subscripts to denote the reaction channels.

In order to estimate cross sections for the reactions, we also measured time of flight spectra for the Na^+ signal under the same experimental conditions. It is known that both NaO and NaO_2 dissociate heavily to Na^+ under electron impact. [22] [23] The collisional dissociation Reaction (iv), if present, would also generate Na^+. But most Na^+ detected came from elastic/inelastic scattering of the Na monomer with O_2 because the number density of the monomers at the collision zone was roughly 20 times higher than that of the dimers. Na^+ time-of-flight spectra at 25° and 30° are given in Figure 2.11. At these angles, nonreactive scattering of Na_2 was negligible. For comparison, the scattering signal of Na from N_2 at corresponding angles was also measured and is plotted in the same

figure. The differences due to the reactions are obvious. We can fit the Na^+ spectra for $Na/Na_2 + O_2$ scattering with four different channels: the elastic scattering from $Na + O_2$, the inelastic scattering from $Na + O_2$, Reaction (i) from $Na_2 + O_2$ and Reaction (iii) from $Na_2 + O_2$. We use the same translational energy and angular distributions as those for the NaO^+ signals to fit the reactive signals in the Na^+ spectra although we have to use different weights (γ') to account for the different fragmentation patterns of NaO and NaO_2 in the ionization region. The results are also plotted in Figure 2.11, where the solid lines show the overall fit and the broken lines indicate the contribution from individual channels, as described in detail in the figure captions. The discrepancies between the fit and the data are possibly due to the collisional dissociation Reaction (iv), which is difficult to account for because it is a three body event. Nevertheless, leaving Reaction (iv) out will not affect our final results of obtaining the cross sections for Reaction (i) and Reaction (iii) because we are comparing these reaction channels with the nonreactive signal only. From the fit, the relative weight for each channel is:

$$\gamma'_{elastic} : \gamma'_{inelastic} : \gamma'_{i} : \gamma'_{iii} = 105 : 171 : 0.5 : 3.0. \qquad (2.3)$$

Because we did not observe any NaO_2 signal, it is safe to assume that NaO_2 molecules, if ionized, dissociated completely to either NaO^+ or Na^+. Figure 2.12 illustrates the relations between the parent molecules directly from the scattering and the measured signal, which will serve as a road map for our discussions in the following sections. Here σ_i and σ_{iii} are the reaction cross sections for Reaction (i) and Reaction (iii), respectively. $\sigma_{elastic}$ and $\sigma_{inelastic}$ are the cross sections for the elastic scattering and the inelastic scattering of $Na + O_2$. $\sigma_{ion}(X)$ denotes the ionization cross section of molecule X by electron bombardment. The ions so formed undergo further dissociation to give the observed sig-

nal. We define ξ as the fraction of NaO^+ among the total Na-containing positive ions produced by electron bombardment. According to the assumption that NaO_2 dissociate completely upon electron bombardment, the fraction of Na^+ from NaO_2 is $(1-\xi)$. In a similar way, we define the fraction of Na^+ among the total Na-containing positive ions produced from ionization of NaO products to be η. Accordingly the branching ratio between Reaction (i) and Reaction (iii) can be obtained. From Equation (2.2), we have:

$$\gamma_i : \gamma_{iii} = [\sigma_{ion}(NaO_2)\times\sigma_i\times\xi] : [2\times\sigma_{ion}(NaO)\times\sigma_{iii}\times(1-\eta)] = 1 : 1.8. \qquad (2.4)$$

The factor "2" accounts for the fact that two NaO were produced in Reaction (iii). Similarly, from Equation (2.3), we draw another relation between σ_i and σ_{iii}:

$$\gamma'_i : \gamma'_{iii} = [\sigma_{ion}(NaO_2)\times\sigma_i\times(1-\xi)] : [2\times\sigma_{ion}(NaO)\times\sigma_{iii}\times\eta] = 0.5 : 3.0. \qquad (2.5)$$

In order to compare the cross section for each channel, we need the ionization cross sections for Na, NaO and NaO_2 by 200 eV electron bombardment. The ionization cross section of Na is known [24], $\sigma_{ion}(Na) = 2.46$ Å^2. The ionization cross section of NaO can be estimated [25] from the ionization cross section of O_2, and the ratio of the polarizabilities(α's) of O_2 [9] and NaO using the following equation:

$$\sigma_{ion}(O_2) : \sigma_{ion}(NaO) = \alpha_{O2} : \alpha_{NaO} = 1.58 : 3.05, \qquad (2.6)$$

where α_{NaO} was obtained by adding the polarizability of Na^+, $\alpha_{Na+} = 0.155$ Å^3, and the polarizability of O^-, $\alpha_{O-} = 2.85$ Å^3. The result is $\sigma_{ion}(NaO) = 5.2$ Å^2. Similarly, we can calculate the ionization cross section for NaO_2, which gives $\sigma_{ion}(NaO_2) = 6.5$ Å^2.

Covinsky [22] measured η as a function of internal excitation of NaO in the Na + O_3 experiment. η is roughly 0.8 for internally cold NaO (which was the case in this experiment because there is very little excess energy for Reaction (iii) and a considerable amount of this excess energy was released into the translational motion of the products).

Using this value, we obtained $\xi = 0.45$ and $\sigma_i : \sigma_{iii} = 1 : 2.5$.

The next step is to compare the reactive signal with the total nonreactive scattering. From Equation (2.3), we have the following relations:

$$\frac{\gamma'_i}{\gamma'_{elastic} + \gamma'_{inelastic}} = \frac{\sigma_{ion}(NaO_2) \times \sigma_i \times (1-\xi)}{20 \times \sigma_{ion}(Na) \times \sigma_{Nonreactive}} = \frac{0.5}{276} \quad , \qquad (2.7)$$

and

$$\frac{\gamma'_{iii}}{\gamma'_{elastic} + \gamma'_{inelastic}} = \frac{2 \times \sigma_{ion}(NaO) \times \sigma_{iii} \times \eta}{20 \times \sigma_{ion}(Na) \times \sigma_{Nonreactive}} = \frac{3.0}{276} \quad , \qquad (2.8)$$

where $\sigma_{Nonreactive}$ is the sum of the cross sections of elastic scattering and inelastic scattering of Na + O_2. We added factors "20" in Equation (2.7) and Equation (2.8) because the number density of the monomers in the collision zone was roughly 20 times higher than that of the dimers. The interaction between Na monomer and O_2 becomes strong at the crossing of the covalent and ionic surfaces because of the charge transfer. If we neglect the long range van der Waals interaction, the internuclear distance at the surface crossing can be estimated using the following equation which is based on the simple "Harpoon Mechanism": [13] [14] [15] [16]

$$R_c = \frac{14.4}{IP_{Na}(eV) - EA_{O_2}(eV)} \qquad (Å), \qquad (2.9)$$

where IP is the ionization potential of Na [9] and EA is the electron affinity of O_2 [9], both in electron-volts. Equation (2.9) gives a value of 3.1 Å for R_c, which is larger than the averaged hard sphere radius between Na and O_2. Since there is no reaction between Na monomer and O_2, we can assume R_c to be the nonreactive collision radius. Therefore we obtain the total nonreactive scattering cross section to be: $\sigma_{Nonreactive} = \pi R_c^2 = 30$ Å^2. Using these numbers in Equation (2.7) and Equation (2.8), we obtain the cross sections for

Reaction (i), $\sigma_i = 0.8$ Å^2 and Reaction (iii), $\sigma_{iii} = 2$ Å^2.

Discussion

The MO_2 molecules have been studied quite extensively in the past. Alexander generated semiempirical potential energy surfaces for LiO_2 and NaO_2. [26] He showed that the ground state NaO_2, which was 1.6 eV more stable than the separated ground state Na and O_2, had C_{2v} geometry with Na at the apex of an isosceles triangle. The interaction within the molecule could be best described as $Na^+...O_2^-$ singly charged ionic bonding. This is in accord with the Infrared and Raman [27] [28] or ESR [29] spectroscopy results in low temperature matrices. Calculations of the NaO molecule also indicates that it is singly ionic, $Na^+...O^-$. [30] These results suggest that during the course of Reaction (i) and Reaction (iii), the $Na_2 + O_2$ system has to experience a change from covalent to ionic character. This resembles the well known M/M_2 + Halogen molecules (XY) reactions and was commonly characterized by the Harpoon Mechanism. Nevertheless, the $Na_2 + O_2$ reaction shows very different results than the M/M_2 + XY system. In the case of M_2 + XY, [31] for example, the main pathways have both M_2 and XY dissociate to form MX + M + Y or MX + MY with the total cross sections larger than 100 Å^2. For the MX + M + Y channel, the MX product peaked strongly toward the M_2 direction in the center of mass velocity space.

M_2 + XY reactions are model systems that proceed via a long range electron transfer mechanism. Due to the low ionization potential of M_2 and high electron affinity of XY, the potential energy surfaces of the ionic state ($M_2^+...XY^-$) and the covalent state ($M_2...XY$) intersect at intermolecular distance R_c = 7-8 Å (Equation (2.9)) which is much larger than the "hard sphere" radius. At this internuclear distance, there is a fair chance for the valence electron to "jump" from M_2 to the XY. A vertical ionization from the outer

turning point of ground state M_2 puts M_2^+ in the attractive well and vertical ionization from the inner turning point sets M_2^+ on the slightly repulsive (1 eV/Å) surface. Because M_2^+ is almost 50% more strongly bound than M_2, [10] along with the fact that both M_2 and M_2^+ have very low vibrational frequencies, the two alkali nuclei will separate only very slowly after electron transfer. On the other hand the XY^- bonding is much weaker than that of XY neutral molecule. A vertical Frank-Condon transition puts XY^- on a very strong repulsive wall (6 eV/Å) above its dissociation limit, primarily due to the strong antibonding orbital σ_{pz}*. As a result, X^- and Y separate promptly after the vertical electron transfer while the M and M^+ will linger together for a longer time. The reaction proceeds as if the M_2^+ "strips" the X^- off to form the M_2X molecules, which peak preferentially towards the M_2 direction, leaving the other halogen atom Y as a "spectator". The highly vibrationally excited M_2X nascent molecule then boils off an M atom to form the final MX product. The initial repulsive force between the two halogens is offset by their attraction at longer distance as the two halogen atoms separate. Consequently, the spectator Y does not carry away much of the excess energy.

For the $Na_2 + O_2$ system, the scenario is quite different. O_2 has the much lower electron affinity of 0.44 eV [9] so that the nominal crossing distance R_c calculated from Equation (2.9) is only 3.2 Å and only collisions with impact parameter smaller than R_c will experience the electron transfer. This limits the total cross section for charge transfer to 32 $Å^2$ at most. Nevertheless, at such short intermolecular distance, the interaction between the ionic surface and the covalent surface is very strong. Once the system arrives at this region, it will have almost unit probability to switch adiabatically from covalent surface to ionic surface. The final outcome of the reaction is determined by the interaction

between Na_2^+ and O_2^- after electron transfer. Unlike the case of XY, the O_2^- bond is only slightly longer than that of O_2 and the binding energy is almost as large. A vertical transition from O_2 to the ground state of O_2^- would put O_2^- in a deep potential well. It takes some extra 90 kcal/mol in order to break O_2^- to form $O + O^-$. On the other hand, the weakly bound Na_2^+ is much more vulnerable to dissociate into $Na + Na^+$ under the influence of the strong Coulomb attraction. In the case when the impact parameter is large, there is little chance to cleave the O_2^- molecule during the time when two molecules glance off each other. The strong Coulomb interaction between Na^+ and O_2^- leads to the formation of NaO_2 molecules that are highly excited along the newly formed bonds. The departing Na atom should hardly be affected during the collision because the interaction between Na^+ and Na is relatively weak compared with the Coulomb interaction between Na^+ and O_2^-. Therefore it acts similarly as a "spectator" in the case of the halogen reactions. The most important role for this Na atom is to carry away excess energy partly through breaking of the Na-Na bond, much like a "third body" as in the recombination reactions, which is the reason why the NaO_2 products are most likely to appear at Θ_m — the result is just like a simple recombination of Na and O_2. Using this "spectator stripping" model, we calculate the translational energy releases for E_c = 8 and 23 kcal/mol to be 2.4 and 6.6 kcal/mol, respectively, matching well with the peaks in the corresponding P(E)'s.

It is worth pointing out that the formation of NaO_2 results from the transfer of only one electron from Na_2 to O_2. If both valence electrons are transferred to O_2, the molecular system is likely to sample the deep well on the potential energy surface, forming the Na_2O_2 complex (cf. Figure 2.1). Since the Na_2O_2 complex dissociates mainly through the

low energy channel, forming NaO_2 + Na, we would expect to see for the NaO_2 products a forward-backward symmetric angular distribution, which is a characteristic of the complex formation. However, in the experiments we observe a very anisotropic angular distribution. Therefore complex formation mechanism can be excluded.

Contrary to the spectator mechanism of Reaction (i), Reaction (iii) requires considerable rearrangement of the electronic configuration of the system. First of all, both valence electrons have to be transferred because each NaO molecule has $Na^+...O^-$ singly ionic character. This requires a close collision and a favorable approaching geometry between the reactants. This was not directly observed for this reaction because the symmetric angular distribution determined by the kinematics does not provide us much information on the scattering. But evidence could be found from the chemi-ionization reaction $Ba + Cl_2 \rightarrow BaCl^+ + Cl^-$ in which case $BaCl^+$ is backward scattered with respect to the Ba beam, demonstrating that the favored geometry for transferring two electrons is a collinear head-on collision. [33] Second, the strong O-O bond has to be broken. The exact pathways leading to the breaking of the O-O bond could not be deduced from our data, but some insights could be gained by looking at early results of dissociative attachment of O_2, and the results of our recent *Ab initio* calculations [34] using *Gaussian 92* . The formation of O + O^- by electron attachment was studied in great detail and a single electronically excited state $^2\Pi_u$ was found to be responsible for this process, although there are many other states in the vicinity. The state specificity is largely due to the symmetry restriction which could be removed in the case of chemical reaction with the presence of the Na atoms. But the results do suggest that breaking of the O-O bond is likely initiated by electron transfer to the excited O_2^- orbital, which will result in substantial bond stretching in O_2^-. The argu-

ment that the excited O_2^- orbital is important to the NaO + NaO reaction is further supported by our recent calculations in which we computed the energetics for the molecular system at various geometries. It is found for all potential energy surfaces with ground state O_2 characteristics, NaO_2 is the dominant product in the exit channel. The details of the calculations will be reported in a forthcoming paper.

References

[1] E. Bulewicz, C. G. James, and T. M. Sugden, Proc. R. Soc. London **235**, 89 (A1956).

[2] M. J. McEwan and L. F. Phillips, Combust. Flame **9**, 420 (1965); *ibid.* **11**, 63 (1967).

[3] C. H. Muller, K. Schofield, and M. Steinerg, J. Chem. Phys. **72**, 6620 (1980).

[4] V. Kempter, W. Mecklenbrauck, M. Menzinger, and Ch. Schlier, Chem. Phys. Lett. **11**, 353 (1971).

[5] H. Hou, K. T. Lu, A. G. Suits, and Y. T. Lee, unpublished results.

[6] A. W. Kleyn, Ph. D. Thesis, "Stichting voor Fundamenteel Onderzoek der Materie", Amsterdam, The Netherlands (1982).

[7] A. W. Kleyn, M. M. Hubers, and J. Los, Chem. Phys. **34**, 55 (1978).

[8] JANAF Thermochemical Tables, 3rd ed., J. Physical and Chemical Ref. Data, 14 (1985), Supp. No.1.

[9] D. R. Lide, Editor-in-Chief, *CRC Handbook of Chemistry and Physics*, 74th edition (1993-1994).

[10] K. P. Huber and G. Herzberg, *Molecular Spectra and Molecular Structure, IV. Constants of Diatomic Molecules*, Van Nostrand Reinhold Company (1979).

[11] H. Figger, W. Schrepp, and X. Zhu, J. Chem. Phys. **79**, 1320 (1983).

[12] A. Goerke, G. Leipelt, H. Palm, C. P. Schulz, and I. V. Hertel, Z. fur Physik D **32**, 311 (1995).

[13] Magee, J. Chem. Phys. **8**, 687 (1940).

[14] A. W. Kleyn in: *Alkali Halide Vapors*, edited by P. Davidovits and D. L. McFadden, Academic Press (1979).

[15] D. R. Herschbach, Appl. Opt. Supp. **2**, 128 (1965).

[16] R. D. Levine and R. B. Berstein, *Molecular Reaction Dynamics and Chemical Reactivity*, Oxford University, New York (1987).

[17] Y. T. Lee, J. D. McDonald, P. R. LeBreton, and D. R. Herschbach, Rev. Sci. Instrum. **40**, 1042 (1969).

[18] H. F. Davis, A. G. Suits, and Y. T. Lee, J. Chem. Phys. **96**, 6710 (1992) and the references therein.

[19] D. R. Herschbach, Disc. Faraday Soc. **33**, 149 (1962).

[20] Y. T. Lee, in: *Atomic and Molecular Beam Methods, Vol. 1*, edited by G. Scoles, Oxford University Press, New York (1988)

[21] W. B. Miller, S. A. Safron, and D. R. Herschbach, J. Chem. Phys. **56**, 3581 (1972).

[22] M. Covinsky, Ph.D. Thesis, University of California at Berkeley (1990).

[23] M. Steinberg and K. Schofield, J. Chem. Phys. **94**, 3901 (1991).

[24] R. H. McFarland and J. D. Kinney, Phys. Rev. **137**, A1058 (1965).

[25] P. S. Weiss, Ph. D Thesis, Chapter III, University of California at Berkeley (1985).

[26] Millard H. Alexander, J. Chem. Phys. **69**, 3502 (1978).

[27] L. Andrews, J. Chem. Phys. **54**, 4935 (1971); R. R. Smardzewski and L. Andrews,

J. Phys. Chem. **77**, 801 (1973); L. Andrews, J. T. Hwang, and C. Trindle, *ibid.* **77**, 1065 (1973).

[28] H. Huber and G. A. Ozin, J. Mol. Spectrosc. **41**, 595 (1972).

[29] D. M. Lindsay, D. R. Herschbach and A. L. Kwiram, Chem. Phys. Lett. **25**, 175 (1974).

[30] P. A. G. O'Hare and A. C. Wahl, J. Chem. Phys. **56**, 4516 (1972).

[31] W. S. Struve, J. R. Krenos, D. L. McFadden, and D. R. Herschbach, J. Chem. Phys. **62**, 404 (1975).

[32] L. King and D. R. Herschbach, Faraday Disc. Chem. Soc. **55**, 331 (1973).

[33] A. G .Suits, H. Hou, and Y. T. Lee, J. Phys. Chem. **94**, 5672 (1990).

[34] K. T. Lu, H. Hou, A. G. Suits, and Y. T. Lee, unpublished results.

Figure Captions

Figure 2.1 The energy level diagram for $Na_2 + O_2$. Shaded regions indicate the uncertainties in the energetics. Computation is done based on changes in the bond dissociation energies ΔD_0 for each reactions. Values for D_0(Na-O), D_0(O-O) and D_0(Na-Na) are from standard handbooks. [8] [9] [10] D_0(Na-ONa) is from the results of M. Steinberg and K. Schofield [23]. D_0(Na-O_2) is from the results of H. Figger and coworkers. [11] The energy of Na_2O_2 complex is obtained from our *ab initio* calculation using *Gaussian 92*. [34]

Figure 2.2 Newton Diagram for $Na_2 + O_2$ at nominal collision energy E_c = 8 kcal/mol. The Circle indicates the limiting velocity of the ground state NaO_2 products obtained using Equation (2.1). Θ_{CM} is the Na_2/O_2 center of mass angle. Θ_m indicates the angle of Na/O_2 center of mass, where we observed maximum

signal for NaO_2 channel.

Figure 2.3 Time-of-flight spectra measured for m/e = 39 (NaO^+) at collision energy 8 kcal/mol. NaO^+ is from the electron impact fragmentation of NaO_2. Open circles are the experimental data. Solid lines indicate the best fit using P(E) and T(θ) shown in Figure 2.5.

Figure 2.4 Laboratory angular distribution of NaO^+ signal at E_c = 8 kcal/mol. Open circles are experimental data. Solid line is the fit using P(E) and T(θ) shown in Figure 2.5.

Figure 2.5 Product center of mass translational energy distribution P(E) and angular distribution T(θ) that best fit the experimental data.

Figure 2.6 Newton Diagram for $Na_2 + O_2$ at nominal collision energy E_c = 23 kcal/mol. The circles indicate the limiting velocities of the ground state products. Θ_{CM} is the Na_2/O_2 center of mass angle. Θ_m indicates the angle of Na/O_2 center of mass, where we observed maximum signal for NaO_2 channel.

Figure 2.7 Time-of-flight spectra measured for m/e = 39 (NaO^+) at collision energy 23 kcal/mol. NaO^+ is from both the NaO_2 and NaO channels. Open circles are the experimental data. Solid lines indicate the total fit. Dotted lines indicate the contribution from the NaO_2 + Na channel and dashed lines indicate the contribution from the NaO + NaO channel.

Figure 2.8 Laboratory angular distribution of NaO^+ signal at E_c = 23 kcal/mol. Solid line indicates the total fit. The dotted line indicates the contribution from the NaO_2 + Na reaction channel and the dashed line is for the NaO + NaO channel.

Figure 2.9 Translational energy distribution P(E) and angular distribution T(θ) that best fit the NaO_2 channel (Reaction (i)).

Figure 2.10 Translational energy distribution P(E) and angular distribution T(θ) that best fit the NaO channel (Reaction (iii)).

Figure 2.11 Na^+ time-of-flight spectra from $Na/Na_2 + O_2$ (Left) and $Na/Na_2 + N_2$ (Right). Open circles are the experimental data. The total fit (solid lines) is composed of four channels including elastic scattering (the fastest, dash-dot-dot), inelastic scattering (the second fastest, long dash), NaO_2 channel (dash-dot) and NaO channel (short dash).

Figure 2.12 Schematic drawing that illustrates the relations between the observed signal and various products. σ_i and σ_{iii} are the reaction cross sections for Reaction (i) and Reaction (iii), respectively. $\sigma_{elastic}$ and $\sigma_{inelastic}$ are the cross sections for the elastic scattering and the inelastic scattering of $Na + O_2$. σ_{ion}'s are the ionization cross sections by electron bombardment. The ions so formed undergo further dissociation to give the observed signal. ξ is defined as the fraction of NaO^+ among the total Na-containing positive ions produced by electron bombardment of NaO_2. According to the assumption that NaO_2 dissociates completely upon electron bombardment, the fraction of Na^+ from NaO_2 is $(1-\xi)$. η is defined as the fraction of Na^+ among the total Na-containing positive ions from the ionization of NaO.

Figures

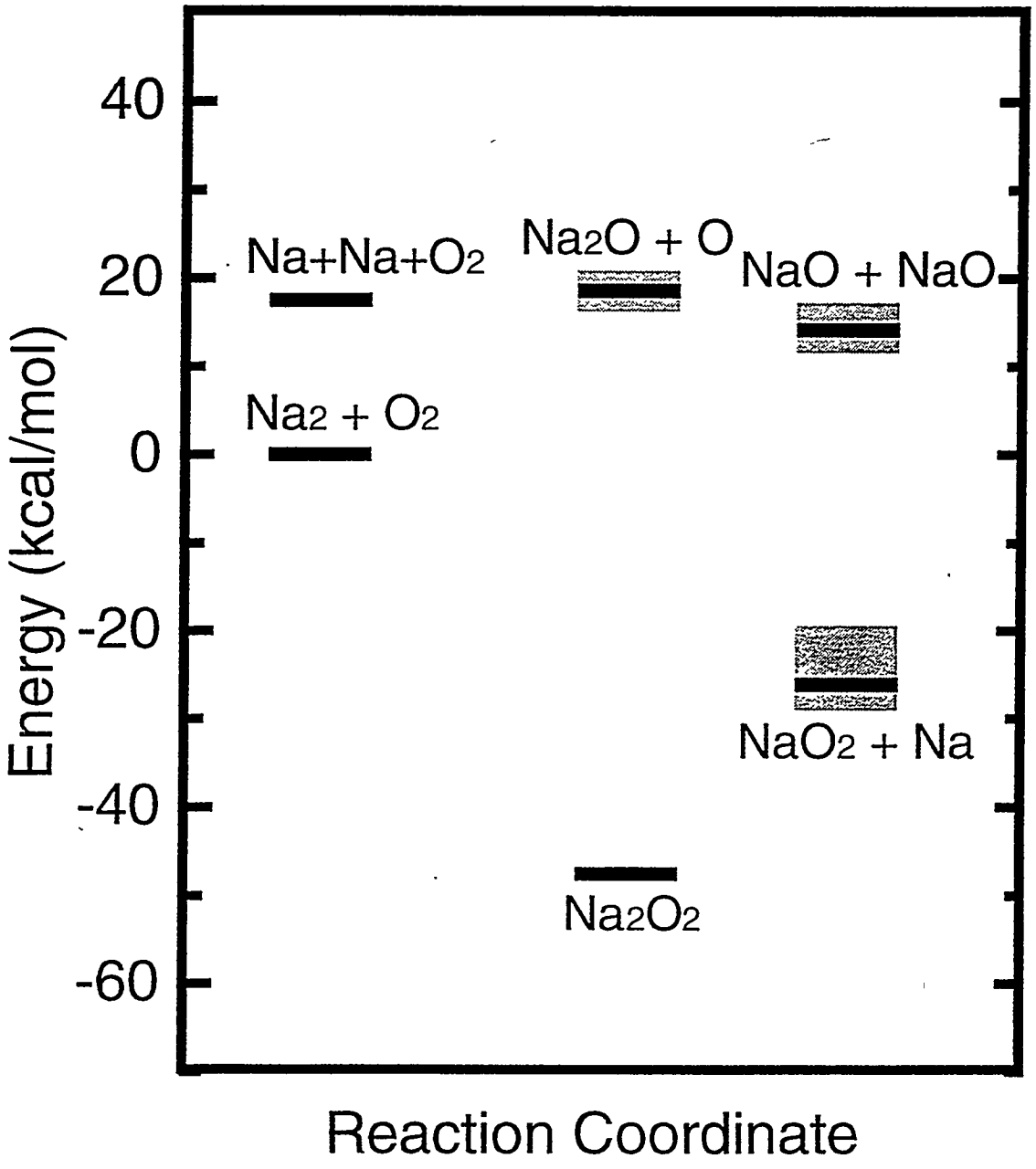
40
20
0
-20
-40
-60
Energy (kcal/mol)
Na+Na+O2
Na2 + O2
Na2O + O
NaO + NaO
NaO2 + Na
Na2O2
Reaction Coordinate

Figure 2.1

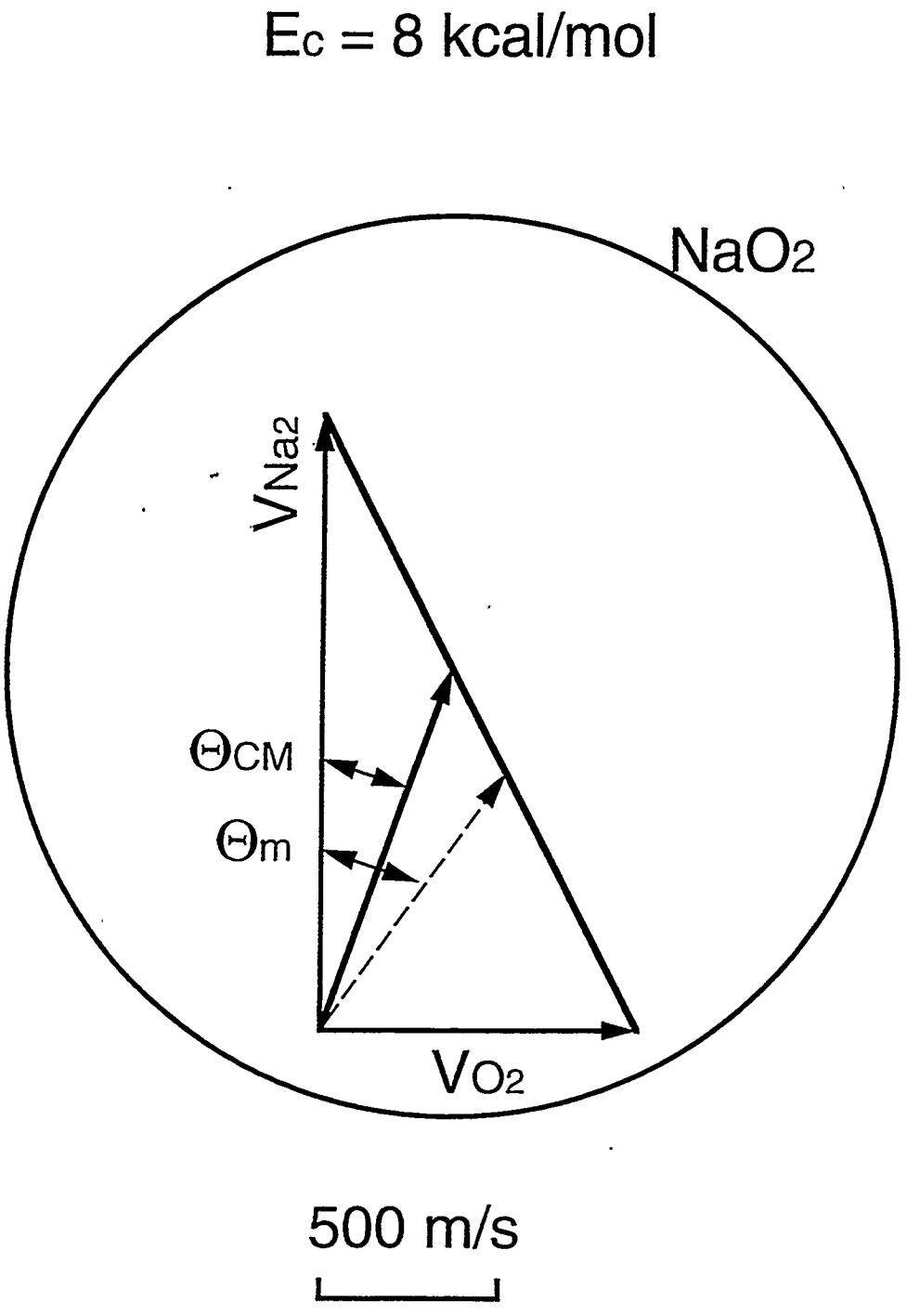

Figure 2.2

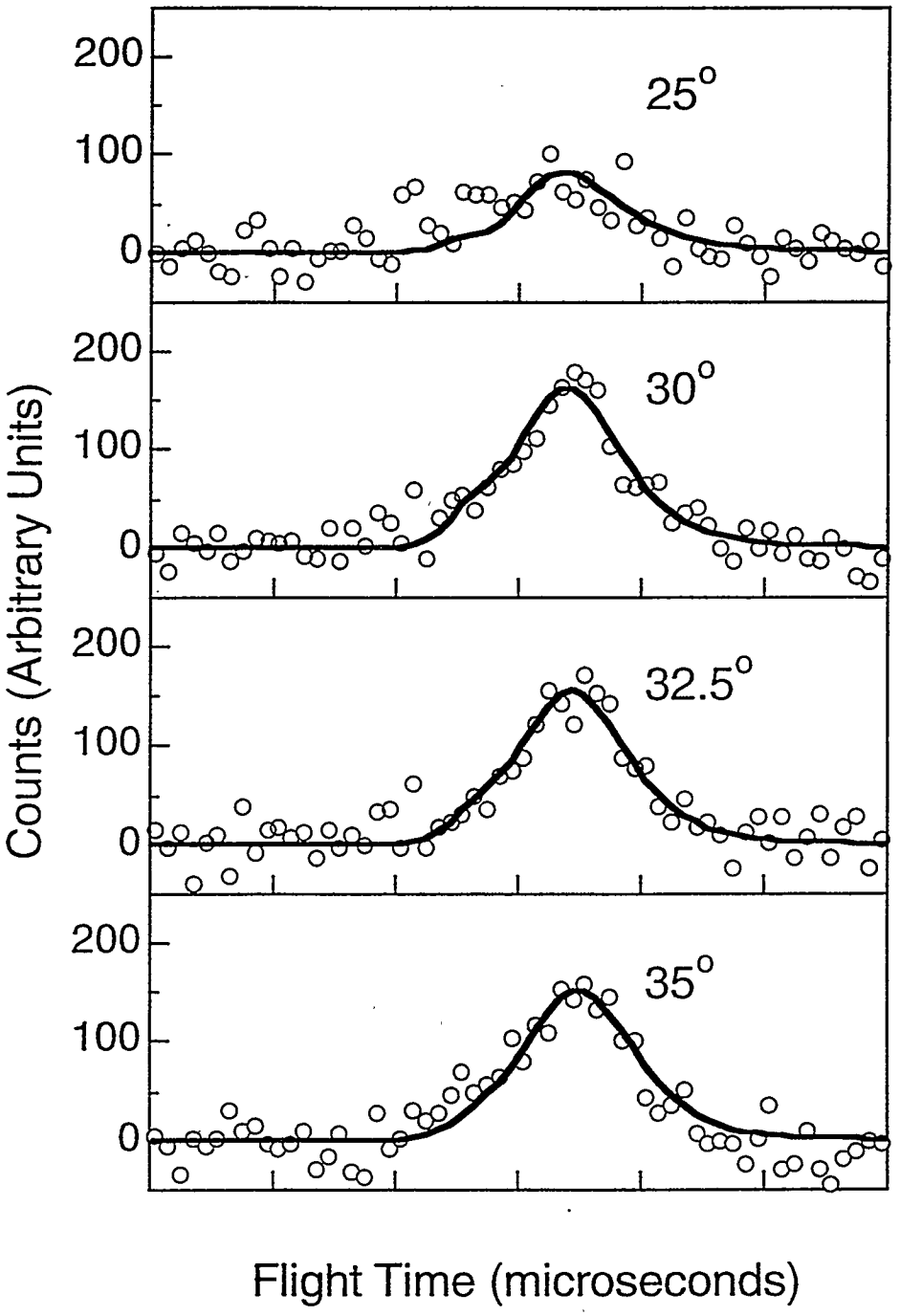
200
100
0
25°
200
100
0
30°
200
100
0
32.5°
200
100
0
35°
Counts (Arbitrary Units)
Flight Time (microseconds)

Figure 2.3

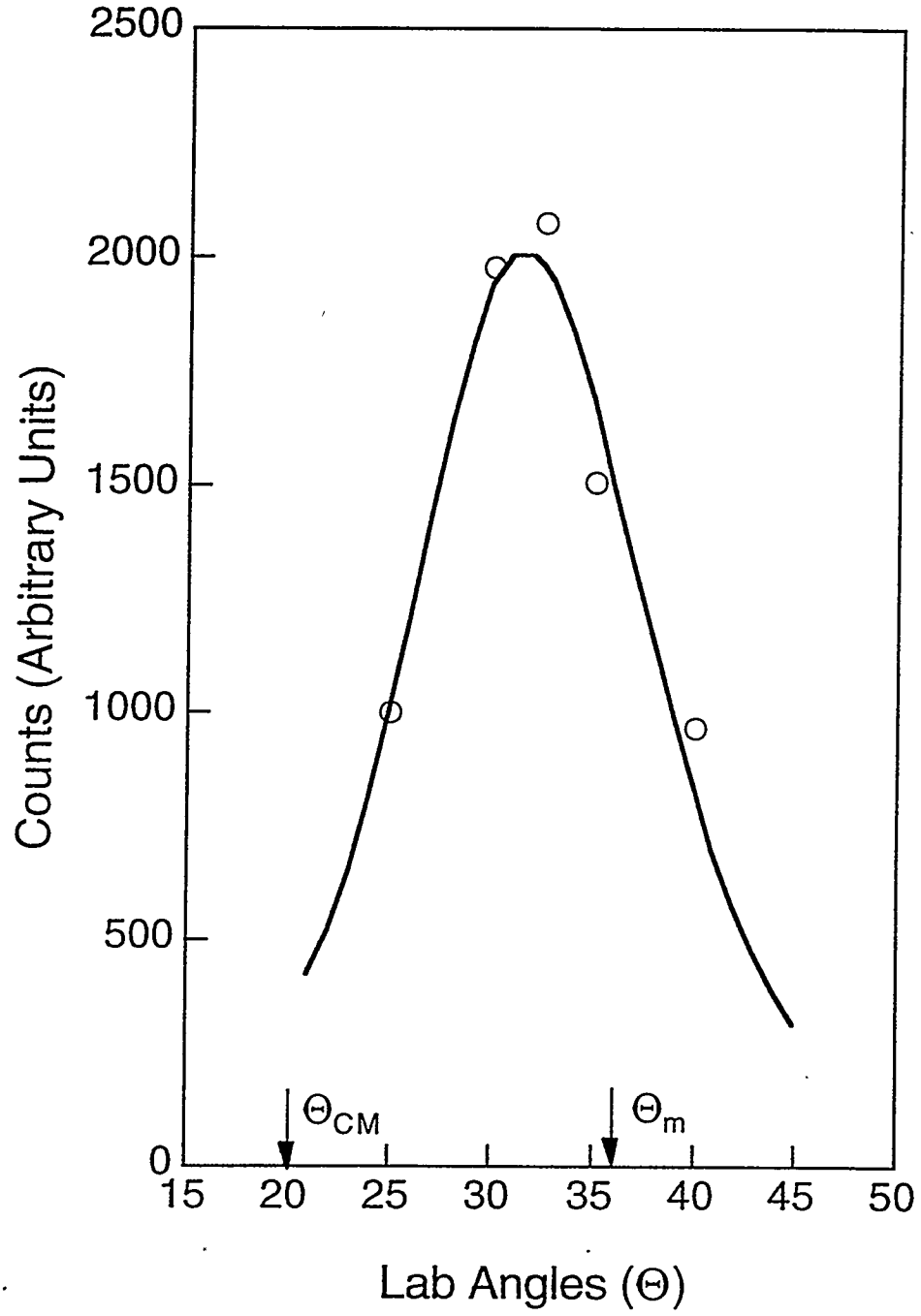
2500
2000
1500
1000
500
0
Counts (Arbitrary Units)
15
20
25
30
35
40
45
50
Lab Angles (Θ)
ΘCM
Θm

Figure 2.4

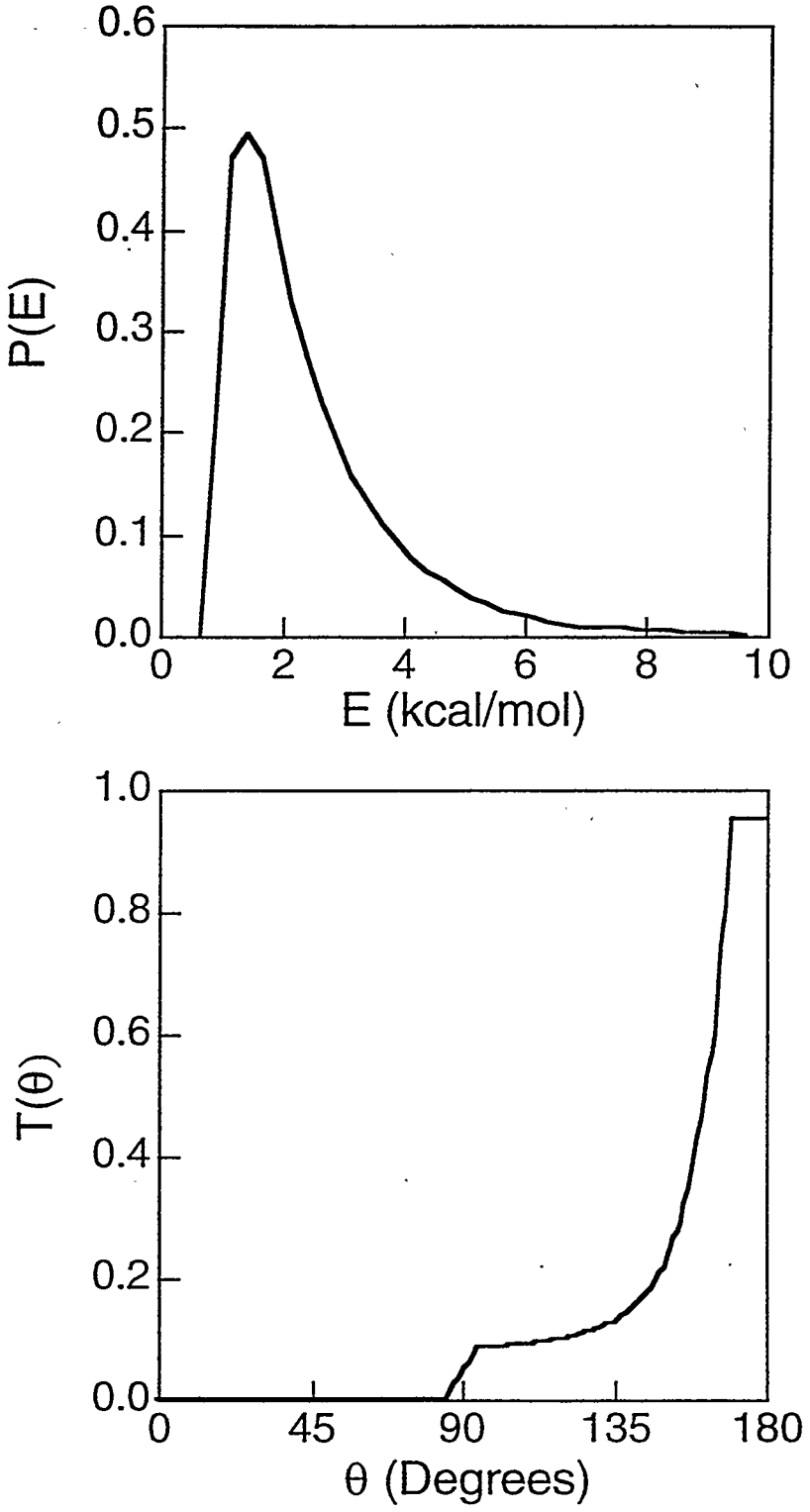
0.6
0.5
0.4
0.3
0.2
0.1
0.0
P(E)
0
2
4
6
8
10
E (kcal/mol)
1.0
0.8
0.6
0.4
0.2
0.0
T(θ)
0
45
90
135
180
θ (Degrees)

Figure 2.5

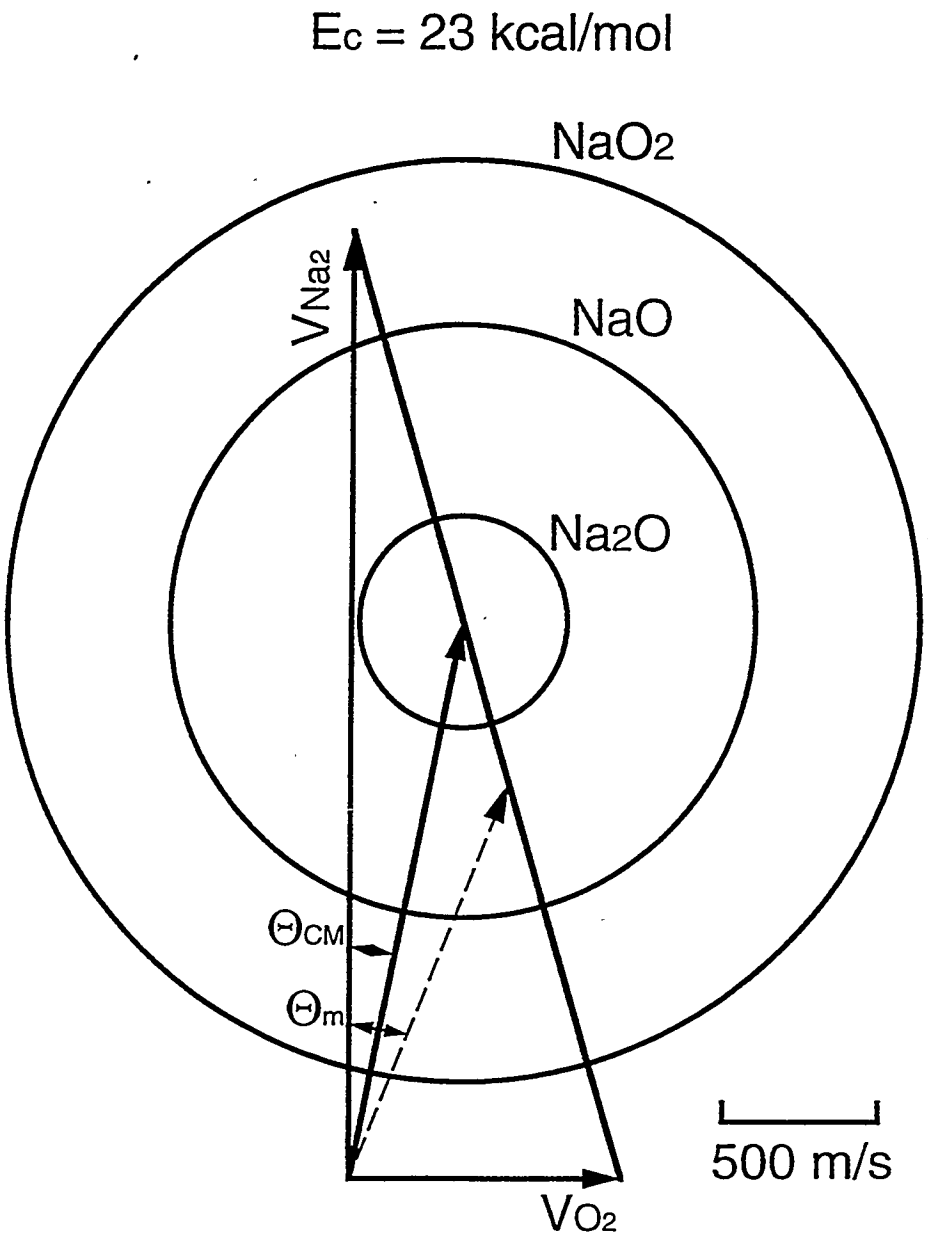

Figure 2.6

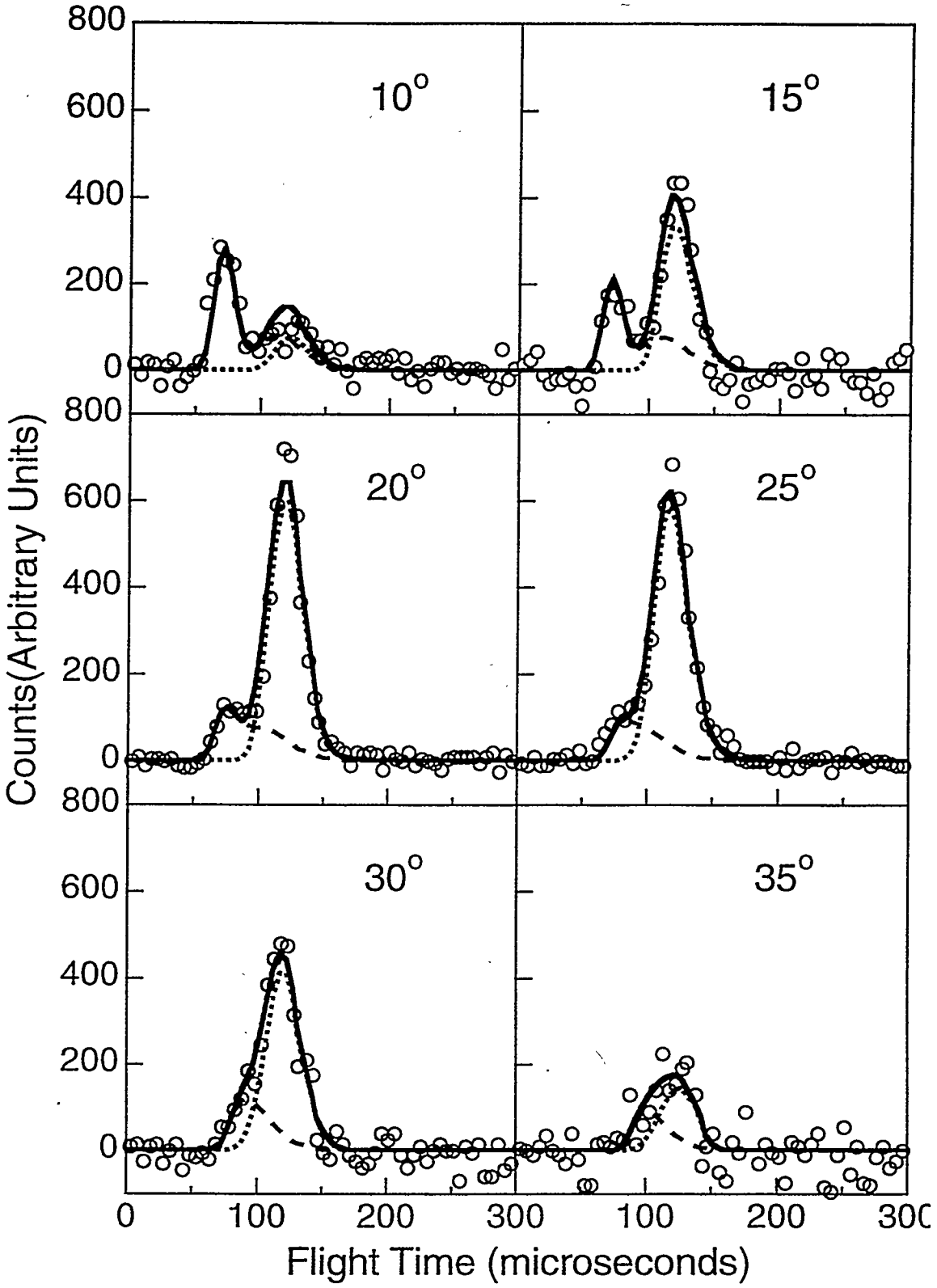
10°
15°
20°
25°
30°
35°
800
600
400
200
0
Counts(Arbitrary Units)
0
100
200
300
Flight Time (microseconds)

Figure 2.7

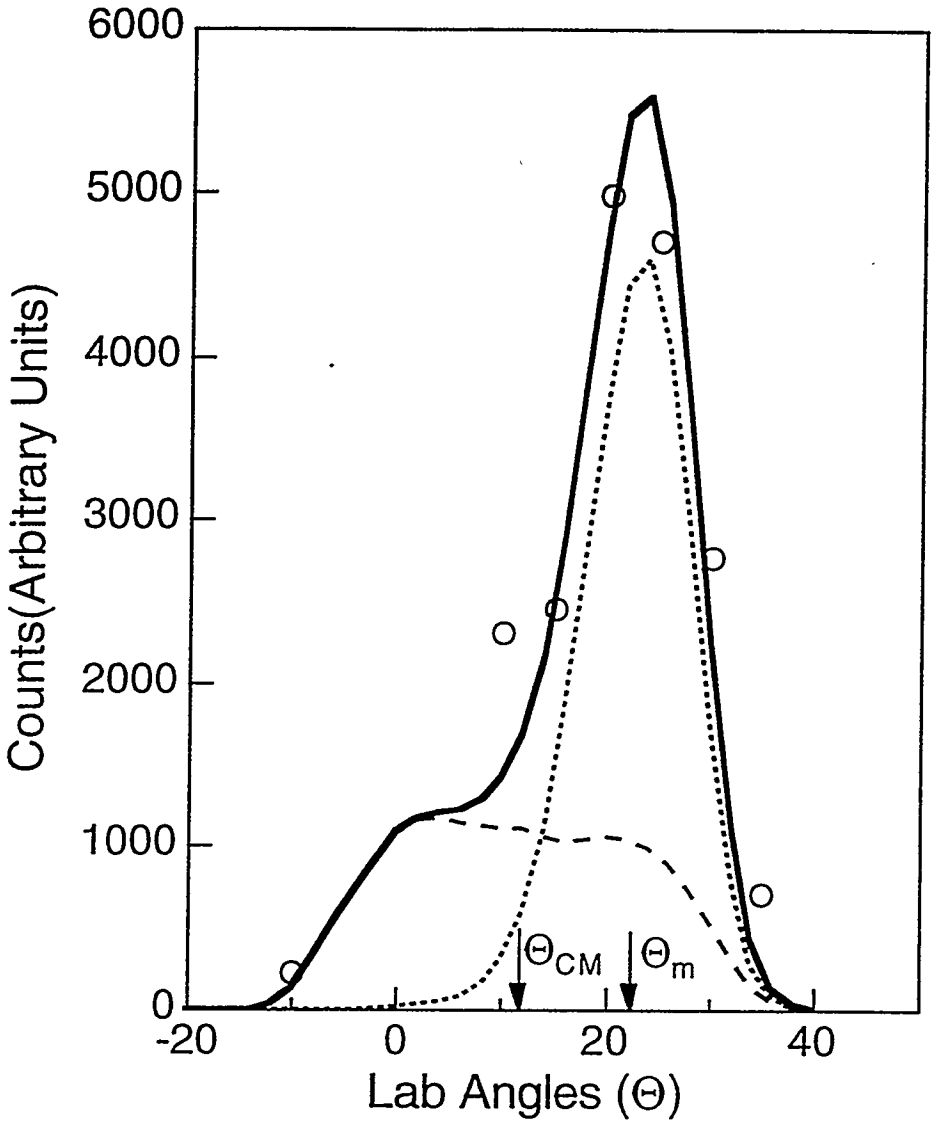
6000
5000
4000
3000
2000
1000
0
Counts(Arbitrary Units)
-20
0
20
40
Lab Angles (Θ)
ΘCM
Θm

Figure 2.8

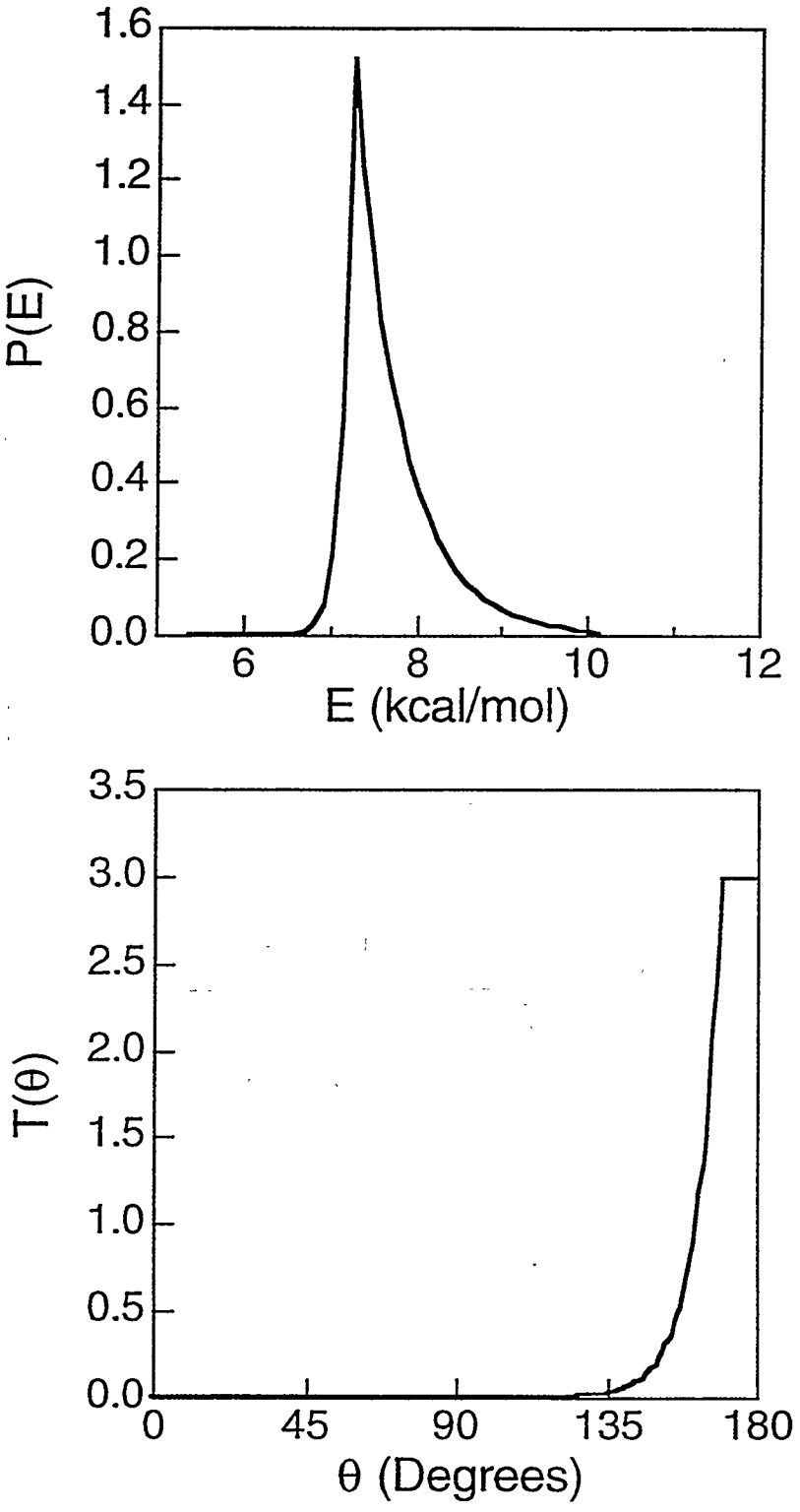
P(E)
1.6
1.4
1.2
1.0
0.8
0.6
0.4
0.2
0.0
6
8
10
12
E (kcal/mol)
T(θ)
3.5
3.0
2.5
2.0
1.5
1.0
0.5
0.0
0
45
90
135
180
θ (Degrees)

Figure 2.9

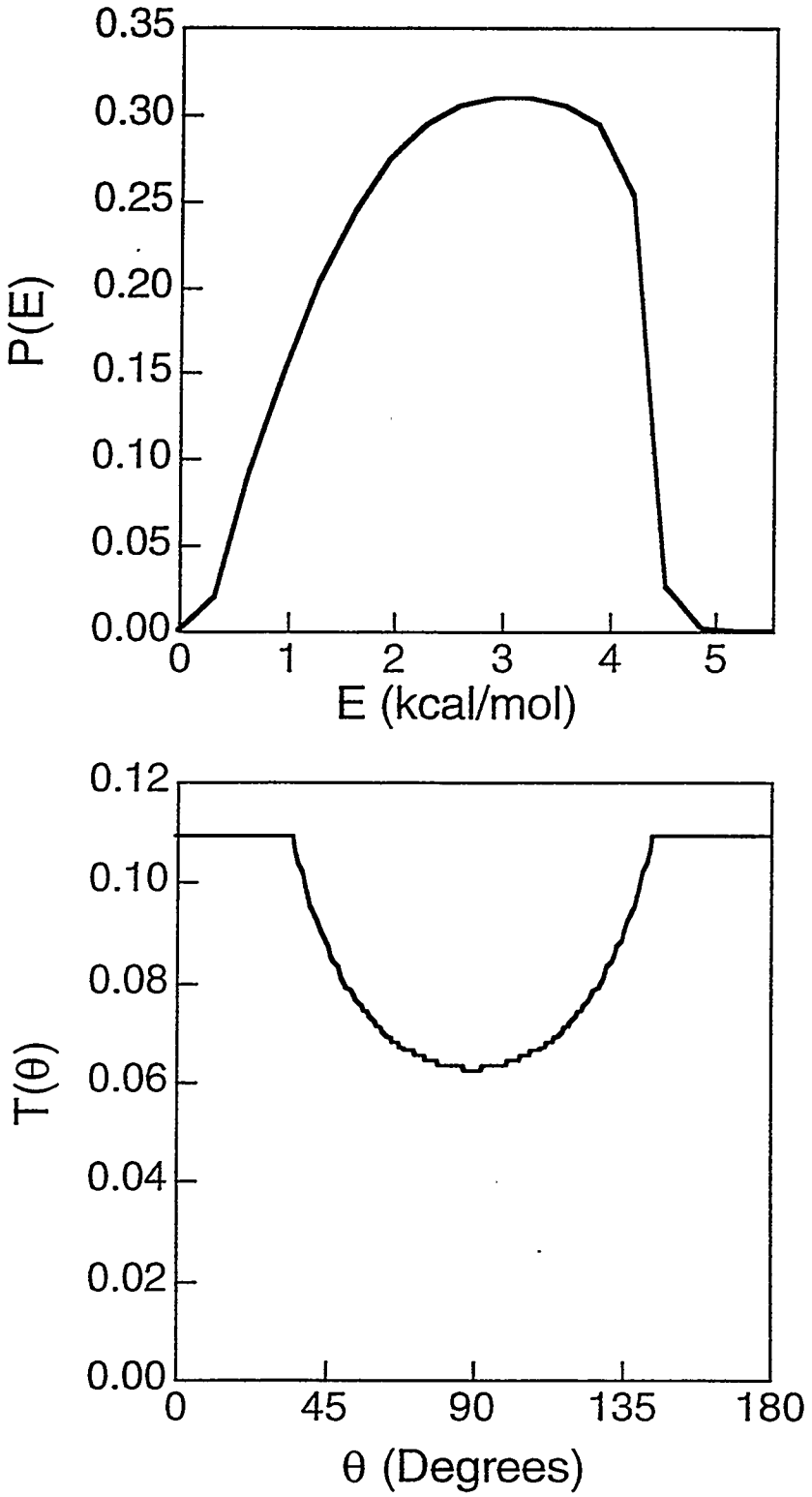
0.35
0.30
0.25
0.20
0.15
0.10
0.05
0.00
P(E)
0
1
2
3
4
5
E (kcal/mol)
0.12
0.10
0.08
0.06
0.04
0.02
0.00
T(θ)
0
45
90
135
180
θ (Degrees)

Figure 2.10

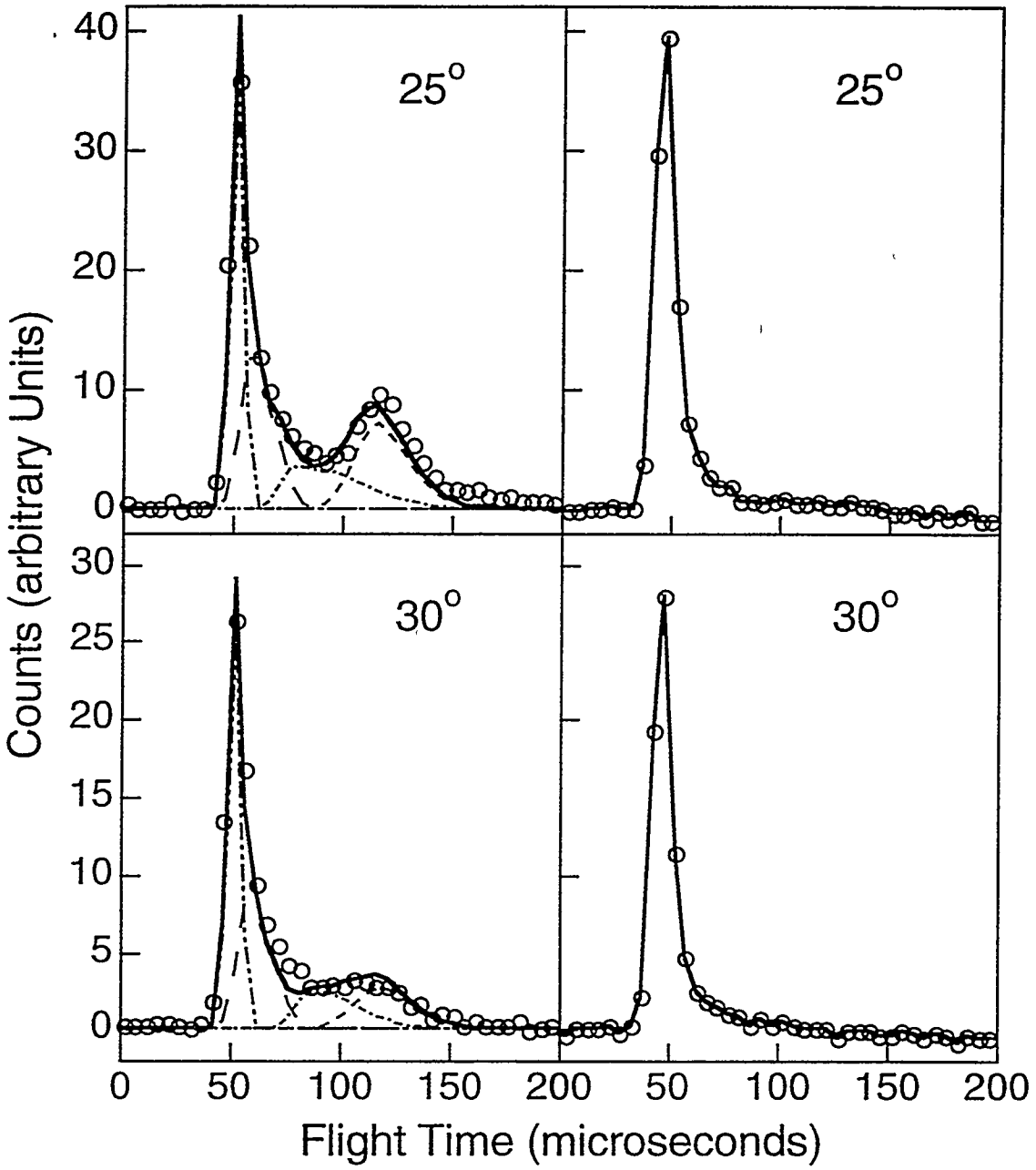
25°
25°
30°
30°
Counts (arbitrary Units)
Flight Time (microseconds)
0
10
20
30
40
5
15
25
50
100
150
200

Figure 2.11

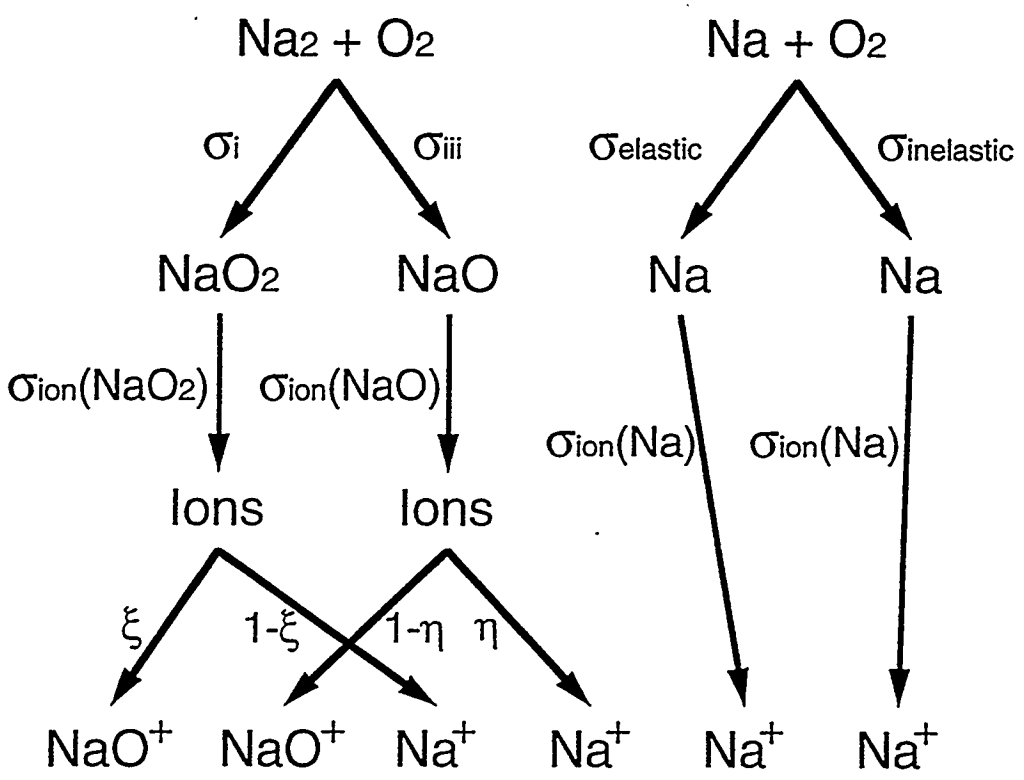
Na2 + O2
σi
σiii
NaO2
NaO
σion(NaO2)
σion(NaO)
Ions
Ions
ξ
1-ξ
1-η
η
NaO+
NaO+
Na+
Na+
Na + O2
σelastic
σinelastic
Na
Na
σion(Na)
σion(Na)
Na+
Na+

Figure 2.12

Chapter 3

The Reactions of Na_2 with NH_3 and CH_3OH*

Abstract

The reactions of Na_2 with NH_3 and CH_3OH were studied in a crossed-beam experiment under single collision conditions. Reaction of Na_2 + NH_3 led to the formation of $NaNH_3$ + Na at a nominal collision energy of 15.5 kcal/mol, with the angular distributions of $NaNH_3$ in the center of mass coordinates peaking strongly forward with respect to the direction of the NH_3 beam in both cases, suggesting that the reaction is completed in a time that is shorter than one rotational period of the molecular system. Only 38% of the total available energy is released to the translation energy of the $NaNH_3$ product, indicating that the products are internally excited. A similar angular distribution but a much broader translation energy distribution was observed for $NaCH_3OH$, a novel molecule from the reaction $Na_2 + CH_3OH \rightarrow NaCH_3OH + Na$ at a nominal collision energy of 26 kcal/mol. From the translation energy distribution, we found that the newly formed $NaCH_3OH$ molecules are also internally excited, with an average of 42% of the available energy appearing in the translational motion of the separating products. These results suggest that the reactions are initiated by impulsive collisions between the reactants, followed by swift contraction of the newly formed chemical bonds, which provide the necessary energy to break the Na—Na bonds. From the high energy tails in the translation energy distributions, the bond dissociation energies, $D_0(NaNH_3)$ and $D_0(Na(CH_3OH))$, are calcu-

---

* This chapter is based on H. Hou, K. T. Lu, A. G. Suits, and Y. T. Lee, submitted to J. Chem. Phys. The experimental work is that of H. Hou, who is the responsible author.

lated to be 19 and 27.6 kcal/mol, respectively. The strong binding energies suggest that the chemical bonds are formed between the 3s orbital of Na and the Rydberg 3s orbitals of the molecules.

Introduction

The reactions of alkali dimer molecules have been studied for nearly 30 years. From the early M_2 + H/D [1] and M_2 + M' [2] reactions which disclosed the importance of the ionic-covalent interactions and the long-lived complex formation, to the prototype M_2 + X_2/X reactions [3] which are initiated by long range electron transfer and characterized by the celebrated "Harpoon Mechanism", up to the recent M_2 + O_2 studies [4] which revealed the involvement of the electronically excited states of O_2^- in the dynamic process of the breaking of the O-O bond, these investigations reflect the progress in studies of alkali dimer molecular dynamics. Alkali dimers have many interesting properties [5] that make their chemistry unique (cf. Table 1 on page 79). The ionization potentials of the dimer molecules are even lower than those of the corresponding monomers such that when dimers interact with electron accepting molecules, the ionic and covalent potential energy surfaces cross at larger intermolecular distances, strongly affecting the charge transfer probabilities and the overall reaction cross sections. The bond lengths of M_2 and M_2^+ are extraordinarily long and although the bond length of M_2^+ is longer, the bond dissociation energy of M_2^+ ion is ~50% higher than those of M_2 neutrals. The covalent bonds of the alkali dimers are abnormally weak, with the bond dissociation energies lower than 1 eV, making many chemical reactions involving the cleavage of the alkali dimer bonds exoergic.

The solvation processes of the alkali metal in the liquid of polar molecules have

been studied since last century. [6] Alkali metal in liquid ammonia, known to be a source of solvated electrons, is widely applied in organic synthesis to reduce free radicals $R^{\cdot}$ to carbanion R^{-} or to initiate Birch reduction reactions which reduce the aromatic rings by adding hydrogen atoms. [7] However, because of the strong influence of the lone pair electrons on the nitrogen atom, the ability of a single ammonium molecule to accommodate an additional electron is limited. Single anion NH_3^- was not previously observed in the gas phase, so the electron affinity of NH_3 is not well known. Nevertheless, it is reasonable to compare NH_3 with its isoelectronic molecule H_2O, whose vertical electron affinity was found to be nearly -6 eV [8], and gain some insight to the energy requirement to put an electron on a single NH_3 molecule. Previous studies found that solvated electrons exist only in a dilute alkali metal-ammonia solution, where the electron is separated from the cation and both are screened individually by the surrounding dielectric medium to form two-center localized states. The first evidence on a microscopic level that indicate the existence of these two-center localized states in the metal-liquid solutions was put forward by Hertel and coworkers in their pioneer studies of the ionization potentials of $Na(NH_3)_n$ and $Na(H_2O)_m$ as functions of cluster sizes n and m ($n \leq 35$, $m \leq 20$), respectively, using photoionization and ion time of flight mass spectrometry techniques. [9] At the same time, similar experiments were also carried out by Misaizu and coworkers for $Cs(H_2O)_n$ and $Cs(NH_3)_n$ systems. [10] Assuming their measured ionization potential of $NaNH_3$ is truly the adiabatic value of the electron binding energy, Hertel's group calculated the value of the bond dissociation energy [11] from the equation:

$$D_0(Na\text{-}NH_3) = IP\ (NaNH_3) + D_0(Na^+\text{-}NH_3) - IP\ (Na). \qquad (3.1)$$

The result, $D_0(Na\text{-}NH_3) = 0.39$ eV (9 kcal/mol), was obtained using the known value for

$D_0(Na^+\text{-}NH_3)$. [12] Hertel's group also reported their spectroscopic studies of the electronically excited states of $NaNH_3$ via a resonant two color two photon ionization scheme, in which case a complex vibrational progression is observed and assigned to the $A^2E \leftarrow X^2A_1$ transition. [13]

The early theoretical calculations of alkali-hydride complexes appeared some 20 years ago. [14] Recent experimental efforts have stimulated theoretical interest in the structural, bonding and spectroscopic properties of the metal-molecule clusters. Greer et al. [15] calculated the potential energy surfaces for the ground state and a number of excited states of $NaNH_3$ using multiconfiguration SCF methods. The resultant binding energy, $D_0(Na\text{-}NH_3)$, of 5 kcal/mol (0.22 eV) [15] is substantially lower than the experimental result [11], possibly due to the exclusion of electron correlation in their calculation. Recently the structure and stability of $Na(H_2O)_n$ and $Na(NH_3)_n$ (n = 1 - 6) have been calculated by Hashimoto and coworkers first at the HF/3-21G level [16] and then at HF/6-3+G(d) level. [17] [18] [19] In the HF/3-21G calculation $Na(NH_3)_n$ was found to be an inclusion complex where Na is surrounded by NH_3 molecules. Water-water hydrogen bonds play an essential role in stabilizing $Na(H_2O)_n$, whereas stabilization by the Na-N bond formation is more important for $Na(NH_3)_n$. This disparity can qualitatively explain the different trends of the ionization potentials between $Na(H_2O)_n$ and $Na(NH_3)_n$ observed by experiment. [9] The calculated binding energy between Na and NH_3 in the $NaNH_3$ molecule is 16.93 kcal/mol, considerably larger than the previously mentioned experimental value of 9 kcal/mol. In the HF/6-3+G(d) calculation, the geometries of $Na(NH_3)_n$ were only slightly different from those from the HF/3-21G calculation, but the bond strength of $Na\text{-}NH_3$ was just 7.0 kcal/mole, almost 10 kcal/mole lower than the pre-

vious HF/3-21G calculation.

In addition to their importance for understanding the mechanism of hydration, alkali-ammonium and alkali-methanol interactions are also interesting because NH_3 and CH_3OH possess only Rydberg-like unfilled molecular orbitals. As a result, the reactions are not expected to be initiated by long range electron transfer, and the well known "harpoon mechanism" is not generally applicable. Instead a close collision is necessary to bring about the chemical reactions, as was the case found in the experiments of $Ba + H_2O$ and $Ba + CH_3OH$. [20] Therefore the reactions are expected to have very small cross sections (< 10 $Å^2$). For this reason, very little gas phase work on the reaction dynamics of NH_3 and CH_3OH with neutral alkali atoms and molecules using crossed molecular beams has been performed.

In this chapter, we present our results from crossed-beam studies of the reactions of sodium dimers with ammonium and methanol molecules. The reactions were investigated under single collision conditions by measuring the angular and velocity distributions of the reaction products. Our results allow us to gain considerable insight into the dynamics of the reactions and to broaden our knowledge of the reactions of the alkali family. Quantitatively, our measurements provide lower limits for the bond dissociation energies of $Na\text{-}NH_3$ and $Na\text{-}(CH_3OH)$ molecules, which are the reaction products.

Experimental

The details of the crossed-beam apparatus can be found in many earlier publications. The primary beam was essentially the same as described in previous chapters. The Na_2 beam was crossed at 90^o by a secondary supersonic beam of either neat ammonia or methanol seeded in helium in the main collision chamber under single collision condi-

tions. The secondary source nozzle was heated to 473°K to prevent cluster formation. Both sources were doubly differentially pumped. The beams were skimmed and collimated to 2° FWHM in the collision chamber. Under these conditions, the nominal collision energies for the reaction are 15.5 kcal/mol for $Na_2 + NH_3$, and 26 kcal/mol for $Na_2 + CH_3OH$, respectively.

The detector configurations were also described in previous chapters. In the current experiment, since we are looking at very weakly bonded products, the energy of the electron beam used to ionize neutral molecules has to be lowered from 200 to 60 volts in order to minimize the fragmentation of the products by electron impact.

Results and Analysis

As mentioned above, the intensity of sodium monomer is very strong in the sodium beam. However, the monomer reactions

$$Na + NH_3 \rightarrow NaNH_2 + H, \quad \text{(i)}$$

$$Na + CH_3OH \rightarrow NaOCH_3 + H, \quad \text{(ii)}$$

$$Na + CH_3OH \rightarrow NaOH + CH_3, \quad \text{(iii)}$$

were not observed. For sodium dimer molecules, there are several thermodynamically accessible reaction pathways as listed in Table 2 on page 79 of this thesis. The energetics for most of these reactions are not known because there exist very few gas phase experiments providing the needed bond dissociation energies.

A. $Na_2 + NH_3$ at E_c = 15.5 kcal/mol

The Newton diagram for $Na_2 + NH_3$ at a nominal collision energy of 15.5 kcal/mol is shown in Figure 3.1. Θ_{CM} denotes the laboratory angle of the center of mass velocity

vector for $Na_2 + NH_3$. In the center of mass coordinate, the direction of the Na_2 beam is defined as $\theta = 0^o$, whereas the direction of the NH_3 beam is $\theta = 180^o$. According to the binding energy of Na-NH_3 given by Hashimoto et al. [16], the total available energy is ~ 15 kcal/mol for the $NaNH_3$ + Na channel so the $NaNH_3$ products should be confined within the solid circle in Figure 3.1. The other reaction channel, $NaNH_2$ + NaH is not shown for the following reasons: First, the bond dissociation energy of Na-NH_2 is unknown. Nevertheless, this channel is likely to be significantly more endoergic than the $NaNH_3$ + Na channel so that it is not accessible with the 15.5 kcal/mol collision energy. Second, this reaction channel is not observed in the experiment.

The time of flight spectra recorded for m/e = 40 ($NaNH_3^+$) are shown in Figure 3.2 (open circles) for several laboratory angles. A number of checks were carefully conducted to prove that the m/e = 40 signal was in fact due to the reaction:

$$Na_2 + NH_3 \rightarrow NaNH_3 + Na. \qquad \text{(iv)}$$

First, the diameter of the primary source was varied while other operation conditions remained the same so that the dimer concentration became negligible whereas the Na monomer intensity was nearly unchanged in the primary beam. [23] With this configuration, the m/e = 40 signal disappeared, which is by far the strongest evidence to prove that the observed signal was indeed from Na_2. Second, it is possible that the residual argon in the gas feeding lines could also give rise to a nonreactive signal at m/e = 40. Therefore each gas line was flushed many times with helium before each run and the beams were examined carefully using the mass spectrometer to make sure there was no m/e = 40 in the beams. Third, the NH_3 beam was scrutinized and ammonium dimers were not seen. Therefore the reaction:

$$Na + (NH_3)_2 \rightarrow NaNH_3 + NH_3, \qquad (v)$$

can be safely excluded.

In the same figure, the solid lines represent the simulation using the forward-convolution method, which is done by assuming the center of mass angular distribution $T(\theta)$ and translation energy distribution P(E). The laboratory angular distribution of the $NaNH_3$ signal is shown in Figure 3.3 where the solid line is the fit using the same P(E) and $T(\theta)$. It is evident that most of the $NaNH_3$ products are scattered into angles larger than the center of mass angle Θ_{CM} toward the NH_3 beam.

The center of mass translation energy distribution P(E) and angular distribution $T(\theta)$ are plotted in Figure 3.4. Based on P(E) and $T(\theta)$, the contour map for the flux of the products is constructed and shown in Figure 3.5. The shape of P(E) is quite narrow, with a sharp rising edge at ~ 4 kcal/mol and a long tail to ~23 kcal/mol at the high energy end. If we assume 23 kcal/mol is the total available energy E_{av} for this reaction, and the internal energy of each reactant in the supersonic beam is negligible, the bond dissociation energy $D_0(Na\text{-}NH_3)$ can be estimated using the following relation:

$$E_{av} = E_{col} + D_0(Na\text{-}NH_3) - D_0(Na\text{-}Na), \qquad (3.2)$$

where E_{col} is the collision energy. Using the known value of 17.5 kcal/mol for D_0(Na-Na), $D_0(Na\text{-}NH_3)$ is calculated to be 25 kcal/mol.

The lower translation energy release corresponds to higher internally excited products. The sharp cut off at low energy in P(E) strongly suggests that the internal excitation of the products has exceeded the dissociation limit of the newly formed bond so that Na and NH_3 can no longer be held together, leading to the collisional dissociation reaction:

$$Na_2 + NH_3 \rightarrow Na + Na + NH_3, \Delta H = 17.6 \text{ kcal/mol}. \qquad (vi)$$

However, the collision energy is only 15.5 kcal/mol, not enough to initiate Reaction (vi), unless the reactants carry some internal energy prior to the reaction.

As described in the experimental section, the secondary beam was formed by a supersonic expansion of neat NH_3. Therefore the expansion is not as "hard" as a seeded beam. It is possible that the expansion led to no vibrational cooling. The vibrational frequencies of the ground state NH_3 as well as the thermal population on each v = 1 state relative to the ground vibrational state are listed in Table 3 on page 79. [24] At 473 K, the v = 932.5 cm^{-1} state is appreciably populated. The ro-vibrational excitation of this state can bring a few kilocalories of energy into the reaction coordinates. If these vibrationally excited NH_3 molecules dominate the reaction, there will be excess energy in the newly formed Na-NH_3 coordinate, leading to its further dissociation into Na + NH_3. The energy equation for Reaction (vi) can be written as:

$$D_0(Na\text{-}Na) = E_{col} + E_{int} - E_0, \qquad (3.3)$$

where E_{int} is the sum of the internal energy in the reactants and E_0 is the cutting energy in P(E) for the $NaNH_3$ products. It follows from Equation (3.3) that the total internal energy carried by the reactants, E_{int}, is 6 kcal/mol. Taking E_{int} into account, Equation (3.2) should be modified to:

$$E_{av} = E_{col} + D_0(Na\text{-}NH_3) - D_0(Na\text{-}Na) + E_{int}. \qquad (3.4)$$

Subsequently the value for D_0(Na-NH_3) is offset to 19 kcal/mol. This number is considerably larger than any of the previously reported values. However the fact that these molecules had survived electron bombardment in the ionization region seems to support a strong binding between Na and NH_3. From P(E), the average translational energy release is 9 kcal/mol, only 39% of the total available energy. This result suggests that nascent

$NaNH_3$ is internally excited, most likely along the newly formed Na-NH_3 bond.

The center of mass angular distribution $T(\theta)$ peaks narrowly towards the NH_3 beam, exhibiting remarkable anisotropy in the forward (0^o) and backward (180^o) directions. This anisotropy indicates that the reaction takes place during a time that is shorter than the rotational period of the molecular system so that the products are separated before they lose the sense of the well defined approaching direction of the reactants. [25]

B. $Na_2 + CH_3OH$ at $E_c = 26$ kcal/mol

The Newton diagram for $Na_2 + CH_3OH$ at a nominal collision energy of 26 kcal/mol is shown in Figure 3.6. Θ_{CM} denotes the laboratory angle of the center of mass velocity vector for $Na_2 + CH_3OH$. In the center of mass coordinate, the direction of the Na_2 beam is defined as $\theta = 0^o$, whereas the direction of the CH_3OH beam is $\theta = 180^o$. Since the bond dissociation energy of Na-(CH_3OH) is not known, the circle in the Newton diagram is actually drawn for the Na-(CH_3OH) products using D_0(Na-(CH_3OH)) = 27.6 kcal/mol, one of the results of this experiment. At this collision energy, CH_3OH can transfer as much as 21 kcal/mol to Na_2 at a collinear "impulsive" impact. (cf. Discussion section) This much energy is enough to break the Na-Na bond, leading directly to the collisional dissociation reaction:

$$Na_2 + CH_3OH \rightarrow Na + Na + CH_3OH, \Delta H = 17.6 \text{ kcal/mol.} \qquad \text{(vii)}$$

However this channel is difficult to measure because of strong non-reactive scattering.

The time of flight spectra recorded for m/e = 55 ($Na(CH_3OH)^+$) are shown in Figure 3.7 for several laboratory angles. Similar checks to those in the $Na_2 + NH_3$ experiment were made to ensure that the observed signal is indeed from the reaction:

$$Na_2 + CH_3OH \rightarrow Na(CH_3OH) + Na. \qquad \text{(viii)}$$

To our knowledge, this is the first time that the $Na(CH_3OH)$ molecule has been observed in the gas phase. In each time of flight spectrum, the solid lines represent the simulation using the forward-convolution method by assuming independent $T(\theta)$ and $P(E)$, which also simultaneously fit the laboratory angular distribution shown in Figure 3.8. Similar to the $Na_2 + NH_3$ case, the $Na(CH_3OH)$ products are also scattered into angles larger than the center of mass angle Θ_{CM} and toward the CH_3OH beam.

Center of mass translation energy distribution $P(E)$ and angular distribution $T(\theta)$ are plotted in Figure 3.9. Based on $P(E)$ and $T(\theta)$, the contour map for the flux of the products is constructed and shown in Figure 3.10. Compared with the distributions of $NaNH_3$, the $P(E)$ for $Na(CH_3OH)$ lacks the sharp rising edge and is also much broader. If we assume that the internal energy of the products is zero at maximum translation energy release, the total available energy E_{av} obtained from $P(E)$ is 36 kcal/mol. Since methanol is seeded in helium, it is less likely to have a substantial fraction of vibrationally hot CH_3OH molecules in the beam. Using Equation (3.2) with NH_3 replaced by CH_3OH, $D_0(Na(CH_3OH))$ is calculated to be 27.6 kcal/mol, assuming no internal excitation in the reactants prior to the collision.

The missing of the sharp rising edge in $P(E)$ suggests that CH_3OH is more flexible in adapting the excess energy, which could be rationalized by the fact that there exist many more vibrational modes in the molecule. $P(E)$ peaks at 12 kcal/mol and the average translation energy release is ~ 15 kcal/mol, which is 42% of the total available energy. So on average, the nascent $Na(CH_3OH)$ molecule is also quite hot internally.

The angular distribution of $Na(CH_3OH)$ is also peaked in the backward direction with respect to the Na_2 beam. Therefore Reaction (viii) follows a similar mechanism to

Reaction (iv), i. e. an impulsive collision which leads to the products in less than the rotational period of the molecular system. $T(\theta)$ is only slightly broader than for $NaNH_3$, whereas P(E) is much broader, and accordingly $Na(CH_3OH)$ is scattered into a wider range in the center of mass coordinates as compared with $NaNH_3$.

Discussion

A. $Na_2 + NH_3 \rightarrow NaNH_3 + Na$.

The molecular orbitals for the ground state NH_3 are: $(2a_1)^2(1e)^4(3a_1)^2$, $^1A_1$. The first electronic transition to state: $(2a_1)^2(1e)^4(3a_1)(4a_1)$, $^1A_2''$ occurs from 2170 to 1700 Å (λ_{max} at *ca.* 1900 Å).[26] The excitation energy at λ_{max} of this transition is ~ 6.5 eV, which can be used to estimate the vertical electron affinity of NH_3 ($EA_v(NH_3) \approx -6.5$ eV). Using the equation:

$$R_c = \frac{14.4}{IP(Na_2) - EA_v(NH_3)} \text{ (Å)}, \qquad (3.5)$$

where IP and EA are in units of eV, the crossing radius of the ionic and covalent potential energy curves can be calculated to be 1.3 Å. Since this distance is of the same order as a bond length, it is inappropriate to describe the reaction dynamics using the celebrated "Harpoon" mechanism, i. e. a long range electron transfer followed by the decay of an ionic intermediate. Based on our measurement, $D_0(Na\text{-}NH_3) = 19$ kcal/mol, it is clear that $NaNH_3$ is a chemically stable molecule. The $Na\text{-}NH_3$ bond is much stronger than if it were just a van der Waals interaction. However, the previously mentioned excited state: $(2a_1)^2(1e)^4(3a_1)(4a_1)$, $^1A_1$, is unlikely to participate in the bond formation, because this state is strongly anti-bonding between the H_3 group and N. This anti-bonding nature tends

to cause the breaking of one or more N-H bond, as in the similar case of the $Ba + H_2O \rightarrow BaO + H_2$ reaction. [20]

Spectroscopy data shows that the region 2170 — 1700 Å may also contain the first Rydberg transition of NH_3. This Rydberg transition can be formulated as:

$$(2a_1)^2(1e)^4(3a_1)(a_13s),\ ^1A_1 \leftarrow (2a_1)^2(1e)^4(3a_1)^2,\ ^1A_1. \qquad (3.6)$$

The upper orbital closely resembles a 3s orbital of the N atom and the transition is optically allowed. Since this upper orbital is non-bonding in nature, the formation of a chemical bond with the 3s electron of Na should not cause sufficient change in the NH_3 structure to induce the dissociation of the molecule. It is possible, therefore, that the newly formed bond is between the 3s orbital of Na and the 3s Rydberg orbital of NH_3, with the ammonium molecule acting as a united atom. An additional factor, the close proximity in energy of these two orbitals, also favors bond formation between them. If this speculation is indeed true, the binding energy could be reasonably strong. For comparison, one may cite Na_2^+ which has a bond dissociation energy of 22 kcal/mol.

An open 3s orbital is quite large, with a radius of 1.713 Å for Na. [27] Instead of long range electron transfer, a direct interaction between Na and NH_3 may cause the overlap of their 3s orbitals. As mentioned earlier, the center of mass angular distribution peaks strongly backward with respect to the Na_2 beam. This anisotropic angular distribution suggests that the interaction which causes the reaction lasts a shorter time than the characteristic rotational period of the system, which is typically on the order of a picosecond. Since the Na-Na bond and the Na-NH_3 bond are of the same strength, it is essential that the collision energy and the energy from the formation of Na-NH_3 bond be channelled into the Na-Na coordinate "impulsively". To illustrate this, we borrow the concept of the

impulse approximation which is formulated to estimate the energy transfer of a collinear collision between an atom A and a diatomic molecule B-C. [28] It follows that the most efficient energy coupling of the translational motion between A and B-C into the B-C bond occurs with:

$$\frac{\Delta E}{E} = \frac{4M_A M_B M_C (M_A + M_B + M_C)}{(M_A + M_B)^2 (M_B + M_C)^2}, \qquad (3.7)$$

where M is the mass of each individual atom. Applying Equation (3.7) to A = NH_3 and B, C = Na, the fractional energy transfer, $\Delta E/E$, is calculated to be 67%, which is ~ 10 kcal/mol out of the 15.5 kcal/mol collision energy. This amount of energy is not sufficient to break the Na-Na bond. Additional energy must be found from the newly formed Na-NH_3 bond. In a collinear configuration, a fast contraction of the Na-NH_3 distance can effectively provide the necessary energy. At the same time, it also causes the vibrational excitation of the Na-NH_3 bond.

B. $Na_2 + CH_3OH \rightarrow Na(CH_3OH) + Na$.

The lowest electronic transition of CH_3OH was observed around 54,500 cm^{-1} (≈ 6.8 eV) by Harrison and coworkers. [29] Using this excitation energy as the electron affinity of CH_3OH (EA_v = - 6.8 eV), the crossing distance of the ionic and covalent potential curves of Na_2 + CH_3OH can be calculated to be 1.2 Å.(Equation (3.5)) As in the Na_2 + NH_3 case, the "Harpoon" Mechanism is again not applicable. The similarity between the angular distributions of Na(CH_3OH) and Na(NH_3) strongly suggests that both reactions follow the same mechanism, i. e. a close collision between Na_2 and CH_3OH followed by

bond formation between Na and CH_3OH. The necessary energy required to break the Na-Na bond is provided by initial impulsive impact as well as contraction of the newly formed chemical bond. The translation energy distribution of $Na(CH_3OH)$ is broader and the percentage of the average translation energy release out of the total available energy is higher.(cf. Table 4 on page 80) This can be explained qualitatively based on the results of the impulse approximation. In this model, the energy transferred from NH_3 to Na_2 is only 10 kcal/mol, while it is 21 kcal/mol for $Na_2 + CH_3OH$. It follows that less energy from the formation of the new chemical bond is needed for $Na_2 + CH_3OH$ to break a Na-Na bond. Therefore on average $Na(CH_3OH)$ products are internally cooler.

The strong binding between Na and CH_3OH suggests that the bond could also be Na^+-like, i. e. the bond is formed between the 3s orbital of Na and the 3s Rydberg orbital of CH_3OH.

Conclusions

We have observed $NaNH_3$ and $Na(CH_3OH)$ molecules in crossed molecular beam experiments from $Na + NH_3$ and $Na_2 + CH_3OH$. The binding energies $D_0(NaNH_3)$ and $D_0(Na(CH_3OH))$ are obtained to be 19 kcal/mol and 27.6 kcal/mol, respectively. The strong bonding between Na and close shell molecules suggests that the Rydberg orbitals of the molecules may play important roles in the chemical bonds.

Tables

Table 1: Properties of Na, Na_2, and Na_2^+ [5]

	Na	Na_2	Na_2^+
IP (eV)	5.139	4.9	—
D_0(eV)	—	0.72	0.96
r_0 (Å)	—	3.1	3.5

Table 2: Reaction pathways for $Na_2 + NH_3$ and $Na_2 + CH_3OH$

Reactants	Products	ΔD_0 (kcal/mol)
$Na_2 + NH_3 \rightarrow$	$NaNH_3 + Na$	- 0.6 [16] [22]
(E_c = 15.5 kcal/mol)	$NaNH_2 + NaH$	—
$Na_2 + CH_3OH \rightarrow$	$Na(CH_3OH) + Na$	—
(E_c = 26 kcal/mol)	$NaOCH_3 + NaH$	—
	$NaOH + NaCH_3$	—

Table 3: The vibrational frequencies of NH_3 and the thermal population at 473 K

Vibrational Modes	Frequencies (cm^{-1})	N (v=1) / N (v=0) (%)
Symmetric Deformation	932.5	5.9
Degenerate Deformation	1626.1	0.7
Symmetric Stretch	3336.2	0.0
Degenerate Stretch	3443.6	0.0

Table 4: Translation energy transfer in the impulse model and the average translation energy release

Reactions	E_{im} (kcal/mol)	E_{im}/E_{col} (%)	E'_{tr}/E_{av} (%)
$Na_2 + NH_3 \rightarrow NaNH_3 + Na$	10	67	38
$Na_2 + CH_3OH \rightarrow Na(CH_3OH) + Na$	21	82	42

References

[1] Y. T. Lee, R. J. Gordon, and D. R. Herschbach, J. Chem. Phys. **54**, 2410 (1971).

[2] P. B. Foreman, G. M. Kendall, and R. Grice, Mol. Phys. **23**, 117 (1972).

[3] W. S. Struve, J. R. Krenos, D. L. McFadden, and D. R. Herschbach, J. Chem. Phys. **62**, 404, (1975).

[4] H. Hou, K. T. Lu, V. Sadchenko, A. G. Suits, and Y. T. Lee, in "Gas Phase Chemical Reaction Systems: Experiments and Models: 100 years after Max Bodenstein" edited by G. C. Schatz and H. Volpp, (1996), in press.

[5] K. P. Huber and G. Herzberg, *Molecular Spectra and Molecular Structure, IV. Constants of Diatomic Molecules*, Van Nostrand Reinhold Company (1979).

[6] W. Weyl, Ann. Phys. (Leipzig) **197**, 601 (1864).

[7] March, *Advanced Organic Chemistry*, John Wiley & Sons (1992).

[8] C. E. Melton, J. Chem. Phys. **57**, 4218 (1972).

[9] I. V. Hertel, C. Hüglin, C. Nitsch, and C. P. Schulz, Phys. Rev. Lett. **67**, 1767 (1991).

[10] F. Misaizu, K. Tsukamoto, M. Sanekata, and K. Fuke, Chem. Phys. Lett. **188**, 241

(1991).

[11] C. Nitsch, C. P. Schulz, A. Gerber, W. Zimmermann-Edling, and I. V. Hertel, Z. Phys. **D 22**, 651 (1992).

[12] A. W. Castleman Jr., P. M. Holland, D. M. Lindsay, and K. I. Peterson, J. Am. Chem. Soc. **100**, 6039 (1978).

[13] C. Nitsch, C. Hüglin, I. V. Hertel, and C. P. Schulz, J. Chem. Phys. **101**, 6559 (1994).

[14] (a) V. A. Nicely, and J. L. Dye, J. Chem. Phys. **52**, 4795 (1970). (b) M. Trenary, H. F. Schaefer III, and P. Kollman, J. Am. Chem. Soc. **99**, 3885 (1977).

[15] J. C. Greer, C. Hüglin, I. V. Hertel, and R. Ahlrichs, Z. Phys. **D 30**, 69 (1994).

[16] K. Hashimoto, S. He, and K. Morokuma, Chem. Phys. Lett. **206**, 297 (1993).

[17] K. Hashimoto, and K. Morokuma, Chem. Phys. Lett. **223**, 423 (1994).

[18] K. Hashimoto, and K. Morokuma, J. Am. Chem. Soc. **116**, 11436 (1994).

[19] K. Hashimoto, and K. Morokuma, J. Am. Chem. Soc. **117**, 4151 (1995).

[20] H. F. Davis, A. G. Suits, Y. T. Lee, C. Alcaraz, and J.-M. Mestdagh, J. Chem. Phys. **98**, 9595 (1993).

[21] JANAF Thermochemical Tables, 3rd ed., J. Physical and Chemical Ref. Data 14, (1985), Supp. No.1.

[22] D. R. Lide, Editor-in-Chief, *CRC Handbook of Chemistry and Physics*, 74th edition (1993-1994).

[23] It was found that the Na dimer concentration dropped severely when the diameter of the nozzle was enlarged from 0.2 mm to 0.3 mm due to the corrosion from the molten/gaseous sodium.

[24] G. Herzberg, *Molecular Spectra and Molecular Structure, Vol. III, Electronic*

Spectra and Electronic Structure of Polyatomic Molecules, Van Nostrand Reinhold, Princeton, New Jersey (1966).

[25] W. B. Miller, S. A. Safron, and D. R. Herschbach, J. Chem. Phys. **56**, 3581, (1972).

[26] (a) Thompson, and Duncan, J. Chem. Phys. **14**, 573 (1946). (b) A. E. Douglas, Disc. Far. Soc. **35**, 158 (1963).

[27] J. C. Slater, *Quantum Theory of Matter*, McGraw Hill, New York (1968).

[28] (a) B. H. Mahan, J. Chem. Phys. **52**, 5221 (1970). (b) F. P. Tully, N. H. Cheung, H. Haberland, and Y. T. Lee, J. Chem. Phys. 73, 4460 (1980).

[29] A. J. Harrison, B. J. Cederholm, and M. A. Terwilliger, J. Chem. Phys. **30**, 355 (1959).

Figure Captions

Figure 3.1 The Newton diagram for Na_2 + NH_3 at a nominal collision energy of 15.5 kcal/mol. Θ_{CM} denotes the laboratory angle of the center of mass velocity vector for Na_2 + NH_3. In the center of mass coordinate, the direction of the Na_2 beam is defined as $\theta = 0^o$, whereas the direction of the NH_3 beam is $\theta = 180^o$. The circle encloses the region in which the $NaNH_3$ products are expected to appear.

Figure 3.2 Time-of-flight spectra measured for m/e = 40 ($NaNH_3^+$) at a collision energy of 15.5 kcal/mol. The open circles are the experimental data, whereas the solid lines indicate the best fit using P(E) and $T(\theta)$ shown in Figure 3.4.

Figure 3.3 Laboratory angular distribution of the $NaNH_3$ products. The open circles are the experimental data, whereas the solid line is the best fit using P(E) and $T(\theta)$ shown in Figure 3.4.

Figures

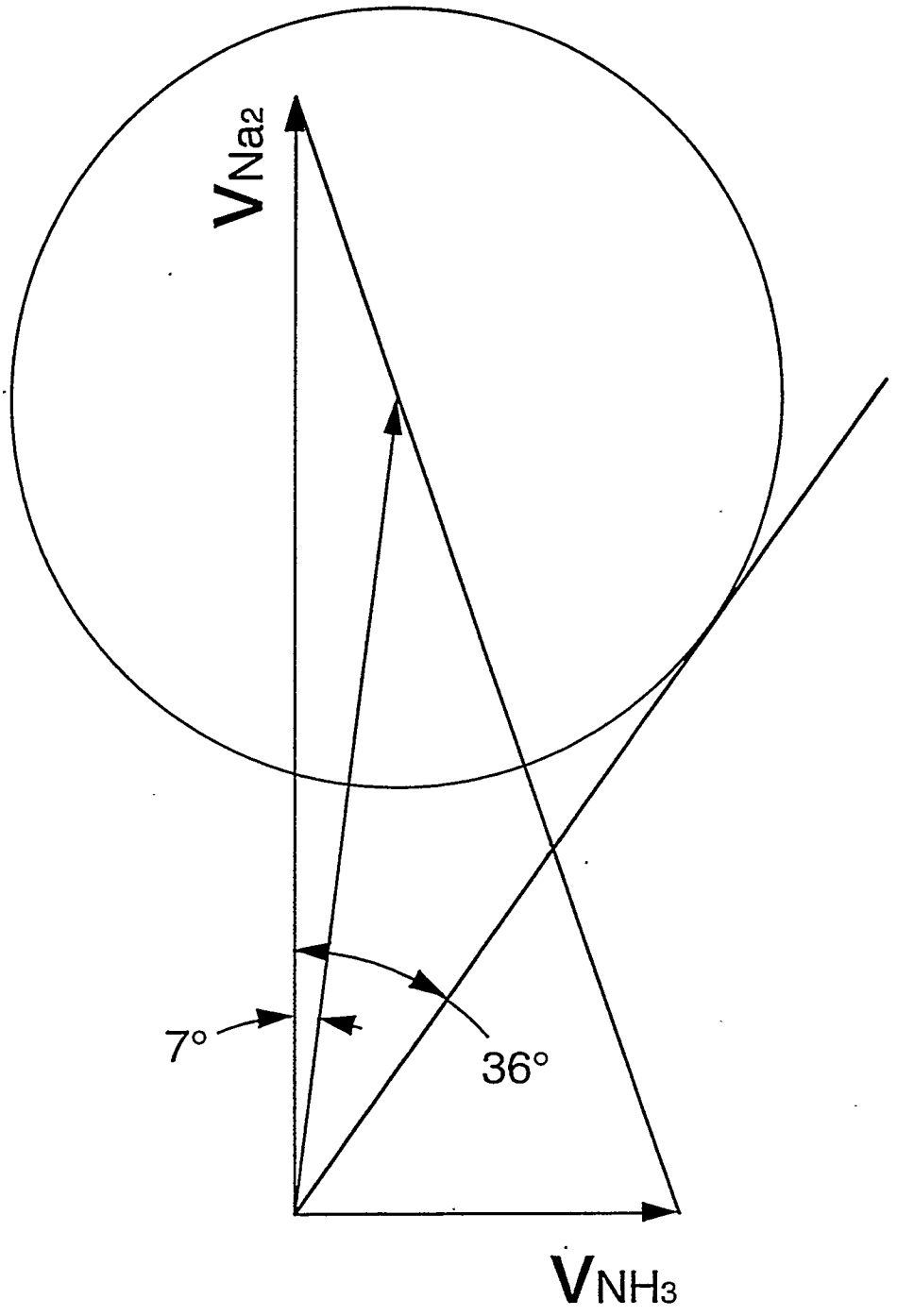

Figure 3.1

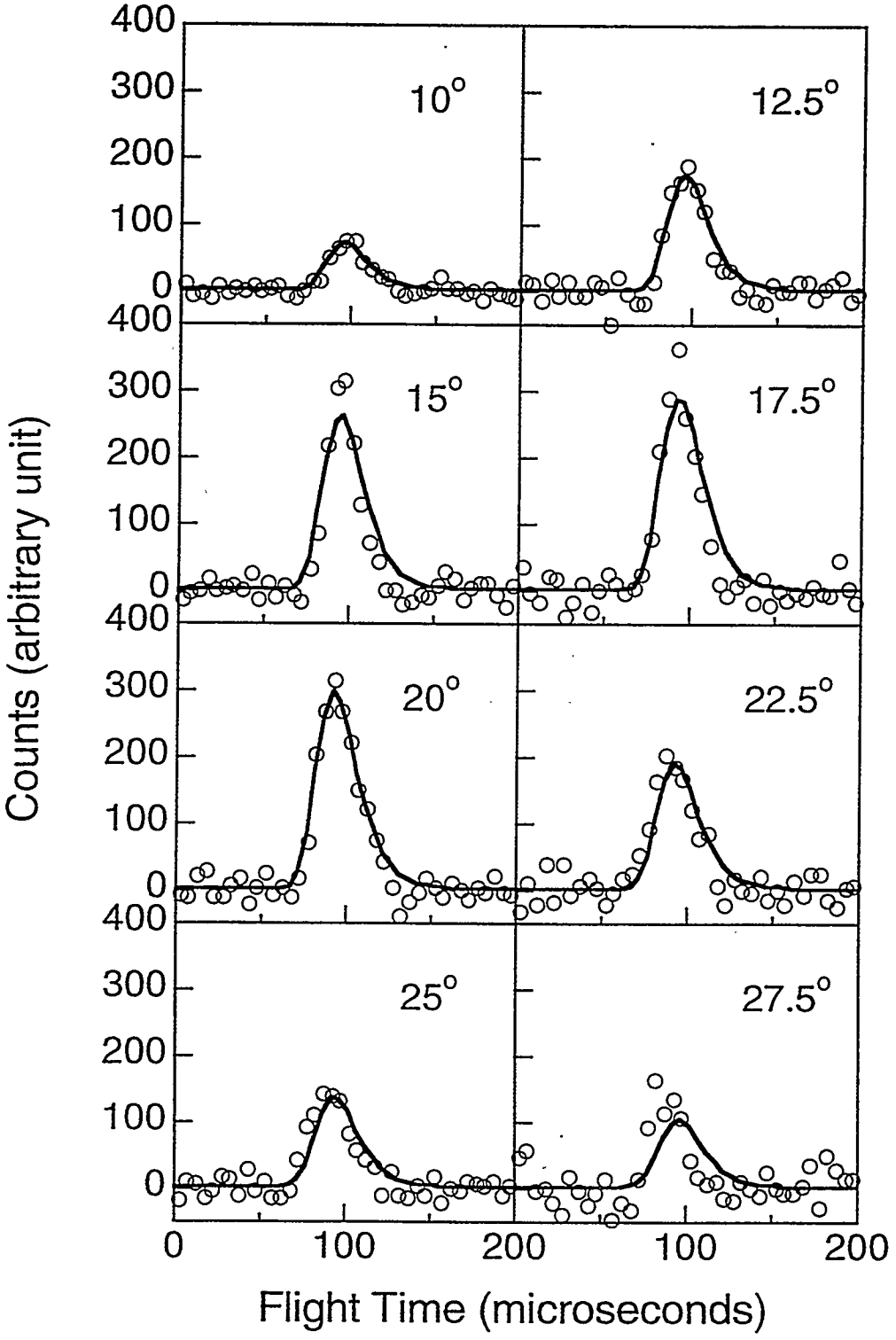
10°
12.5°
15°
17.5°
20°
22.5°
25°
27.5°
400
300
200
100
0
Counts (arbitrary unit)
0
100
200
100
200
Flight Time (microseconds)

Figure 3.2

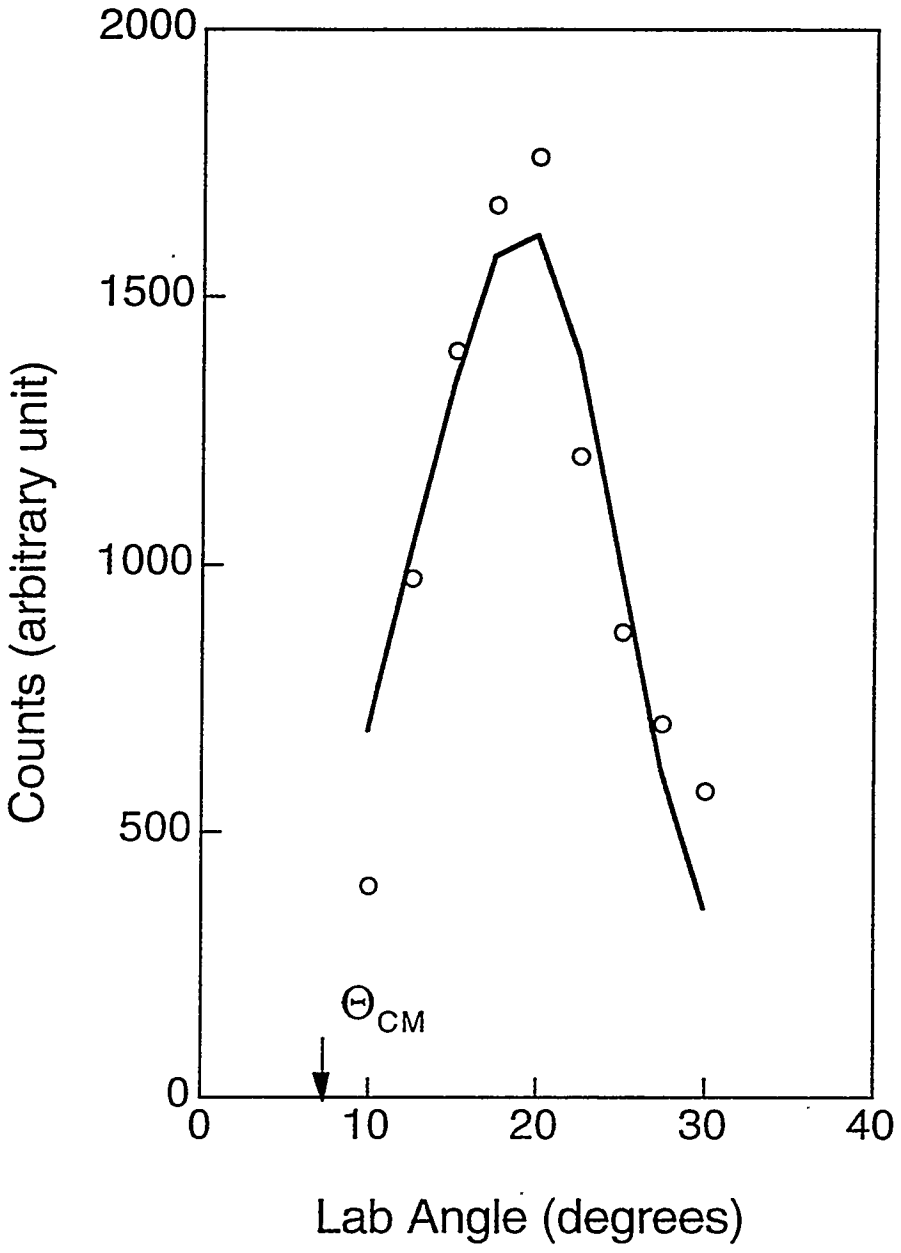
2000
1500
1000
500
0
Counts (arbitrary unit)
Θ_{CM}
0
10
20
30
40
Lab Angle (degrees)

Figure 3.3

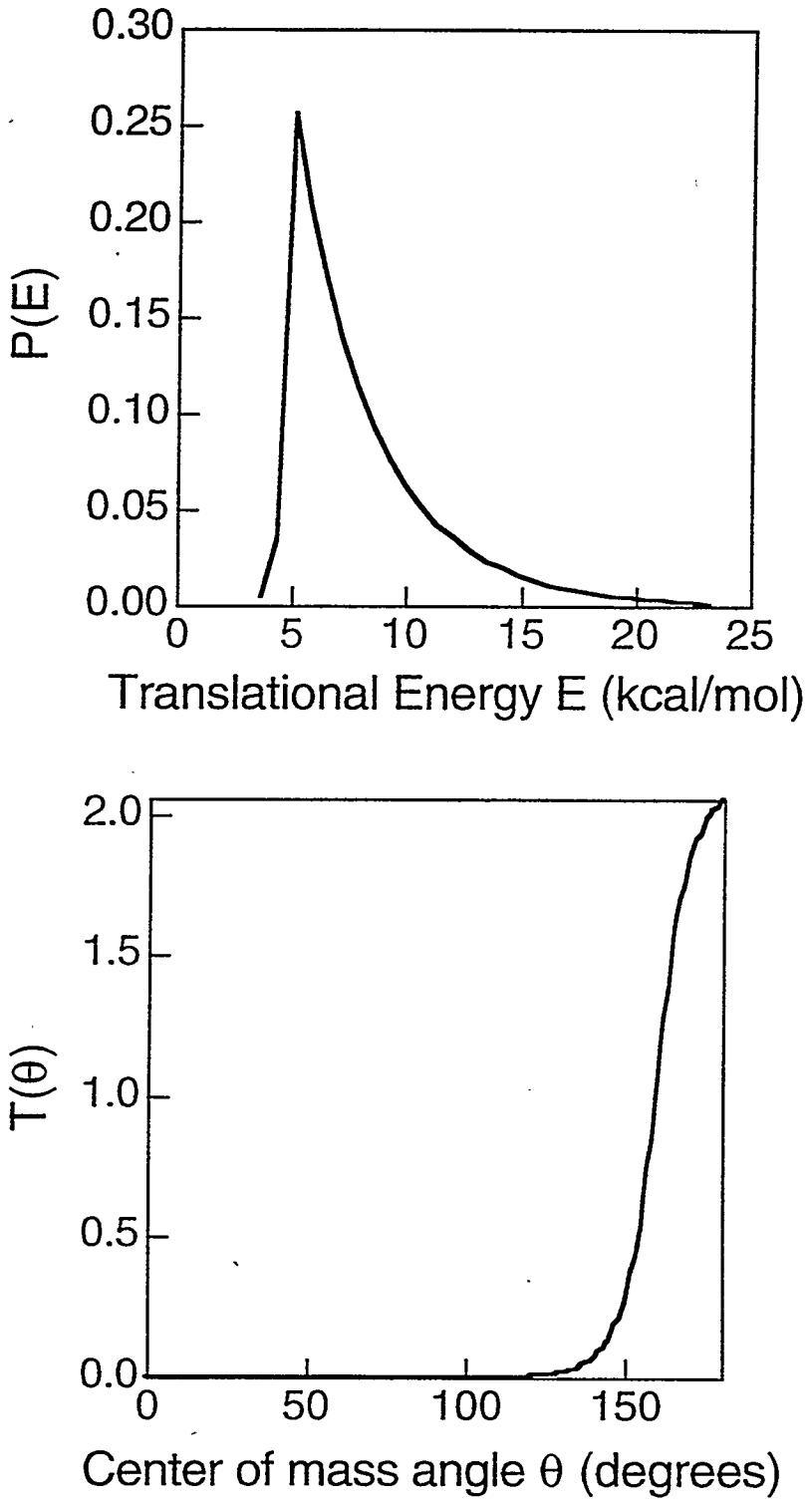
0.30
0.25
0.20
0.15
0.10
0.05
0.00
P(E)
0
5
10
15
20
25
Translational Energy E (kcal/mol)
2.0
1.5
1.0
0.5
0.0
T(θ)
0
50
100
150
Center of mass angle θ (degrees)

Figure 3.4

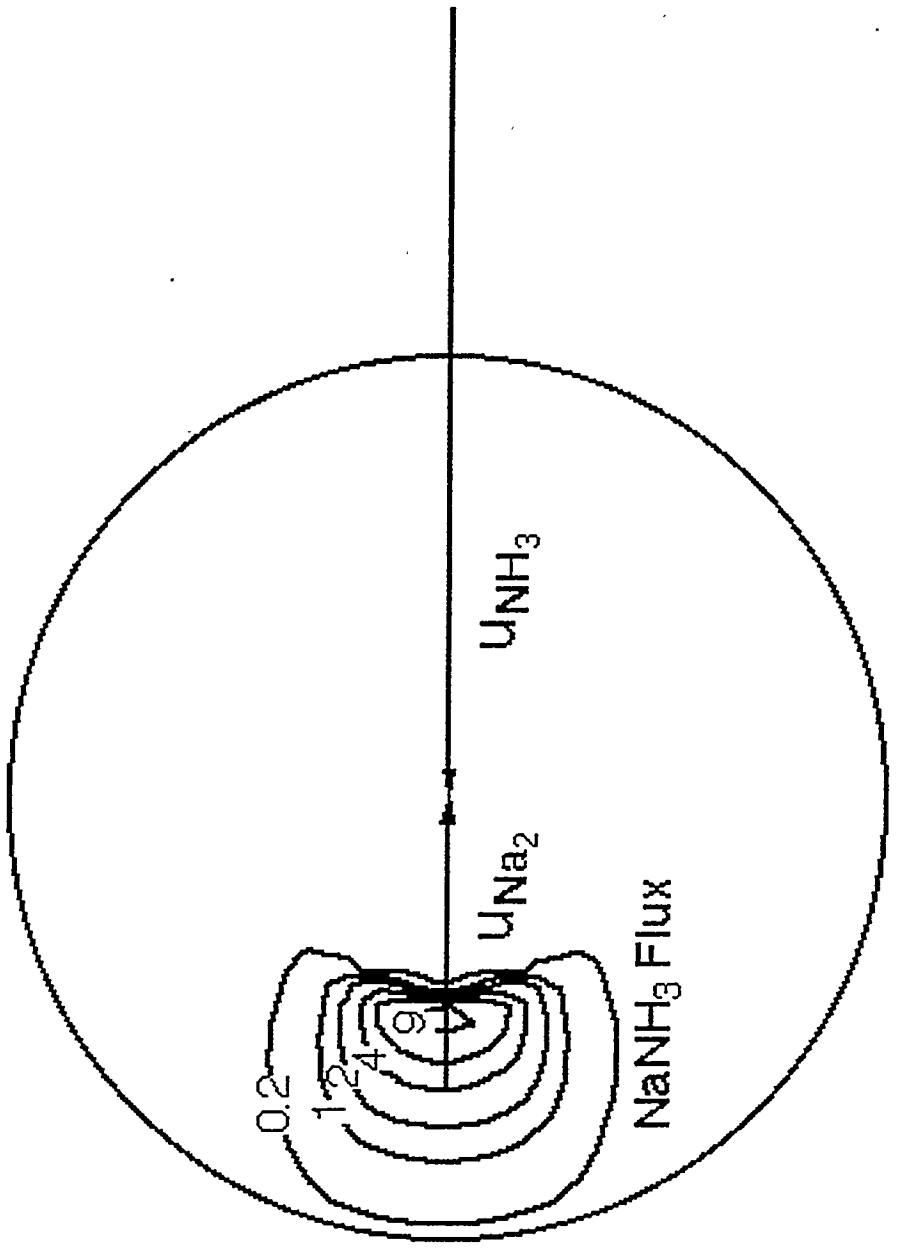

Figure 3.5

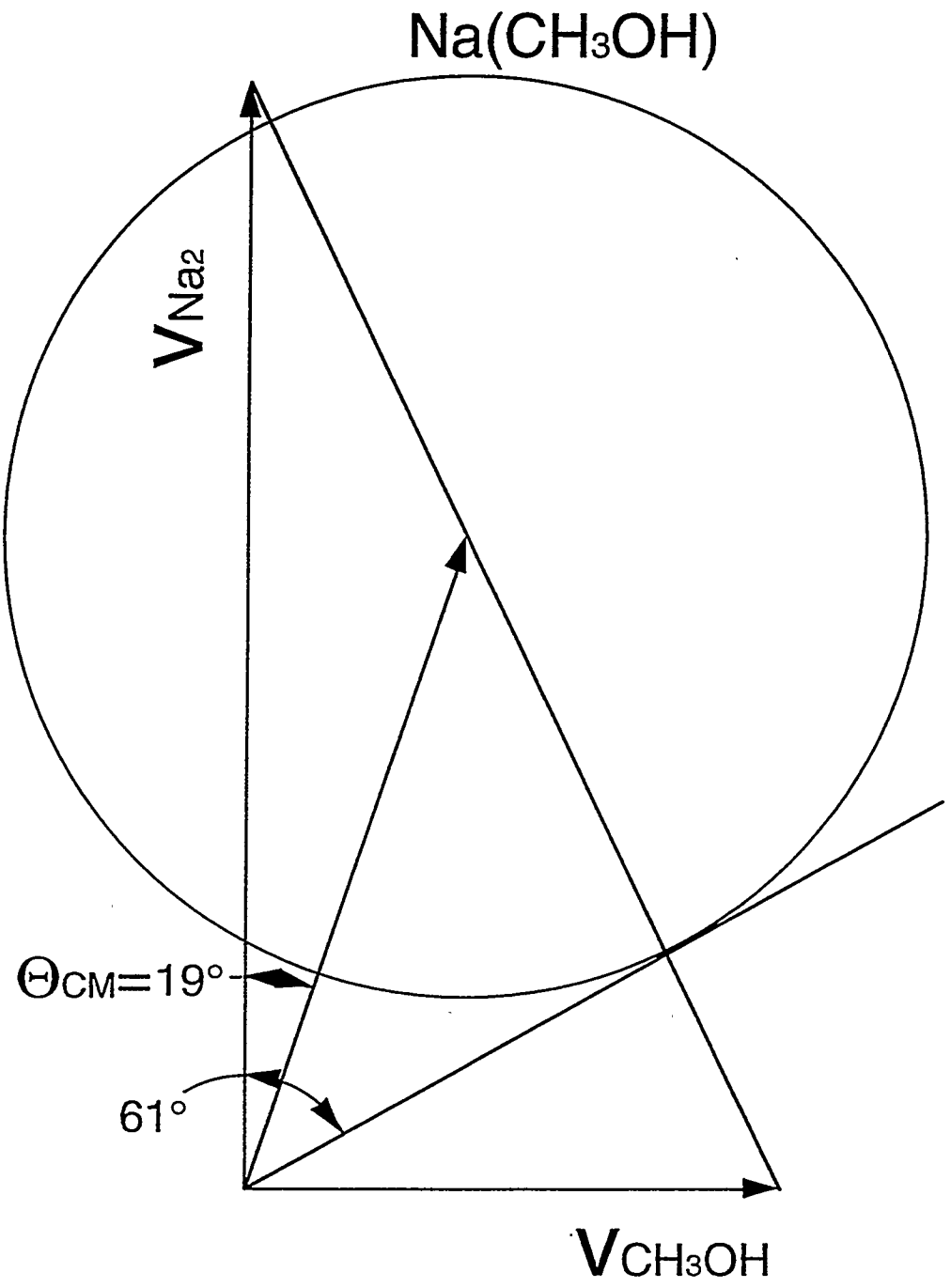

Figure 3.6

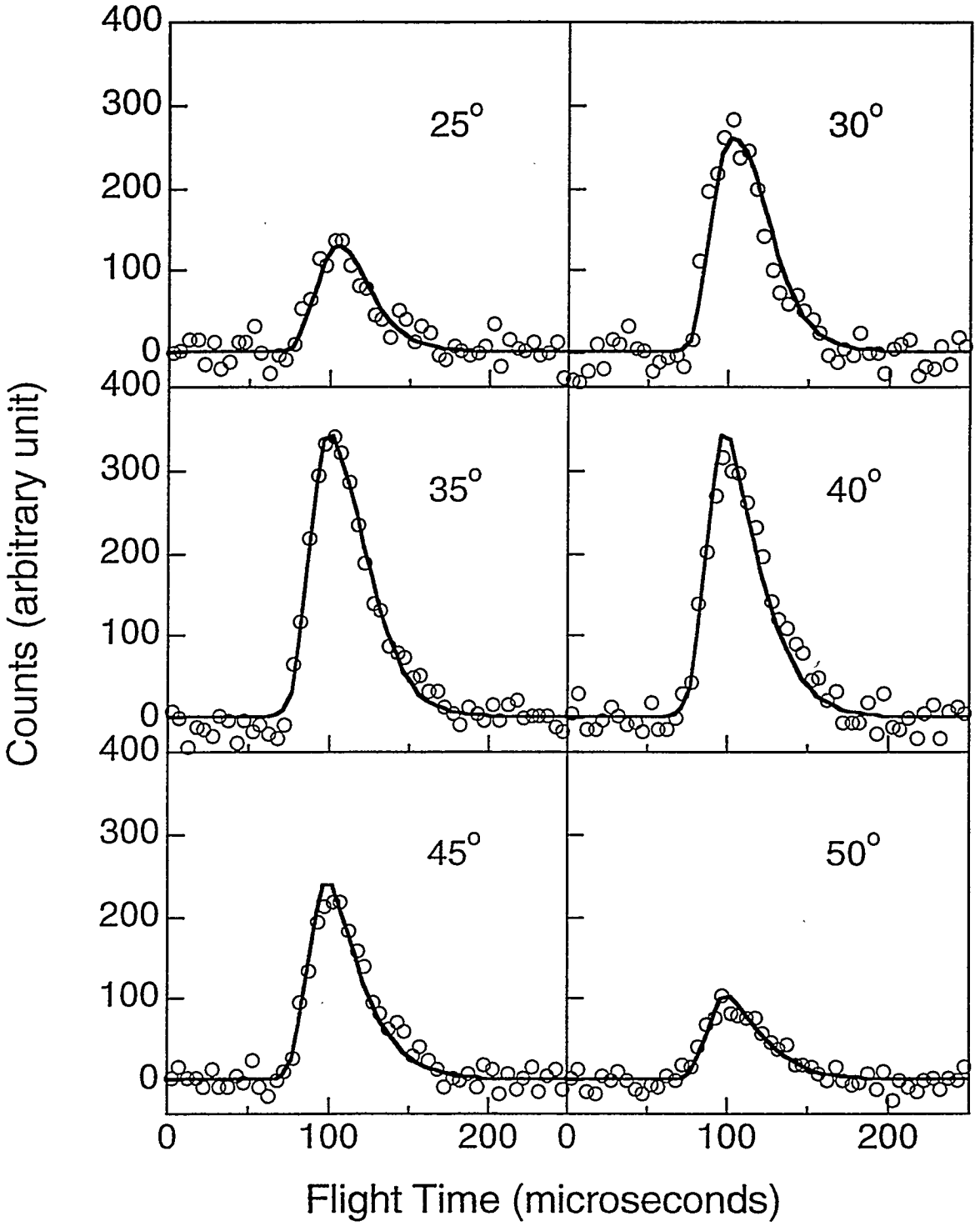
25°
30°
35°
40°
45°
50°
Counts (arbitrary unit)
Flight Time (microseconds)
0
100
200
300
400

Figure 3.7

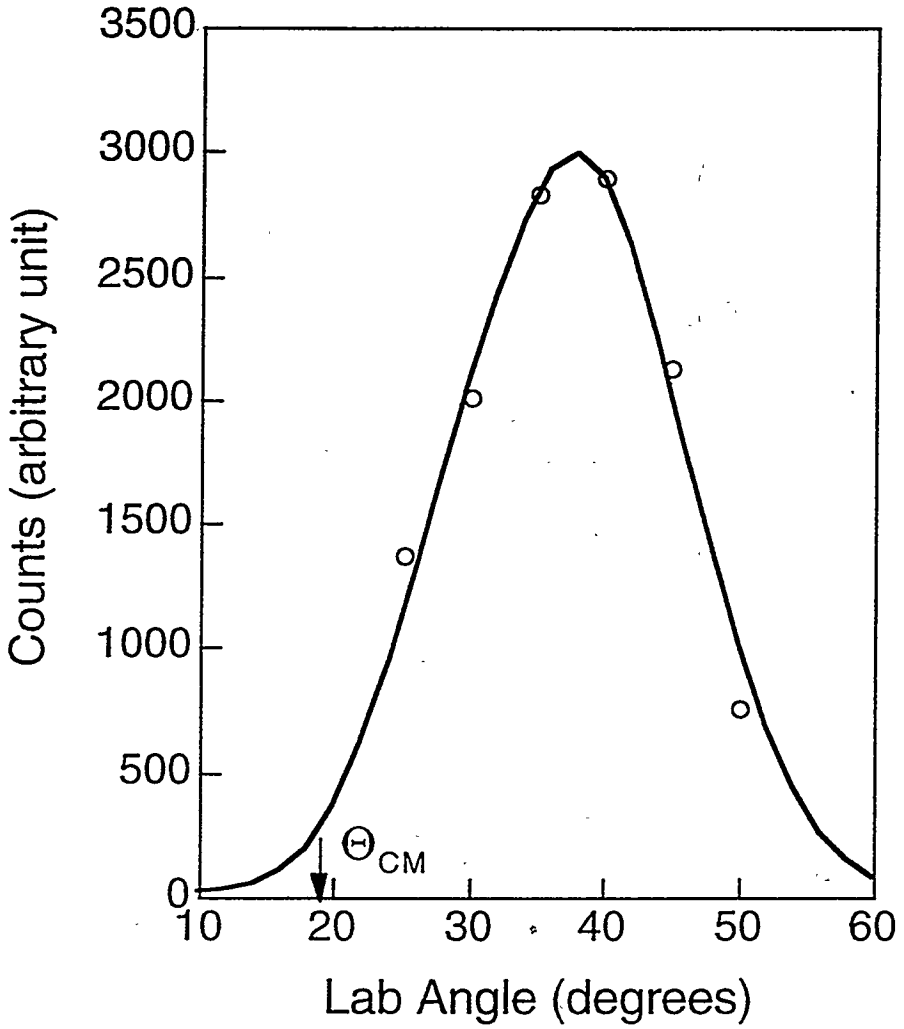
3500
3000
2500
2000
1500
1000
500
0
Counts (arbitrary unit)
Θ_{CM}
10
20
30
40
50
60
Lab Angle (degrees)

Figure 3.8

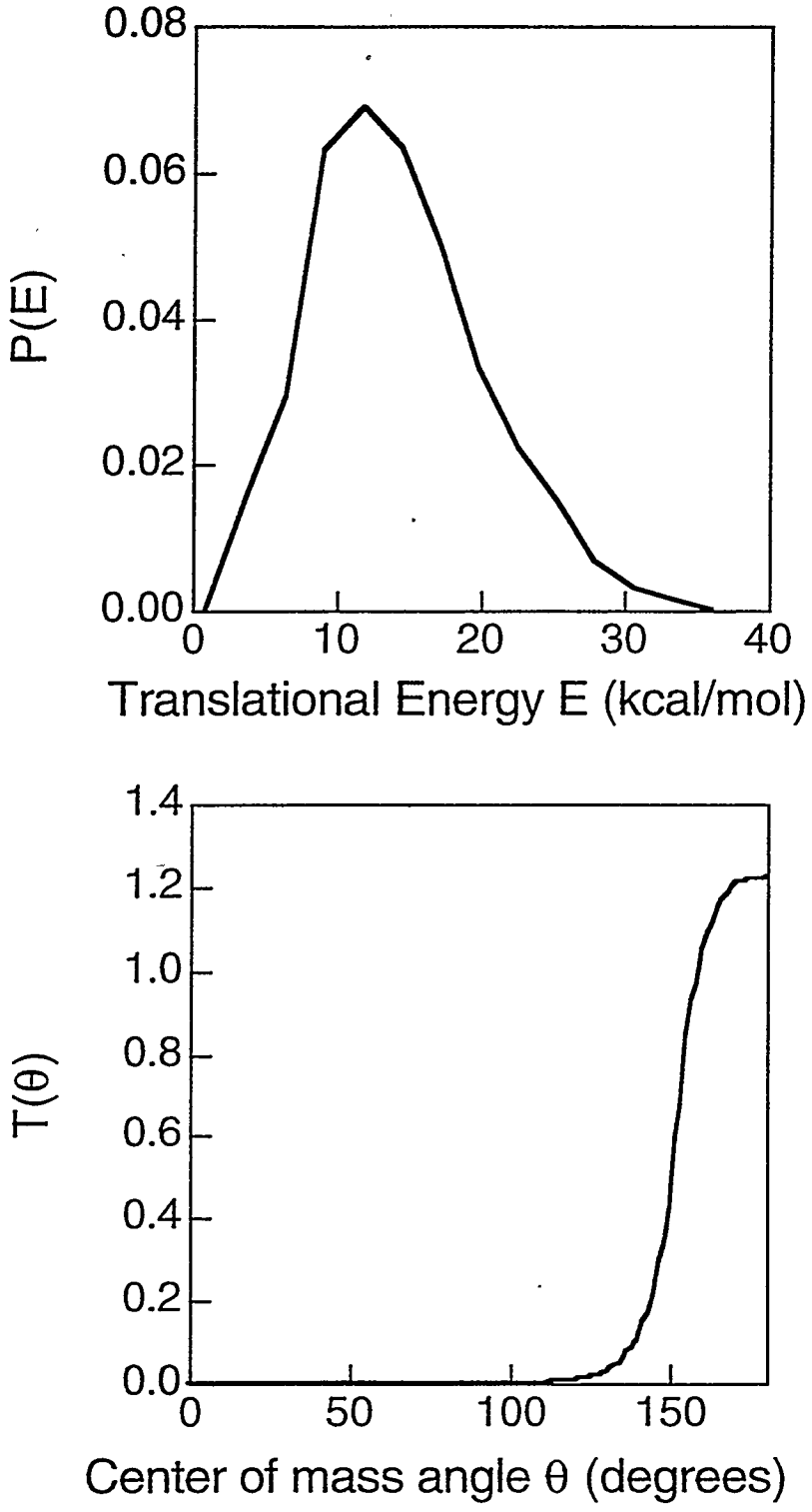
0.08
0.06
0.04
0.02
0.00
P(E)
0
10
20
30
40
Translational Energy E (kcal/mol)
1.4
1.2
1.0
0.8
0.6
0.4
0.2
0.0
T(θ)
0
50
100
150
Center of mass angle θ (degrees)

Figure 3.9

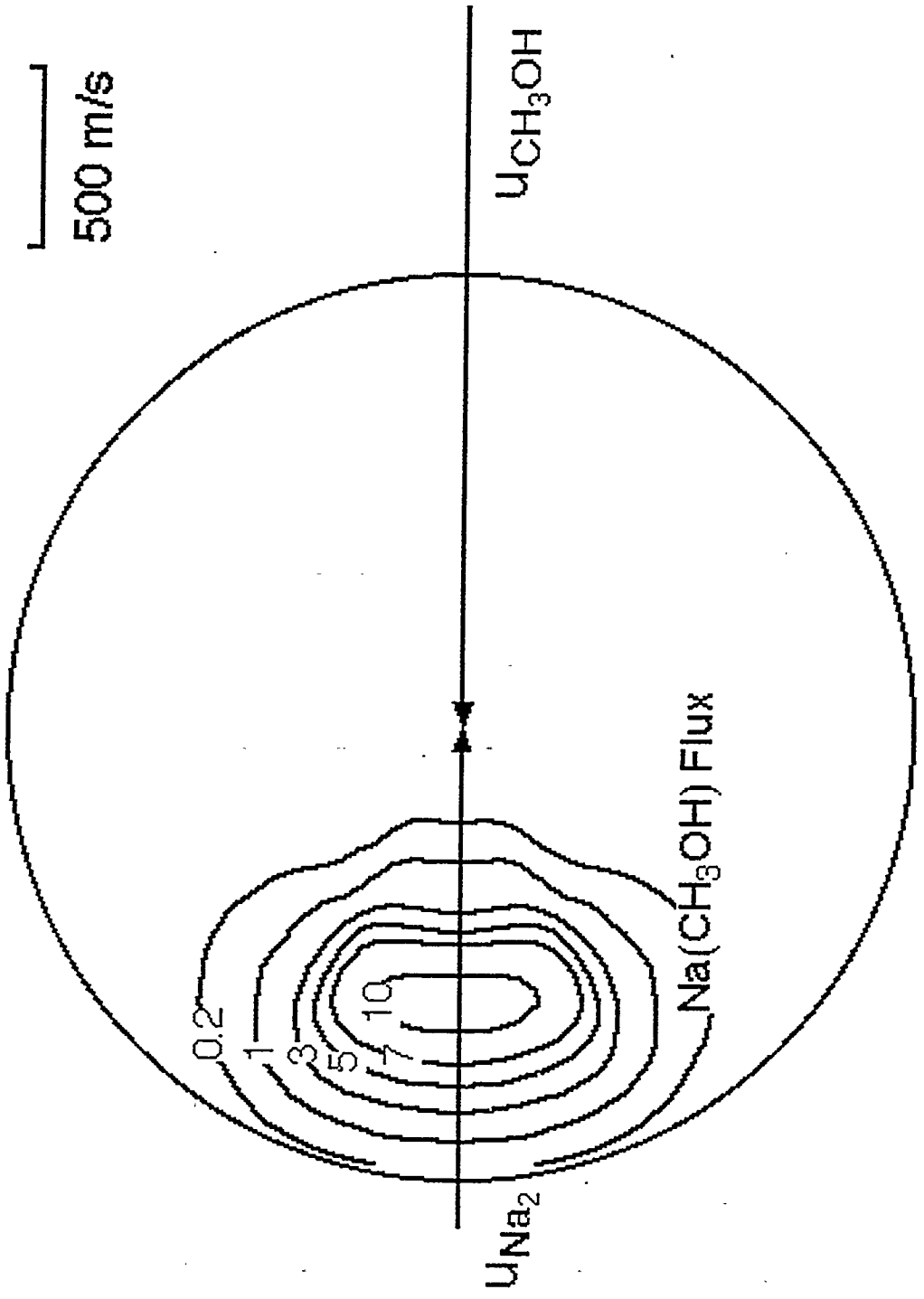

Figure 3.10

Chapter 4

Collisional Excitation of Na(4D) by Oxygen Molecules*

Abstract

Scattering of Na(4D) with ground state O_2, N_2, NO and CO molecules at a collision energy of 16 kcal/mol was studied in a crossed molecular beam apparatus. An inelastic scattering process producing Rydberg Na was observed only for the Na(4D) + O_2 system. The time of flight spectra and angular distribution of the Rydberg products show that most of the collision energy is turned into the electronic excitation of Na. High lying Rydberg states were observed with lifetime as long as 350 μs. A simple treatment based on classical mechanics is carried out to account for the experimental data.

Introduction

Chemical reactions can be affected or even controlled by judicious choice of the electronic states of the reactants, as demonstrated in the study of the reactions of Ba($6s^2$-$^1S_0$) and Ba(6s5d-$^1D_2$) with water and methanol. [1] Electronic excitation can change the course of a reaction by either simply adding energy into the chemical system to overcome barriers along the reaction coordinates, or changing the topologies of the potential energy surfaces. It is important to understand the role of the electronic excitation in the study of reaction dynamics.

The interactions of the sodium atoms in their 3S, 3P, 4D and 5S states with oxygen

---

* This chapter is based on H. Hou, K. T. Lu, A. G. Suits, and Y. T. Lee, to be submitted to J. Chem. Phys. The experimental work is that of H. Hou, who is the responsible author.

molecules were studied in a previous crossed beam experiment in which a strong inelastic scattering signal was observed only when Na was excited to the 4D state. [2] [3] The signal appeared at a threshold translational energy of ~ 11 kcal/mol. The angular distribution of the signal showed a strong dependence on the alignment of the 4D orbital of Na with respect to the relative velocity, implying that the symmetry of the electronic configuration is crucial in determining the outcome of the scattering. In spite of the great effort made in the study, the identity of the products remained uncertain. In this paper, we report our follow-up measurements which definitively determined the chemical nature of the products from Na(4D) + O_2 scattering. A simple model to interpret the data is proposed.

Experimental

The details of the experimental setup can be found in many previous publications. [4] Briefly, a supersonic beam of Na and a supersonic beam of O_2 are crossed orthogonally under single collision conditions. Na(4D) was prepared at the interaction region using two single frequency ring dye lasers via a stepwise excitation scheme. [2] The laser beams are perpendicular to the scattering plane. Both lasers are linearly polarized and the direction of the polarization can be rotated in the scattering plane. Scattered products are detected with a triply differentially pumped mass spectrometer which is rotatable about the interaction region in the scattering plane. A mechanical chopper wheel can be mounted just outside the entrance of the detector for the time of flight measurement. The schematic drawing of the detector is shown in Figure 4.1.

In the experiment, the detector could be set in two detection configurations: The first configuration(Configuration I), which was used in most of the previous measurements, uses a tungsten filament as the electron bombardment ionizer, with the ion lenses

set at the optimal voltages to extract ions formed at the ionizer region, the quadrupole mass filter tuned at a certain mass to charge ratio, and the high voltage electrode in the Daly counter region at -30 kV. Using this configuration, time-of-flight spectra for the neutral scattering products could be recorded, with the flight length measured from the chopper wheel to the ionizer.

In the cases when the scattering processes produce long-lived Rydberg state atoms or molecules, which can survive the long flight path until they arrive at the Daly detector region, where they can be field ionized, the detector can be set at a different configuration (Configuration II). In this configuration the electron bombardment ionizer and its associated ion optics are all turned off while the settings of the Daly detector are unchanged. In this way the time-of-flight spectra of the products can be recorded as the products fly from the chopper wheel to the Daly detector region. If the Rydberg signal is laser related as is the case in our experiment, no ions are produced when either or both of the lasers are tuned off the excitation line because under our experimental conditions only the Rydberg atoms or molecules can be ionized by the electric field. Therefore the angular distribution of the products can be obtained by directly measuring the ion counts at different angles.

Results and Analysis

For Na(4D, 3S) + O_2 at a nominal collision energy of 16 kcal/mol, the time of flight spectra at a lab angle of 25 degrees taken under Configuration I with the quadrupole mass filter set at m/e = 23 for Na^+ are shown in (a) and (b) of Figure 4.2. The corresponding Newton diagram is given in Figure 4.3. The fast peaks at ~50 μs are the elastic scattering signals which are nearly the same for the ground and excited Na. This implies that the attenuation of ground state scattering by laser excitation is insignificant and the fraction of

the excited Na is very small, unless elastic scattering of the ground and excited Na off O_2 follow exactly the same mechanism. The most striking feature arrives at ~ 120 μs for the Na(4D) scattering, and appears even stronger than the elastic scattering. Besides this strong peak, there are also laser dependent products arriving at a much later time (~ 330 μs), corresponding to the atoms that fly extremely slowly in the laboratory frame and also ionized at the electron bombardment ionizer. In the center of mass coordinates, these extremely slow products could only be the ones that were produced with large velocities flying away from the detector. Due to the cylindrical symmetry with respect to the relative velocity in this experiment, there should exist a fast signal corresponding to the extremely slow one that scatters toward the detector. This faster signal was not seen. The slow signal was also seen in the previous experiment [2] [3] but the mechanism was not fully understood.

Two simple tests were done to examine the nature of the slow signal in (a) of Figure 4.2. The first test was to tune the mass filter to allow an odd m/e other than m/e = 23 to transmit. In this way, Na^+ ions formed in the electron bombardment region were not able to reach the Daly ion counter. The second test was to turn the ionizer off so that no ions were formed in the electron bombardment region. The time of flight spectra thus obtained are shown in (c) and (d) of Figure 4.2 respectively for the same lab angle. In both tests the elastic scattering peaks disappeared, as expected. The strong laser related peak at ~ 120 μs also went away, proving that it is truly the Na^+ from electron bombardment ionization. On the other hand, the later-arriving signals persist in both tests. These results reveal two facts: First, these signals are not affected by the mass filter, which shows that the ions are not formed in the electron bombardment region. Second, there exist means other than

electron bombardment that can ionize the scattered products at farther distances away from the chopper wheel than the filament ionizer. In fact, we found that an electric field as low as 25 V/cm would give rise to the ion signal, which became stronger with the increase of the electric field.

These facts lead to one logical conclusion: Long-lived Rydberg state Na(nl) are formed in the collision of Na(4D) with O_2. Some of these Rydberg products are ionized by electron bombardment and then mass selected and counted, while some of the remaining ones are subsequently field ionized by the electric field along the flight path, resulting in multiple peaks in the time of flight spectra.

Since the distance from the chopper wheel to the filament can be accurately determined, it is the best to analyze the ion signals generated by the electron bombardment. Figure 4.4 shows the time of flight signals at selected laboratory angles for the Rydberg products which are ionized in the electron bombardment region. In the same figure, the simulation of the experimental data [5] is also given for each angle, assuming the center of mass angular distribution $T(\theta)$ and energy distribution P(E) shown in Figure 4.5.

The angular distribution of the Rydberg products measured using detector Configuration II described in the experimental section of this chapter is shown in Figure 4.6. Strictly speaking the signals so measured are not exactly the same as those measured with Configuration I because some Rydberg state Na might decay to lower lying states along the path from the filament to the Daly counter and the field strength in the latter region is not sufficient to ionize these decayed atoms. Nevertheless, after comparing this angular distribution with the one obtained by integrating the time of flight spectra shown in Figure 4.4, we find no noticeable difference between them. The same $T(\theta)$ and P(E) used for the

simulation of time of flight spectra also generate a satisfactory fit to the angular distribution.

The alignment effects reported previously [2] [3] are not observed in the current experiment. NaO molecules from the reactive scattering $Na + O_2 \rightarrow NaO + O$, which were proposed previously as the sources of the laser related Na^+ signal, [2], [3] were not observed either. Similar experiments were also carried out using N_2, NO and CO molecules in place of O_2, in which cases no Rydberg products were detected.

Discussion

The energetics of the $Na(nl) + O_2$ system is shown in Figure 4.7. Two-photon excitation brings 98.7 kcal/mol to the sodium atoms which in their 4D state are only 19 kcal/mol below their ionization limit. The additional 16 kcal/mol nominal collision energy is certainly enough to produce Rydberg state Na. The ionic state $Na^+ + O_2^-$ is also within the reach of the system.

From the translational energy distribution P(E), it is evident that most of the collision energy is transferred to the electronic excitation of Na and possibly the vibrational and rotational excitation of the O_2 so that the center of mass velocity of the Rydberg products is very slow. Consequently most of the signal appeared in a range that is very close to the center of mass angle, resulting in a very narrow angular distribution as shown in Figure 4.6. For the same reason, the Jacobian for the center of mass $\rightarrow$ laboratory transformation [6] v/u^2 is very large, where v and u are velocities in the lab and center of mass coordinates, respectively. Therefore the recorded signals are severely distorted, especially near the center of mass angle. This is one of the reasons that at some angles the Rydberg signals appear even stronger than the elastic scattering signal. A second reason lies in the

fact that the ionization probability for the Rydberg products could be orders of magnitude higher in the electron bombardment region compared with that of the ground state Na, which is typically 10^{-4}. [2] Taking these factors into account, the cross section for producing Rydberg Na is estimated to be of the same order of magnitude as that for the elastic scattering.

The time that Rydberg products remain in the highly excited electronic states has to be extremely long in order for them to survive the long flight into the Daly counter region and became field ionized. Figure 4.2 shows that the products live in these Rydberg states for at least 350 μs (without even taking into account the flight time from the interaction region to the chopper wheel) before they are finally ionized, indicating that the products are in very high n and/or l states. [7] Evidence is also found from the fact that an electric field as low as 25 V/cm can produce an ion signal. Classically, the field required to ionize a Rydberg atom in state nl is: [7], [8]

$$E = 1/(16n^4)\ a.u. \qquad (4.1)$$

Thus a field of 25 V/cm can ionize atoms with $n \approx 40$.

Therefore we can conclude that during the collision, most of the translational energy is turned into the electronic excitation of Na to form the highly excited Rydberg products. However, we have also learned from similar experiments where N_2, NO and CO molecules were used in place of O_2 that "brute force" collisions do not lead to Rydberg products. In these parallel experiments, N_2, NO and CO molecules have nearly the same mass as O_2 so that the kinematics of the scattering system are virtually unchanged. These results suggest that an unique intermediate leading to electronic excitation must exist during the collisional process for Na(4D) + O_2.

The various collisional processes of alkali atoms with oxygen molecules have been investigated extensively during the past fifteen years. Previous laboratory studies showed that electronic excitations of the alkali atoms $M + O_2 \rightarrow M^* + O_2$ were the main processes in the collisions of ground state alkali atoms with oxygen molecules at collision energies of 2 ~ 10 eV. [9] In the $Na + O_2$ collision, Na D-line fluorescence was observed as soon as the collision energy was above the $3P \leftarrow 3S$ excitation energy of 2.1 eV, with its intensity becoming stronger as the collision energy was increased. When the collision energy was above 8 eV, fluorescence from higher electronic states appeared. The cross section for this process was found to be 26 $Å^2$ at a collision energy of 5 eV. Hertel's group studied quenching in the collisions of electronically excited sodium with O_2. [10] In all these investigations, the ionic intermediate $M^+O_2^-$ was found to be necessary to cause the change of the electronic states of the alkali atoms.

It is therefore reasonable to conclude that the production of the Rydberg Na proceeds via the formation of an $Na^+O_2^-$ ionic complex which possesses unique characteristics distinguishing it from the complexes formed between Na and other molecules. The uniqueness of the $Na(4D) + O_2$ system could also come from the non-adiabatic interactions between the covalent and ionic potential energy surfaces. A detailed solution of the dynamics is difficult to obtain because there exist a large number of electronic states in the vicinity of the ionic-covalent interactions of the system over a wide range of the scattering coordinate. Still, it is useful to describe the behavior of the system qualitatively with a simple classical model [11] which can also provide a straight forward method in predicting the outcomes for other scattering systems.

Electronic excitation of Na can be viewed as a process in which one electron is

promoted to the orbitals having larger radii. Because the radius of a Rydberg atom is usually a few hundred angstroms, Na can be excited to long-lived Rydberg states in the collision with O_2 only if O_2 has the chance and ability to pull an electron to a much larger distance from the core of the sodium atom. One necessary condition is that after charge transfer, the two charged particles in the coulomb field can be separated to a distance that is much greater than at charge transfer. In the center of mass coordinates, this is equivalent to:

$$r_{max} >> r_c, \tag{4.2}$$

where r_{max} is the maximum separation between the positive and negative charge centers in the ionic complex and r_c is the charge transfer radius. At r_{max}, the radial velocity becomes zero, and the centrifugal force resulting from the angular motion is balanced by the Coulomb attraction between the ions:

$$\frac{2E_c b^2}{r_{max}^3} = \frac{14.4}{r_{max}^2}, \tag{4.3}$$

where E_c is the collision energy in eV and b is the impact parameter in Å. It follows that:

$$r_{max} = (2E_c b^2/14.4). \tag{4.4}$$

Therefore Equation (4.2) can be re-written as:

$$b \gg \sqrt{\frac{14.4}{2E_c} r_c}. \tag{4.5}$$

Here E_c takes the unit of eV while b is in Å. Equation (4.5) is equivalent to the requirement that after charge transfer, the system is set at the outer turning point on the effective potential energy surface (including the centrifugal term) because the condition

$$(dr/dt)_{r=rc} >> 0 \qquad (4.6)$$

will lead to the same result as Equation (4.5). At the same time the simple condition,

$$b \leq r_c, \qquad (4.7)$$

has to be satisfied for the charge transfer to take place. It follows from Equation (4.5) and Equation (4.7) that

$$r_c \gg \frac{14.4}{2E_c} \text{ (Å)}. \qquad (4.8)$$

For a typical value, E_c = 16 kcal/mol (0.7 eV), r_c has to be much larger than 10 Å. In Table 1, numerical values for the charge transfer distance r_c and the maximum separation r_{max} are listed for several (Na(nl) + Molecule) systems at E_c = 16 kcal/mol. r_c is calculated using the equation:

$$r_c = \frac{14.4}{IP - EA} \text{ (Å)}, \qquad (4.9)$$

where IP is the ionization potential of Na(nl) and EA is the electron affinity of the molecule, both in eV. r_{max} is calculated for $b = r_c$. The equation shows that at this collision energy, only Na(4D) + O_2 system has the opportunity to produce a well separated ($Na^+...O_2^-$) ion pair, largely due to the close match of the ionization potential of Na(4D)

with the electron affinity of O_2 and the resulting large electron transfer radius r_c. Under these conditions, the nearly parallel covalent and ionic potential energy curves could have a strong interaction over a wide range and the probability for the electron to undergo a nonadiabatic transition is strongly enhanced. It is also worth noticing how sensitive r_{max} is to the slight difference in (IP - EA), which is likely to be the reason why no long-lived Rydberg products were observed in Na(5S) + O_2 scattering. For the systems having small electron transfer radius, increasing the collision energy might help to excite Na, although in an inefficient way. For instance, let us examine the collisional excitation process Na(3S) + O_2 → Na(Rydberg) + O_2, which has a charge transfer distance of 3.1 Å. According to Equation (4.4), in order to reach a maximum separation of 100 Å, E_c must be at least 75 eV. Confirmation can be found in the experiments of Kleyn and coworkers on the charge transfer processes M + O_2 → M^+ + O_2^- at collision energies ranging from 4 to 2000 eV, [12] [13] which is high enough to remove an electron from the alkali atom completely.

Conclusion

It appears that the inelastic signal observed in the Na(4D) + O_2 experiment results from a energy resonance between the covalent and ionic states. The topologies of the potential energy surfaces have little influence on the scattering results.

Tables

Table 1: Charge transfer distances (r_c) and maximum separations of the ion pairs at a collisional energy of 16 kcal/mol, calculated with Equation (4.4) and Equation (4.9).

Chemical System	IP - EA (eV) [14]	r_c (Å)	r_{max} (b = r_c) (Å)
Na(3S) + O_2	4.7	3.1	0.9
Na(3P) + O_2	2.6	5.5	3.0
Na(5S) + O_2	0.57	25.3	62.0
Na(4D) + O_2	0.41	35.1	120.0
Na(4D) + N_2	2.8	5.2	2.6
Na(4D) + NO	0.83	17.3	29.0
Na(4D) + CO	2.4	6.1	3.6

References

[1] H. F. Davis, A. G. Suits, Y. T. Lee, C. Alcaraz, and J. -M. Mestdagh, J. Chem. Phys.**98**, 9595 (1993), and the references therein.

[2] P. S. Weiss, Ph. D. Thesis, "The Reaction Dynamics of Electronically Excited Alkali Atoms with Simple Molecules", University of California, Berkeley, March 1986.

[3] P. S. Weiss, M. H. Covinsky, H. Schmidt, B. A. Balko, Y. T. Lee, and J. M. Mestdagh, Z. Phys. D — Atoms, Molecules and Clusters **10**, 227 (1988).

[4] (a) Y. T. Lee, J. D. McDonald, P. R. LeBreton, and D. R. Herschbach, Rev. Sci. Instrum. **40**, 1042 (1969). (b) H. F. Davis, A. G. Suits, and Y. T. Lee, J. Chem. Phys. **96**, 6710 (1992).

[5] P. E. Siska, J. Chem. Phys. **59**, 6052 (1973).

[6] Y. T. Lee, in: *Atomic and Molecular Beam Methods, Vol. 1*, edited by G. Scoles (Oxford University Press, New York, 1988).

[7] R. F. Stebbings and F. B. Dunning, Editors, *Rydberg states of atoms and molecules*, Cambridge University Press (1983).

[8] S. A. Edelstein and T. F. Gallagher. Adv. At. Mol. Phys. **14**, 365 (1978).

[9] V. Kempter, W. Mecklenbrauck, M. Menzinger, Ch. Schlier, Chem. Phys. Lett. **11**, 353 (1971).

[10] (a) I. V. Hertel, H. Hofmann, and K. A. Rost, J. Chem. Phys. **71**, 674 (1979). (b) G. Jamieson, W. Reiland, C. P. Schulz, H. U. Tittes, and I. V. Hertel, J. Chem. Phys. **81**, 5805 (1984).

[11] see, for example, H. Goldstein, *Classical Mechanics*, 2nd edition. Addison Wesley (1980).

[12] A. W. Kleyn, Ph. D. Thesis, "Stichting voor Fundamenteel Onderzoek der Materie", Amsterdam, The Netherlands (1982).

[13] A. W. Kleyn, M. M. Hubers, and J. Los, Chem. Phys. **34**, 55 (1978).

[14] (a) D. R. Lide, Editor-in-Chief, *CRC Handbook of Chemistry and Physics*, 74th edition (1993-1994). (b) K. P. Huber and G. Herzberg, *Molecular Spectra and Molecular Structure, IV. Constants of Diatomic Molecules*, Van Nostrand Reinhold Company (1979).

Figure Captions

Figure 4.1 Schematic drawing of the rotatable detector. c.c. is the interaction region of the molecular beams. The products pass through a series of defining slits before they reach the electron bombardment ionization region (1). The ions

are then mass selected by the quadrupole mass filter (2) and focused by ion lenses (3) into the Daly ion counter, which houses a high voltage electrode (4) and a scintillator-PMT assembly (5).

Figure 4.2 Time of flight spectra recorded at a lab angle of 25 degrees. (a) is recorded at m/e = 23, with both lasers tuned on resonances. The electron bombardment ionizer and its associated ion lenses are in operation. (b) is taken under the same conditions as in (a) except the 4D ← 3P laser is tuned off resonance. The spectrum looks the same when either or both lasers are tuned off resonance. (c) is taken under the same conditions as in (a) except that the mass filter is set to allow an odd mass to transmit. In this case, m/e = 10. (d) is taken for m/e = 23 under the same conditions as in (a) except the electron bombardment ionizer is turned off.

Figure 4.3 Newton diagram for Na + O_2 at a nominal collisional energy of 16 kcal/mol. θ is the center of mass angle and Θ is the lab angles. It is shown in Figure 4.5 that most products appear with less than 1 kcal/mol of translational energy.

Figure 4.4 Na^+ time of flight spectra recorded under same conditions as in (a), Figure 4.2, at E_c = 16 kcal/mol. The open circles are the experimental data and the solid lines are simulations using the center of mass energy and angular distributions shown in Figure 4.5.

Figure 4.5 Center of mass angular and energy distributions of the Rydberg products at E_c = 16 kcal/mol.

Figure 4.6 Laboratory angular distribution of the Rydberg products at E_c = 16 kcal/mol. The open circles are experimental data recorded with the electron bombard-

ment ionizer and the ion lenses turned off. The solid line is the simulation using the center of mass energy and angular distributions shown in Figure 4.5.

Figure 4.7 Energetics for the $Na + O_2$ system. Data are adapted from reference [14].

Figures

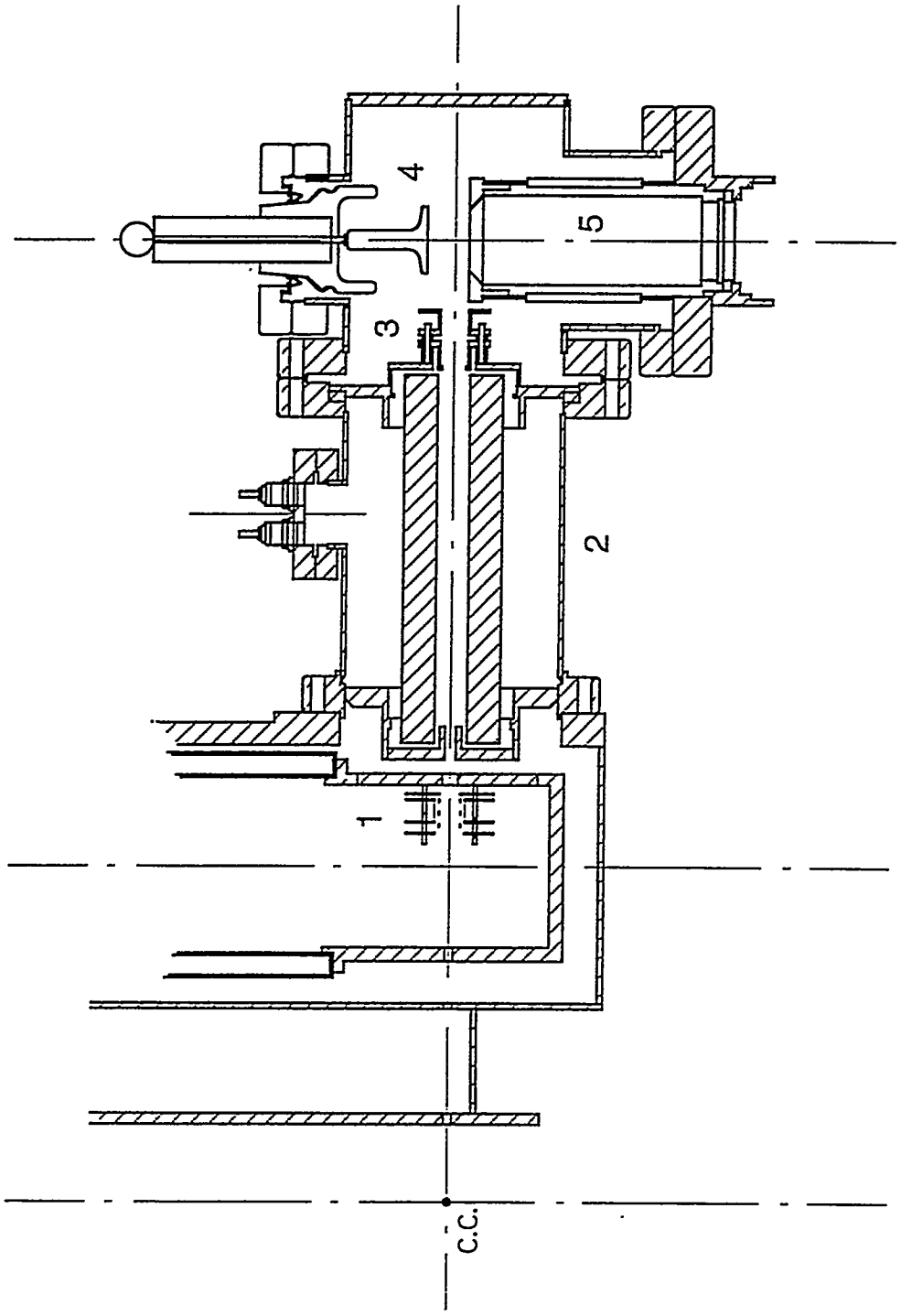

Figure 4.1

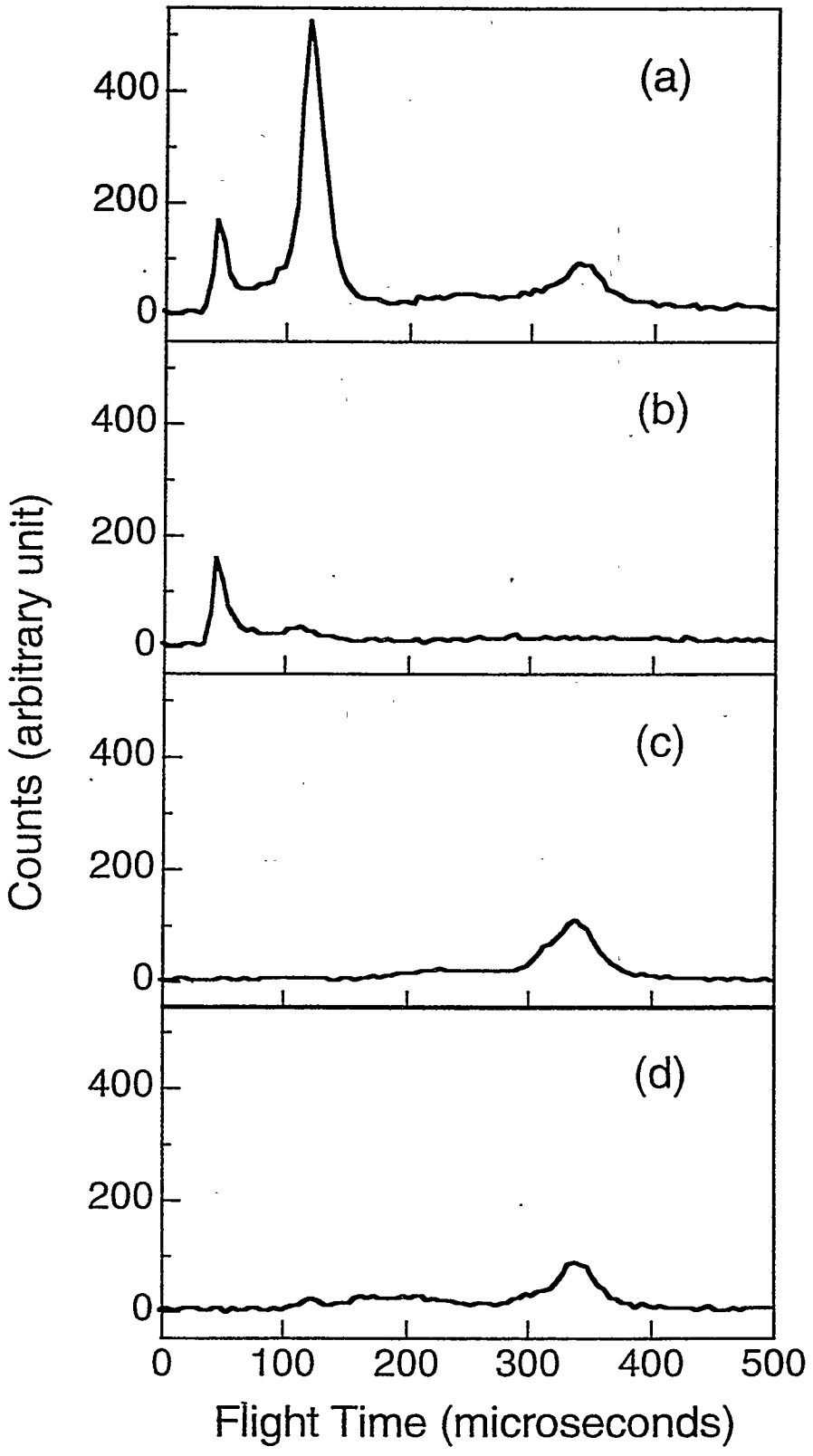
(a)
(b)
(c)
(d)
400
200
0
Counts (arbitrary unit)
0
100
200
300
400
500
Flight Time (microseconds)

Figure 4.2

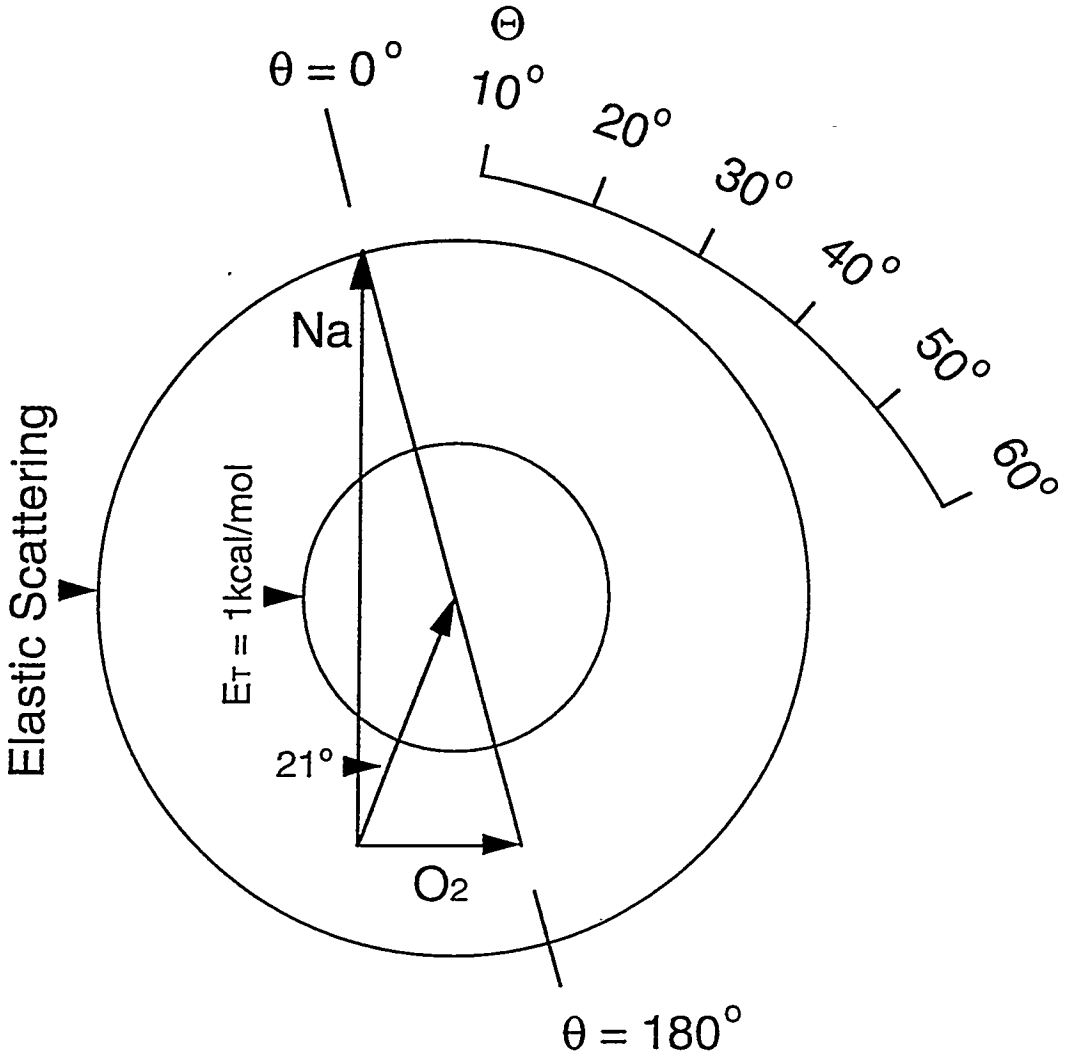
Θ
θ = 0°
10°
20°
30°
40°
50°
60°
Na
Elastic Scattering
ET = 1kcal/mol
21°
O2
θ = 180°

Figure 4.3

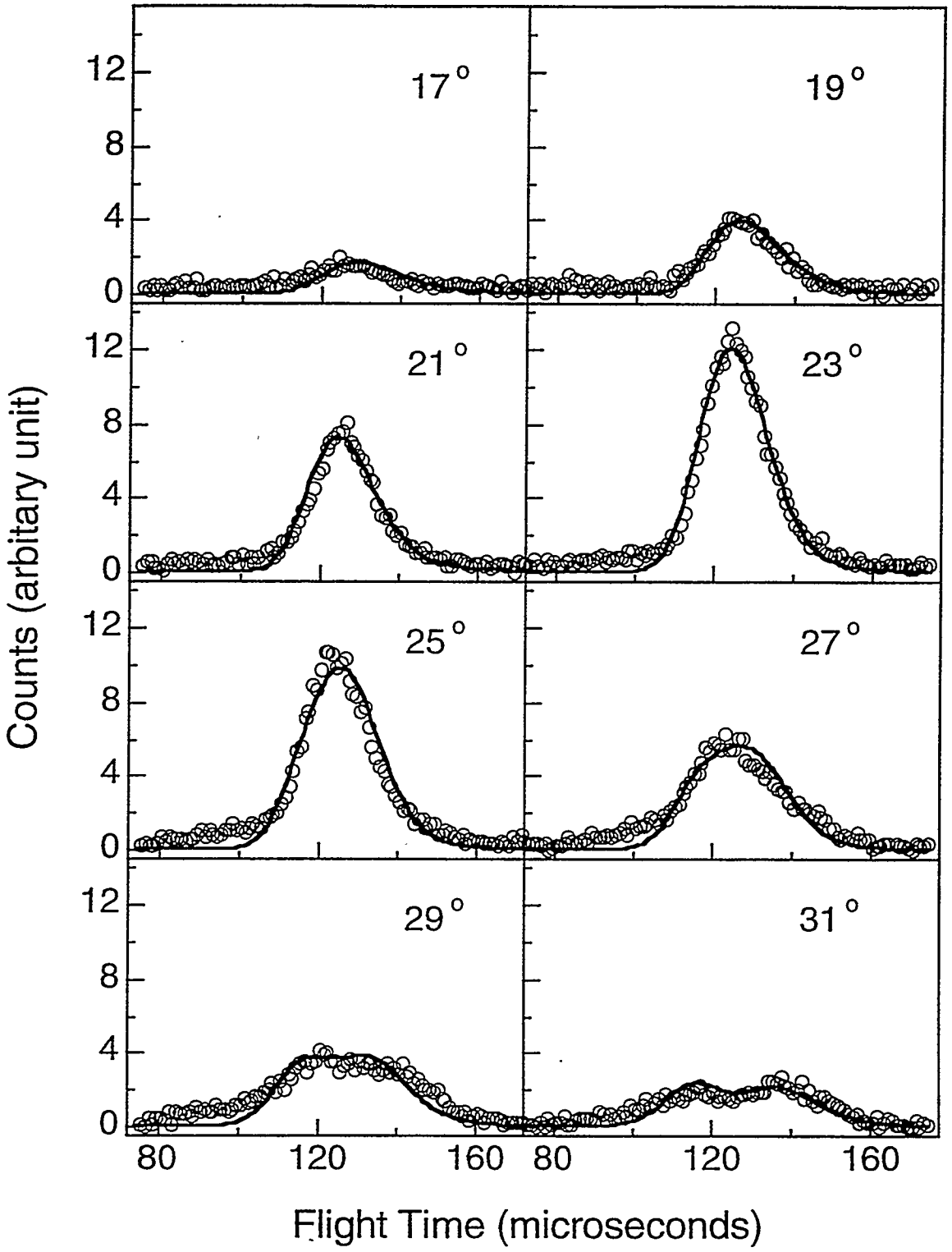
17°
19°
21°
23°
25°
27°
29°
31°
12
8
4
0
80
120
160
Counts (arbitary unit)
Flight Time (microseconds)

Figure 4.4

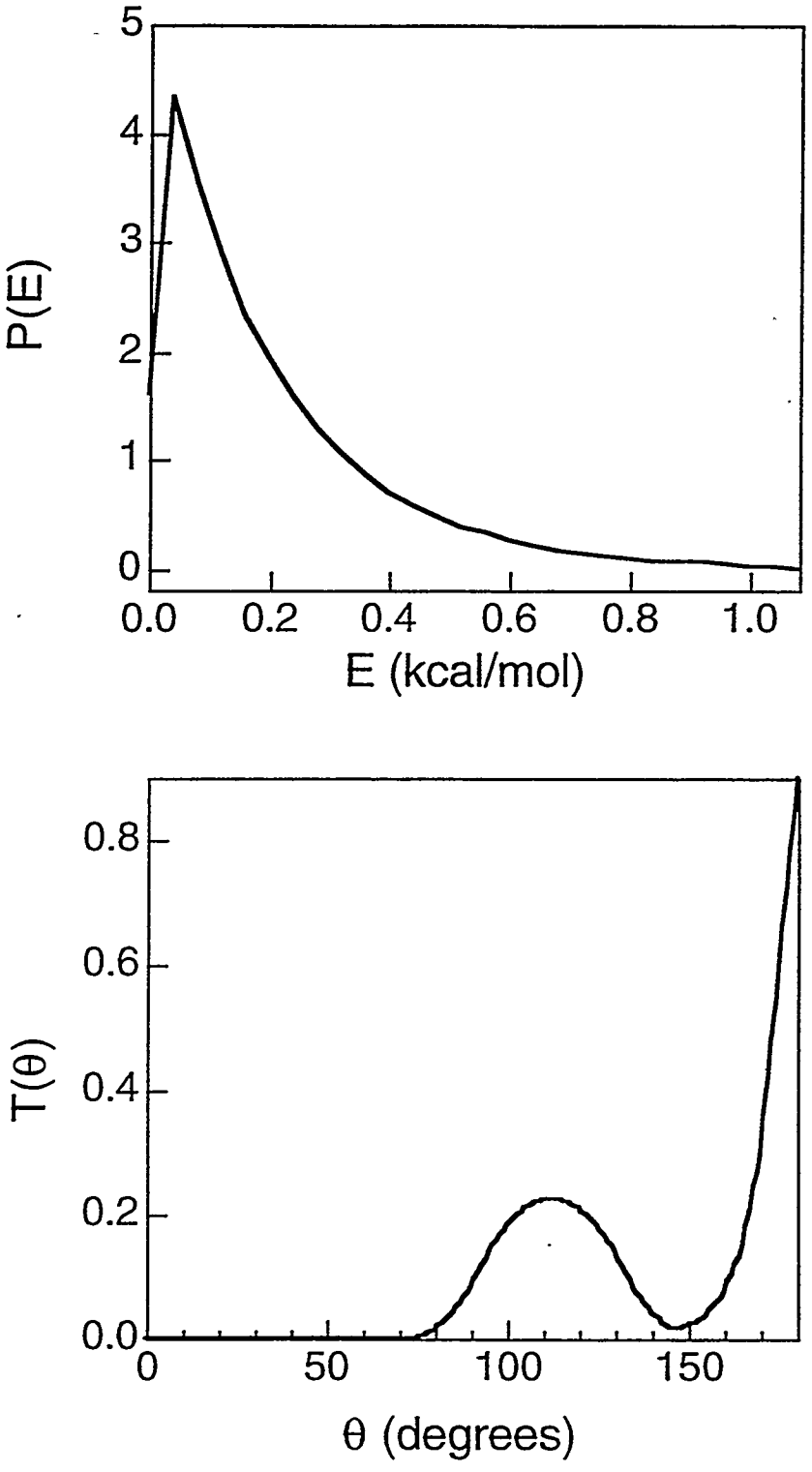
P(E)
5
4
3
2
1
0
0.0
0.2
0.4
0.6
0.8
1.0
E (kcal/mol)
T(θ)
0.8
0.6
0.4
0.2
0.0
0
50
100
150
θ (degrees)

Figure 4.5

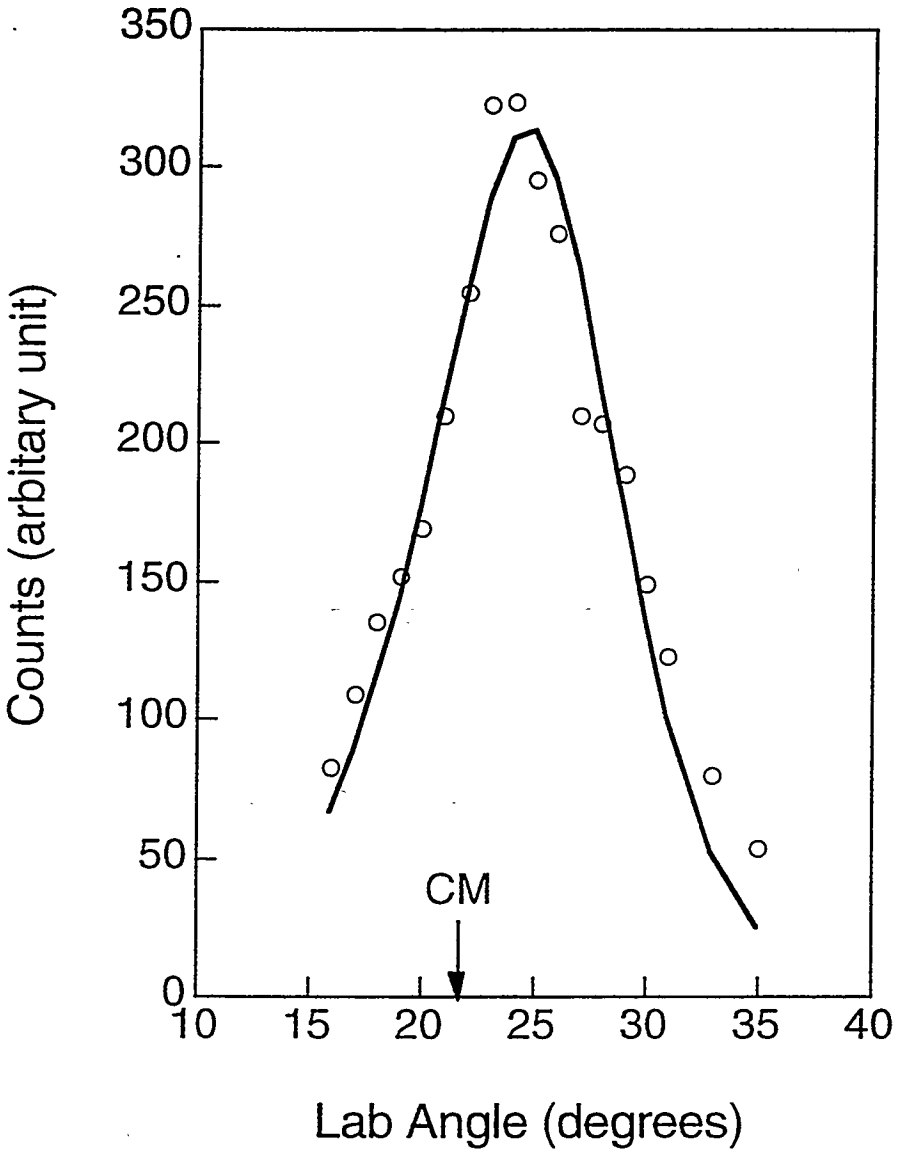
350
300
250
200
150
100
50
0
Counts (arbitary unit)
CM
10
15
20
25
30
35
40
Lab Angle (degrees)

Figure 4.6

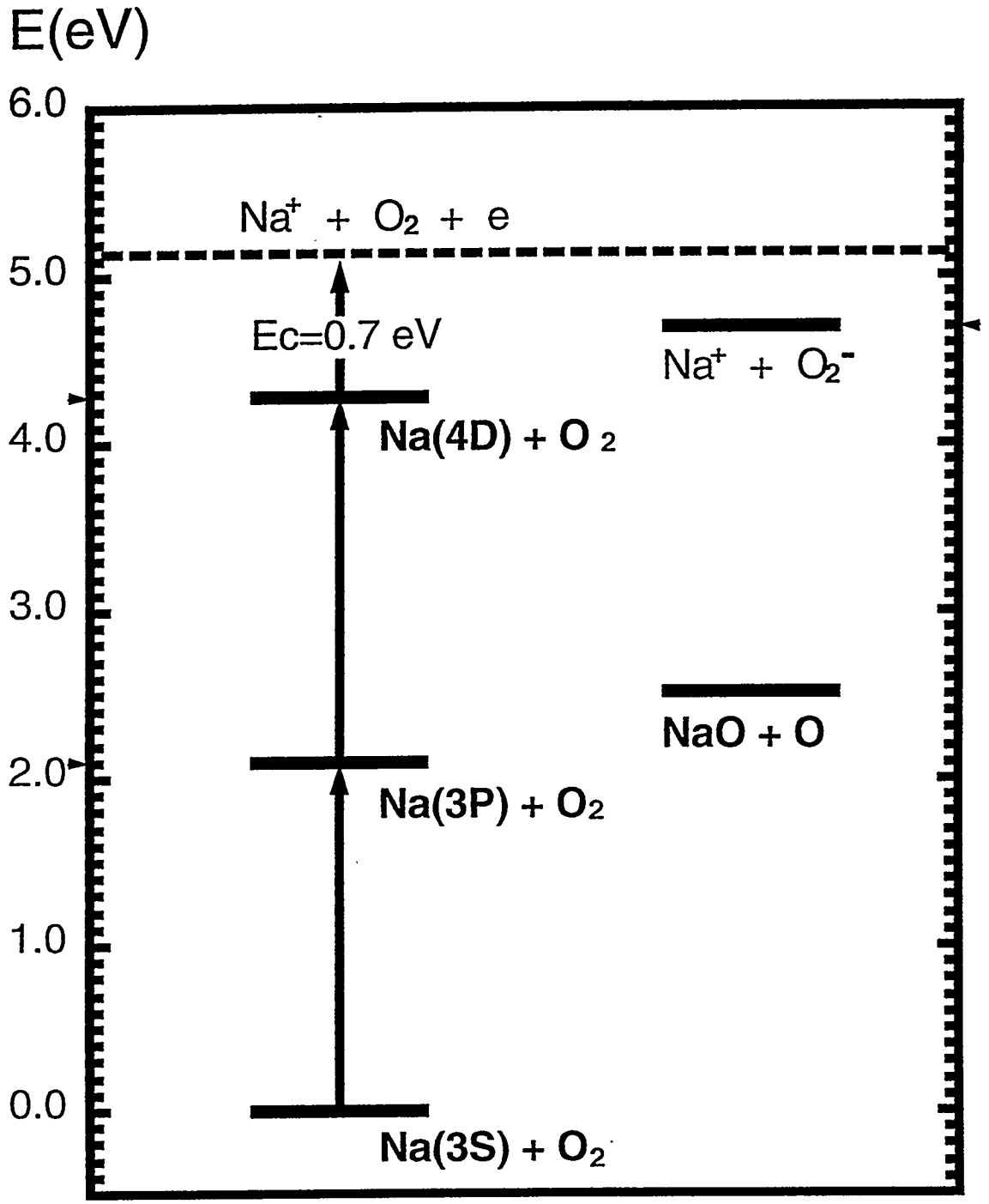
E(eV)
6.0
5.0
4.0
3.0
2.0
1.0
0.0
Na+ + O2 + e
Ec=0.7 eV
Na+ + O2-
Na(4D) + O 2
NaO + O
Na(3P) + O2
Na(3S) + O2

Figure 4.7